14:16:45 OCA PAD INITIATION - PROJECT HEADER INFORMATION 10/02/87

Active

Project #: E-21-J33 Cost share #: Rev #: 0
Center # : R5962-BC3 Center shr #: OCA file #: 93
Work type : RES
Contract#: N61331-85-D--0025-0033 Mod #: INITIATION Document : DO
Prime #: Contract entity: GTRC

Subprojects ? : N
Main project #:

Project unit: EE Unit code: 02.010.118
Project director(s):
PARIS D T EE

Sponsor/division names: NAVY / NAVAL COASTAL SYS, FL
Sponsor/division codes: 103 / 001

Award period: 870818 to 880331 (performance) 880331 (reports)

Sponsor amount	New this change	Total to date
Contract value	48,780.00	48,780.00
Funded	48,780.00	48,780.00
Cost sharing amount		0.00

Does subcontracting plan apply ?: N

Title: FREQUENCY AGILE BEAMFORMER

PROJECT ADMINISTRATION DATA

OCA contact: E. Faith Gleason 894-4820

Sponsor technical contact

MR. EDWARD L. PIPKIN / CODE 4120
(904)234-4281
NAVAL COASTAL SYSTEMS CENTER
PANAMA CITY, FL 32407-5000

Sponsor issuing office

ALLEN HOTTELL / CODE 0654
(904)234-4309
NAVAL COASTAL SYSTEMS CENTER
PANAMA CITY, FL 32407-5000

Security class (U,C,S,TS): U ONR resident rep. is ACO (Y/N): Y
Defense priority rating : DO-S10 GOVT supplemental sheet
Equipment title vests with: Sponsor X GIT

Administrative comments -
INITIATION: INCLUDES SUBCONTRACT TO MISSISSIPPI STATE UNIVERSITY FOR $44,02

EORGIA INSTITUTE OF TECHNOLOGY OFFICE OF CONTRACT ADMINISTRATION

SPONSORED PROJECT TERMINATION/CLOSEOUT SHEET

Date 5/11/88

roject No. E-21-J33 School/Lab EE

ncludes Subproject No.(s) N/A

roject Director(s) D. T. Paris GTRC/[redacted]

ponsor

itle Frequency Agile Beamformer

ffective Completion Date: 3/31/88 (Performance) 3/31/88 (Reports)

rant/Contract Closeout Actions Remaining:

- [ ] None
- [X] Final Invoice or Copy of Last Invoice Serving as Final
- [X] Release and Assignment
- [X] Final Report of Inventions and/or Subcontract:
  Patent and Subcontract Questionnaire sent to Project Director [X]
- [X] Govt. Property Inventory & Related Certificate
- [X] Classified Material Certificate
- [ ] Other

ontinues Project No. Continued by Project No.

OPIES TO:

roject Director
esearch Administrative Network
esearch Property Management
ccounting
rocurement/GTRI Supply Services
esearch Security Services
eports Coordinator (OCA)
rogram Administration Division
ontract Support Division
Facilities Management - ERB
Library
GTRC
Project File
Other

E-21-J33

MISSISSIPPI STATE UNIVERSITY
COLLEGE OF ENGINEERING

DEPARTMENT OF ELECTRICAL ENGINEERING
DRAWER EE
MISSISSIPPI STATE, MISSISSIPPI 39762
PHONE (601) 325-3912

December 10, 1987

Dr. D. T. Paris, EE
Georgia Institute of Technology
Atlanta, GA 30332-0258

Dear Dr. Paris:

Enclosed is a copy of the progress report for Subcontract E-21-J33-S1 under IQC No. N61331-85-D-0025; D.O. 0033. Please note three copies of this report have been sent to Dr. Larry Howell, Code 4230, NCSC, Panama City, FL 32407-5000, in accordance with Exhibit A of the contract document.

Sincerely,

J. Patrick Donohoe
Co-Investigator

Frank M. Ingels
Co-Investigator

asd

Enclosure

FREQUENCY AGILE BEAMFORMER

PROGRESS REPORT

15 December 1987

Contract No. E-21-J33-S1 (Ga. Tech Omnibus)
Naval Contract N61331-85-D-0025; D.O. 0033

Deliver To:

Dr. Larry Howell
Code 4230
Naval Coastal System Laboratory
Panama City, FL 32407-5000

P. Donohoe
F. Ingels
Department of Electrical Engineering
Mississippi State University
Drawer EE
Miss. State, MS 39762
601+325-3912

TABLE OF CONTENTS

Section		Page
1.0	Introduction	1
	1.1 General	1
	1.2 Receiver Types	2
	1.3 Conclusions	10
2.0	Low Probability of Intercept Approaches	12
	2.1 Spread Spectrum Direct Sequence	12
	2.2 Spread Spectrum Frequency Hopping	14
3.0	Welch Sequence Frequency Hopper	19
	3.1 Why a Welch Sequence?	19
	3.2 Welch Sequence Generation	24
	3.2.1 Generation Technique	25
	3.2.2 A Welch Sequence Beamformer Example	28
4.0	Summary of Work To Date	40
5.0	Budget Statement	41

1.0 INTRODUCTION

1.1 GENERAL

This contract has as its objective a frequency agile beamformer. This term, frequency agile, is meant to imply a beamformer that is capable of transmitting acoustic pulses over a wide frequency range and at the same time possessing properties that would classify the array's transmissions as a low probability of intercept (LPI) type of signal.

The development of LPI for radar and sonar has been claimed by some to be impossible since the electronic surveillance monitor (ESM) one is trying to prevent from detecting the signal is detecting over a one-way path whereas the signal user is attempting detection over a two-way path (the round trip path). However, this criticism is only a valid criticism if the ESM is monitoring a signal at a known frequency and time location and is, in fact, in the one-way detection range of the intercept receiver.

Consider the ESM receiver that is monitoring a frequency range by selective band monitoring, changing those bands periodically, and that is a long distance away compared to the one-way maximum distance the sender can use. The sender then has the option of spreading the energy density over a wider frequency band than necessary, say two or three times the normal bandwidth. For example, a 100KHz carrier with a millisecond pulse burst requires a 2000 Hz bandwidth for 90% power. If the energy transmitted with a normal 90% power bandwidth of 2000 Hz is 50 watts, then the energy density would be (50/2000) watts per Hz or 25.0 mw per Hz. Spreading the signal to a 10,000 Hz bandwidth would lower the instantaneous energy density to 5.0 mw per pulse. This effectively cuts by a factor of 5 the maximum detectable distance of a

receiver with the 2000 Hz bandwidth relative to the original unspread maximum detectable distance.

The sender can also use frequency hopping to select one of, say, 10 frequencies. If the upper frequency is, say, 250 KHz and the lower frequency is 50 KHz, the total frequency range is 200 KHz. If a total of 10 frequencies in this frequency range with a bandwidth of 10,000 Hz are utilized for transmission one at a time, the percentage utilized of the total frequency range is 100 KHz out of 200 KHz or 50.0% utilized at a 5% rate. Thus, a receiver looking at random with ten frequencies in the 200 KHz range from 50 KHz to 250 KHz using a receiver with a normal bandwidth of 2000 Hz will have approximately a 5.0% chance per listening frequency of hearing the emitted signal. If the receiver is using only two detection frequencies in the range at one time, the probability of hearing the emitted signal is roughly 10.0%. However, the intercept receiver is forced to work with one-fifth the energy-to-noise ratio due to the unspread bandwidth of the receiver.

The sender can also use time hopping (or random time intervals between pulses) to further complicate the detection problem.

1.2 RECEIVER TYPES

The key to all of the above is to know the detector receiver characteristics of the detector one is trying to defeat. In fact, there is no single LPI technique suitable for all applications other than instantaneous spreading of the energy density to a value lower than the ambient noise spectral density, a technique limited by the bandwidth of transmitter and receiver acoustic transducers.

One may also choose to operate in a frequency band of high acoustic energy absorption so that detectable energy is not transmitted very far outside twice the maximum detection range (one-way trip) of the user. This technique may be self-defeating in some respects, however.

Receiver characteristics may be grouped into energy detectors and envelope detectors. Neyman-Pearson criterion of setting the detection threshold, V, so that the false alarm probability is tolerable is assumed. Thus, the noise level is used to set the threshold value V.

An energy detector is illustrated in Figure 1. The received signal is

$$r(t) = A\, s(t) + n(t) \qquad (1)$$

where A = 1 if signal is present and 0 if signal is not present and n(t) is white Gaussian noise.

The output of the bandpass filter is

$$f(t) = A\, s'(t) + n'(t) \qquad (2)$$

where the primes denote the bandpass filtered quantities.

The probability of false alarm and of signal detection for this type of receiver is well known and documented in a classical paper by H. Urkowitz, ''Energy Detection of Unknown Deterministic Signals,'' IEEE Proc., Vol. 55, pp. 523-531, April, 1967, and in other publications such as textbooks.

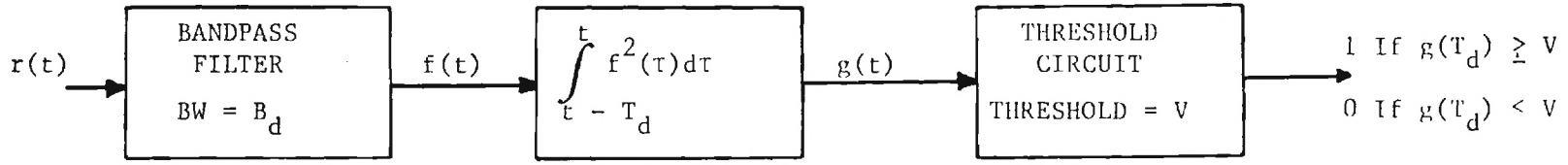

a) Energy Detector

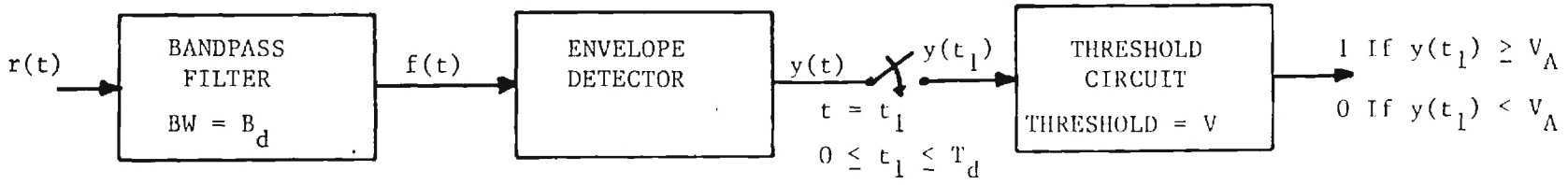

b) Single Sample Envelope Detector

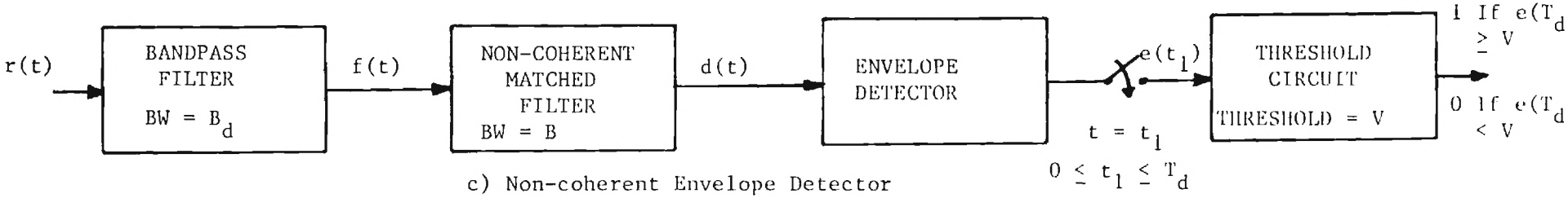

c) Non-coherent Envelope Detector
With Matched Filter

FIGURE 1 VARIOUS RECEIVER TYPES CONSIDERED

The resultant output g(t) at time T_d for noise only, assuming the worst case of the integrator timing being synchronized with the message timing, is a chi-square distribution with D_F degrees of freedom where

$$D_F = 2T_dB_d \tag{3}$$

and T_d is the integrator time duration and B_d is the receiver bandwidth. The output with signal is non-central chi-squared with non-centrality parameter $2E/N_o$ where E is the signal energy and N_o the noise spectral energy density (one-sided). The false alarm probability and signal detection probability are respectively:

$$P_{fa} = P[g(T_d) \geq V|A=0] = P\left[\sum_{i=1}^{2T_dB_d} g_i^2 \geq \frac{2V}{N_o}\right] \tag{4}$$

and

$$P_d = P[g(T_d) \geq V|A=1] = P\left[\sum_{i=1}^{2T_dB_d} (g_i + \overline{g_i})^2 \geq \frac{2V}{N_o}\right] \tag{5}$$

where V is the detector threshold, g_i is a zero mean unity variance random variable and $\overline{g_i}$ is the integrated signal at sample time

$$\overline{g_i} = \frac{S_i(t = i/2B_d)}{\sqrt{N_oB_d}} \tag{6}$$

[Reference: Urkowitz, previous reference on page 3, or E. W. Chandler, ''Optimizing the LPI Performance of a Spread Spectrum Receiver, Dissertation, 1985, UMI, 8519989]

The threshold V is determined by setting the desired false alarm rate and then calculating V from the probability of false alarm equation above.

For large T_dB_d products, the probability of detection is approximated by

$$P_d = Q\left[\frac{Q^{-1}(P_{fa}) - \sqrt{\frac{E/N_o}{T_dB_d}}}{\sqrt{1 + \frac{2E/N_o}{T_dB_d}}}\right] \qquad (7)$$

where Q(x) is the standard error function,

$$Q(x) = \frac{1}{\sqrt{2\pi}} \int_x^\infty e^{-u^2/2}\,du \quad . \qquad (8)$$

As an example of the benefit of direct spread spectrum that achieves instantaneous spectral spreading, consider a band spreading factor of 10 (from 2000 Hz to 20,000 Hz for a 100 KHz signal). If the false alarm probability is set to 10^{-4} for a spread time bandwidth product (T_dB_d) of 10, the normalized threshold setting is 52.66. For a signal energy to noise spectral energy density ratio of 31.6 (15dB signal-to-noise power ratio), the probability of detection is .9743 (read from standard curves or calculated from above equations). In contrast, the intercept receiver of Figure 1a using standard bandwidth and a false alarm probability of 10^{-4} has a time bandwidth product of

1.0, a normalized threshold setting of 19.29 and a detection probability of .024. Note that the E/N_o of 31.6 is spread by a factor of 10 to an energy density of 3.16 over the spread bandwidth and that a normal bandwidth receiver (detecting with no despreading) works or detects with an E/N_o of 3.16. This is a significant processing gain for a band spreading factor of only 10 to 1.

An envelope detector is illustrated in Figure 1 as well. The analysis for this detector for a sinusoidal pulse waveform with pulse duration T and carrier frequency f_c is found in either of the two previous references. For the sinusoidal pulse waveform and receiver type B in Figure 1, the false alarm probability, the threshold setting and the probability of detection are respectively:

$$P_{f_a} = P[Y(t_d) \geq V/A \sim 0] = P\left[\sum_{i=1}^{2T_dB_d} Y_i^2 \geq \frac{2v}{N_o}\right] \tag{9}$$

$$V = \sqrt{-2N_oB_d \ln(P_{fa})} \tag{10}$$

and

$$P_d = \int_v^\infty ze^{-z^2/2} e^{-P/N} I_o(z\sqrt{2P/N})dz \tag{11}$$

where the parameter z^2 is the signal plus noise to noise power ratio and is

$$z^2 = g^2/N_oB_d \tag{12}$$

and

$$N = N_o B_d \qquad (13)$$

and g is the envelope of signal plus noise. [Also see Page 140 of Radar System Design and Analysis by S. A. Hovenessian, 1984, Artech House.]

For the receiver in part C of Figure 1, the results for sinusoidal signal with duration T and carrier frequency f_c is the same as for receiver A except that the noise power is now

$$N = N_o B_d/4 \qquad (14)$$

due to the matched filter (non-coherent) and the signal power is

$$P = E\, B_d/4 \qquad (15)$$

and E = PT where T is the signal bandwidth period and T_d is detector sample period. Thus, the detection probability equation is the same but with P/N replaced by E/N_o:

$$P_d = \int_v^\infty z e^{-z^2/2}\, e^{-E/N_o}\, I_o\left(z\sqrt{\frac{2E}{N_o}}\right) dz \qquad (16)$$

where B is signal bandwidth and B = 1/T and B_d is detector bandpass filter bandwidth and T_d is the sample time out of the envelope detector.

The data in Table 1 drawn from the Chandler reference page 46 illustrates the detection probability for various values of the parameter X which is either P/N for receiver B or E/N_o for receiver C.

TABLE 1

Detection Probability P_d for Envelope Detectors

(Drawn From the Chandler Reference, Page 46)

X	P_d 10^{-2}	10^{-4}	10^{-6}
.0001	.010005	1.001E-4	1.0015E-6
.000316	.01001	1.003E-4	1.0045E-6
.001	.01005	1.009E-4	1.0140E-6
.00306	.01015	1.029E-4	1.0442E-6
.01	.0105	1.094E-4	1.142E-6
.0316	.0115	1.308E-4	1.479E-6
.1	.0149	2.096E-4	2.836E-6
.316	.0275	5.872E-4	1.104E-5
1.0	.0845	.00368	1.222E-4
3.16	.3688	.05225	.004585
10	.9422	.6161	.2481

where X = P/N for receiver type B

X = E/N_o for receiver type C

Since the parameter E/N_o is larger than P/N by the factor T_dB_d, the receiver C can perform better than receiver B for some circumstances.

Consider again the performance for a sinusoidal pulse waveform and an energy detector which has managed to determine a close estimate of the pulsed carrier duration, T, and the assumed radiated BW for 90% signal power of B = 2/T. If the energy detector has set T_d = T and B_d = B (i.e., T_dB_d = 2), then the probability of detection performance for 10^{-4} false alarm probability and an energy-to-noise ratio of, say, 10 is .4521. If T_dB_d is not optimum but, say, 3.16 meaning the receiver system is integrating for too long of a period or using too much bandwidth, then the performance for E/N_o = 10 is .3551, a lower performance figure. For the envelope detector receiver type C with E/N_o = 10 and a false alarm probability of 10^{-4} the performance figure is .6161. Similarly for receiver type B, single sample only, with P/N = 5 = $(E/N_o)/2$, the performance figure is about .2.

1.3 CONCLUSIONS

From the above discussion in the previous section, we see that the hardest receiver to defeat is the envelope detector with non-coherent matched filter IF THE SIGNAL PULSE AND BW ARE KNOWN AND SIGNAL BIT TIMES ARE KNOWN! Again, however, spreading the signal energy density over a ten to one ratio will lower performance of an intercept receiver type C from .6161 to .00368 probability of detection. The bottom line is that even small spreading factors can help tremendously!

The use of frequency hopping can also be a great help in that the detecting receiver now has a more difficult time looking at the right frequency. If the receiver uses a wideband detector, this in effect

increases B_d thus increasing the input noise power and in effect reduces receiver performance.

The impact of this discussion is that a frequency hopping system using high speed pulses for signal energy density spreading on an instantaneous basis is the most attractive method for achieving LPI properties against energy or envelope detector receivers. Several questions remain:

1) What is the best frequency hopping sequence to use from a range/doppler ambiguity point of view?

2) What are reasonable bandwidth spreading factors that can be obtained from state-of-the-art acoustic transmitters and receiver sensors?

3) What type of wide frequency band constant beamwidth arrays could be designed with the above techniques?

This report addresses the frequency hopping sequence and the array design in the following sections.

2.0 LOW PROBABILITY OF INTERCEPT APPROACHES

There are two basic methods of achieving a low probability of intercept signal. These two basic methods are spread spectrum methods - achieved through either direct sequence spectral density spreading of the carrier or through frequency hopping the transmitted carrier over a broad frequency range. The first method achieves a low spectral energy density of the transmitted signal at all times and is a spread spectrum technique in the purest sense. The second method achieves a time average low spectral energy density by transmitting a specific frequency at high spectral energy density but only for a short period of time relative to the total time period of the basic signal. The second method can only achieve a spectral energy density spreading if the total frequency content used is small relative to the total end-to-end frequency range of the signals used.

Other techniques use time hopping or time and frequency hopping or even time and frequency hopping with direct sequence spreading of the radiated signals.

2.1 SPREAD SPECTRUM DIRECT SEQUENCE

Spectral energy density spreading achieves a very low energy density by spreading a signal's energy density over a frequency range orders of magnitude wider than required to send the signal. By spreading the acoustic energy by a factor of 5 or 10, as demonstrated in the previous section, a significant advantage can be gained by reducing the range at which an intercept receiver can detect the radiated acoustics. If a one millisecond pulse is to be radiated at a frequency of 50 KHz, the signal bandwidth is effectively 2000 Hz for 90% of the

energy to be transmitted. By using a fast code, say, 5 or 10 times faster than the base pulse which is 1.0 milliseconds long and by sending a Barker Code sequence at the carrier frequency, one may spread the spectral energy by a factor of the ratio of one millisecond divided by the smallest bit width of the Barker Code. If the Barker Code chosen is five bits long, with the five bits occurring in one millisecond, then the smallest bit width is two-tenths of a millisecond, and the signal bandwidth is now 10,000 Hz or five times wider than the base pulse. The same 90% energy is now effectively spread over this wider bandwidth and the signal energy-to-noise power spectral density (E/N_o) is now lowered by a factor of five. Thus, an intercept receiver must move a factor of $\sqrt{5}$ = 2.236 times closer to maintain a specific probability of detection since the energy is diminished with inverse range squared. Alternatively, a Barker Code of 7 or 11 or 13 could be used for larger signal spectral spreading with associated wider acoustic transducer bandwidth required.

Assuming a transducer Q of 10 at 100 KHz driving frequency, a bandwidth of 10 KHz is available. Thus, a 5-bit Barker Code could be used with .2 millisecond pulse widths. If a transducer with a Q of 4.5 can be built, then the available bandwidth is 22.2 KHz, and a spectral spreading factor of 11 relative to the 2.0 KHz unspread signal is possible using a Barker Code of 11 bits with .091 millisecond pulse widths.

For a spreading factor of 10, the intercept receiver must move a factor of 3.16 closer in distance to compensate for reduced signal power density. If the intercept receiver is four times as sensitive as the user's receiver, then the intercept receiver could work with an unspread

signal at a distance of 2 * 2 = 4 times the maximum one way detection range of the user. However, by spreading by a factor of 10, the intercept receiver must move to within .316 times the maximum one way detection range of the user, that is almost within detection range of the user, provided the intercept receiver is not aware of the spreading code. Table 2 summarizes these relationships.

This is a promising start. Now if frequency hopping is added to the users bag of tricks, the intercepter problems will be compounded. The next section discusses the frequency hopping aspects.

2.2 SPREAD SPECTRUM FREQUENCY HOPPING

In an acoustic system a wideband constant beamwidth array might be used for transmission or reception. If the wideband array covers the frequency range with a series of, say, 7 frequencies spaced at various intervals, then a possible signalling scheme is to transmit first one frequency, then another sequentially to cover the frequency range. As long as the frequency range has a large bandwidth and only a few frequencies are used to cover the range, the intercept receiver must either use a wideband detector or, if the detector only covers a portion of the frequency band, use a series of contiguous detectors. For example, consider an intercept receiver that has transducers with a bandwidth four times the user transmitter transducer. Assume further that the intercept system has four receivers each with 8 KHz bandwidth listening in a 200 KHz frequency range. If the transmitter system sends on one of seven possible frequencies with a 2 KHz bandwidth, the

TABLE 2

ILLUSTRATION OF SPECTRAL SPREADING FACTORS

ASSUME FALSE ALARM PROBABILITY IS SET TO 10^{-4}. ASSUME E/N_o UNSPREAD IS 31.6 (15dB).

ASSUME UNSPREAD SIGNAL TRANSMITTED BANDWIDTH IS 2000 Hz.

ASSUME INTERCEPT RECEIVER USES 2000 Hz BANDWIDTH FOR EACH DETECTION FREQUENCY.

ASSUME MAXIMUM DETECTION RANGE OF USER RECEIVER IS R. (ONE-WAY RANGE).

ASSUME INTERCEPT RECEIVER HAS FOUR TIMES AS SENSITIVE RECEIVER (I.E., CAN DETECT WITH FOUR TIMES LESS E/N_o RATIO).

E/N_o VARIES INVERSELY WITH RANGE SQUARED.

	DETECTION RANGE (USER)	DETECTION RANGE (INTERCEPTER)
Unspread Signal SF = 1.0	R_u (one way)	$R_I = 2(2R_u) = 4R_u$ (one way)
Spread By SF = 5 (Hence E is reduced by 5 or $E_{us} = E_u/5$)	R_u (one way)	$R_I = .447(4R_u) = 1.788\ R_u$ (one way)
Spread By SF = 10 (Hence E is reduced By 10 or $E_{us} = E_u/10$)	R_u (one way)	$R_I = .316(2R_u) = 1.264\ R_u$ (one way)

E_I=Intercept Receiver Energy E_u=User Receiver Energy E_{us}=Unspread Energy Density SF=Spreading Factor

$$E_I \sim 1/R_I^2 \qquad \text{Thus} \quad E_I R_I^2 \sim E_u R_u^2$$

$$\text{or} \quad R_I \sim R_u \sqrt{\frac{E_u}{E_I}} = R_u \sqrt{\frac{E_{us}}{SF\ E_I}}$$

If E_I detectable is one-fourth E_u detectable, then $R_I \sim 2\ R_u$.

TABLE 2 (continued)

ASSUME E/N_o = 10dB (UNSPREAD) SPREADING FACTOR ASSUMED = 10

INTERCEPT RECEIVER TYPE	INTERCEPT RECEIVER PROBABILITY OF DETECTION AGAINST UNSPREAD SIGNAL	INTERCEPT RECEIVER PROBABILITY OF DETECTION AGAINST SPREAD SIGNAL (SF=10)
	$T_dB_d = 2.0$	$T_dB_d = 2.0$
Energy Detector Figure 1a	.4521	.00154
Envelope Detector Figure 1b	$\sim.2^+$	~.0015
Envelope Detector Figure 1c	.6161	.00368

probability of intercepting the transmission with one of the four receivers would be as follows. The 8 KHz bandwidth intercept receivers need 25 center frequencies to cover the 200 total KHz bandwidth. We assume the seven user frequencies lie anywhere in the 200 KHz range at random and that at the maximum intercept range only 6 KHz of the 8 KHz is useable due to the roll off 3dB attenuation at 8KHz. Then the chance a user frequency lies within the useable 6 KHz of a receiver center frequency is .75. The chance that any single user frequency will be in one of the four intercept receiver's detection bands is 4 out of 25, or .16. Thus, the chance that a single user frequency is within 6 KHz of one of the four intercept receivers detection range is (.16) (.75) = .12.

When sending two of seven user frequencies simultaneously, the possibility of one or more landing in an intercept receiver detection range is (.12) + (.12) + (.12) (.12) = .24 + .0144 = .2544. By using a wideband array and a few discrete frequencies to sample the frequency range, it is thus possible to lower the intercept receivers probability of detection to less than one, even if the intercept receiver has a wider receiver bandwidth.

From the above example one may observe that it is better to transmit only one frequency at a time. Given this single frequency at a time signalling technique, is there a best way to select a relationship between frequencies to be transmitted? The next section of this report discusses this point.

Before proceeding, however, it should be mentioned that using three frequencies, one from each of three distinct sets, and distributing the power of the single frequency approach amongst the three frequencies, it

would be feasible to signal with a Reed Solomon (or other) error correcting code. Thus, if the power is lower to the point that one or two sets of frequencies are not received properly, it would be possible to correct the errors and to establish a synchronization on the return signal for ranging purposes. This technique will be addressed at a later time in this contract.

A second point of consideration is the sensitivity of the multi-sensor array to frequencies off the design frequency. For a 10% lower frequency, the beam response is approximately 10% broader and vice versa. Thus, a spreading factor of 10 or 11 is possibly an optimum spread considering array beam skew.

3.0 WELCH SEQUENCE FREQUENCY HOPPER

3.1 WHY A WELCH SEQUENCE?

Although Doppler shifts are small for sea surface reverberation due to a rough-moving sea surface, being typically in the 25 Hz or less for 85 KHz signals and 10 Hz for 60 KHz signals [Reference page 284-285, Urick, Principles of Underwater Sound, 1983, 3rd Edition.] the Doppler shift for a moving target is more significant. The Doppler shift is easily calculated by

$$\Delta f = \frac{2v}{C} f = \frac{2v\ f}{1500\ m/s} = \frac{2v\ f}{4900\ f/s} = \pm .69\ Hz/(kt)(KHz) \ .$$

Thus for a 10-knot movement and a 100 KHz signal frequency, the Doppler shift expected is

$$\Delta f = (.69)(10)(10^2) = 690\ Hz \ .$$

and for 250 KHz signal frequencies, Δf = 1725 Hz.

The Doppler shift for 10Knot velocity and a 250 Hz signal is seen to be significant compared to the possible RF signal bandwidth of 200 Hz. A shift of 1725 Hz of the signal carrier would, in fact, move the signal out of a typical non-Doppler compensating bandpass filter with a 2000 Hz bandwidth ($\pm$1000 Hz about the carrier frequency.)

Another effect which must be accounted for is the possibility of return echo elongation due to target length. For a target length L at an aspect angle Θ, the return echo is lengthened by an approximate factor

$$\frac{2L\cos\theta}{C} \quad . \qquad (17)$$

The signal processing of the return echo data should be designed to accommodate the echo elongation. For mines the echo elongation is not the severe problem it can be for submarine detection. This phenomena will not be considered for this specific contract.

The Doppler shift of the return echo is a phenomena that must be considered in this signalling design. If two frequencies in a frequency hopping signal set are spaced within 2000 Hz of each other, it is obvious that for a 10Knot velocity and signals in the 250 KHz frequency range, the prime signal could be moved out of the pass band of the receiving filter. At the same time the secondary signal could be shifted into the pass band of the receiving filter.

For example, consider a two-pulse transmission with the first pulse using 248 KHz. If up Doppler of 1725 Hz is experienced, the 248 KHz signal will be detected by the filter whose center frequency is 250 KHz, and the 250 KHz signal will return at 251.725 KHz shifted out of the detection filter region. Hence for non-Doppler compensating receiver system, the 248 KHz pulse is detected in the wrong filter and is thus confused with the 250 KHz pulse. The response in the 250 KHz filter will be used to determine range, but based on the assumed time difference between transmission and assumed reception of the 250 KHz pulse, which of course creates a range error.

Correct frequency spacing of the pulses to be used in a set of frequency hopping pulses is an important design consideration. This problem has been addressed by radar designers for many years. The use of a range/velocity ambiguity function, which is in effect a two

dimensional correlation equation, has been the typical figure of merit for investigating signal waveforms that exhibit good range/velocity ambiguities.

The ideal signal shape with regards to not producing ambiguous returns due to range timing shifts or velocity induced frequency shifts is a signal whose two-dimensional correlation function is a ''thumb tack'' or impulse shape, as illustrated in Figure 2 for the delay - Doppler ambiguity function defined as

$$X(\tau,v) = \frac{1}{2E}\int_{-\infty}^{\infty} \mu^*(\sigma)\mu(\sigma-\tau)e^{j2\pi v\sigma}d\sigma \qquad (18)$$

where E is the total energy of the signal pulse $\mu(t)$. Consider a pulsed sinusoid

$$\mu(t) = \Pi(\frac{t}{T})\ \cos W_o t \qquad (19)$$

where T is the pulse duration and W_o is the carrier radian frequency. For this signal shape, the energy E is

$$E = \int_{-\infty}^{\infty} \mu(t)\ \mu^*(t)\ dt = \int_0^T \cos^2 W_o t\ dt = \frac{T}{2} \qquad (20)$$

and for N contiguous pulses, the total energy is $\frac{NT}{2}$.

Also illustrated in Figure 2 is an ambiguity response for a single CW pulse, such as the pulsed sinusoid signal used previously. The

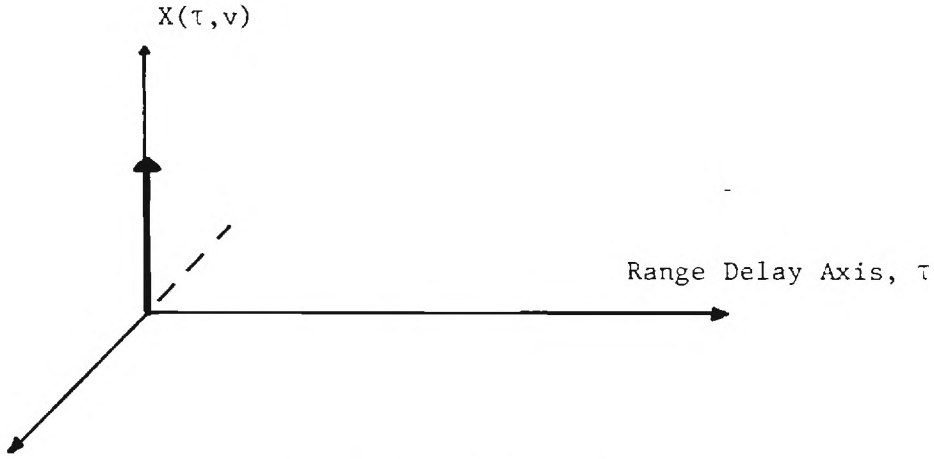

a) Ideal Ambiguity Function Response

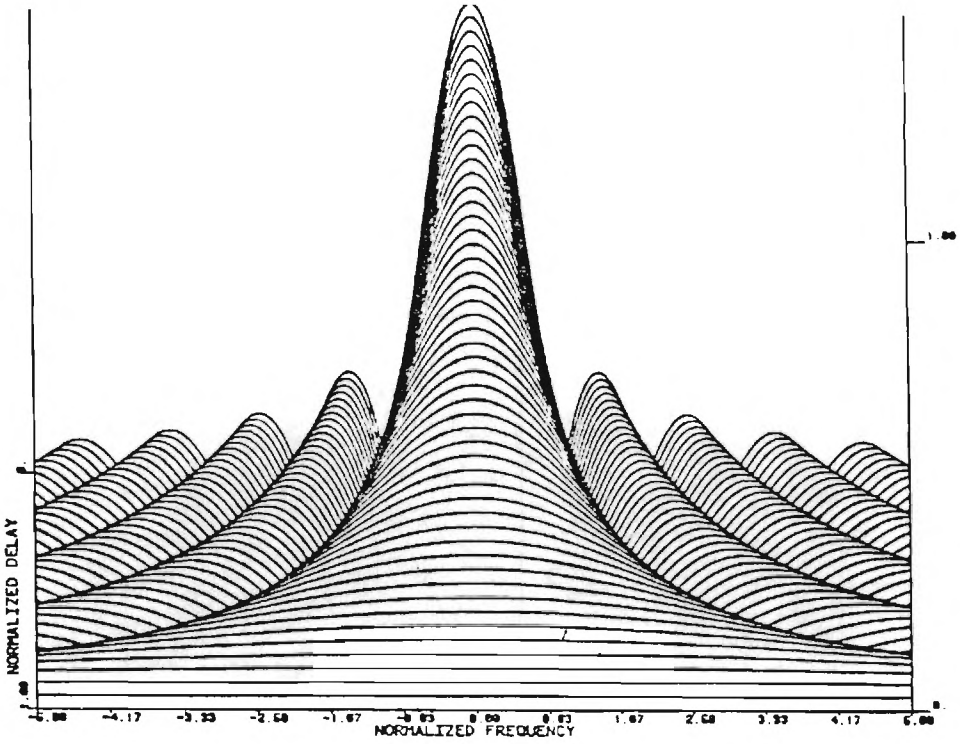

b) Pulsed Sinusoid Ambiguity Function Response

(From Costas, "A Study of a Class of Detection Waveforms Having Nearly Ideal Range-Doppler Ambiguity Properties," IEEE Proceedings, Vol. 72, No. 8, August 1984, Page 1001.)

Figure 2 Ambiguity Function Responses

ridges on the plot are areas of high response due to frequency shift, and it is easily observed that strong return echoes with, say, 1.67 normalized frequency would produce a correlator output that could indicate a false return due to range delay. Contrast this ambiguity plot with that for the ideal ambiguity plot in which any Doppler shift will cause the correlation response to be zero and hence precludes a false range delay indication.

A paper by John P. Costas [Reference Costas, A Study of a Class of Detection Waveforms Having Nearly Ideal Range-Doppler Ambiguity Properties, IEEE Proceedings, Vol. 72, No. 8, August 1984, pages 996-1009] has investigated a signalling set for frequency hopping using a Welch sequence to determine the order of use of the various frequencies and also has made use of the fact previously determined by others that the frequency differences of the signals should be equal to the reciprocal of the pulse length to prevent ambiguities along the range delay axis.

Furthermore Costas, in this paper, has made a good argument for one pulse per time period and no more than one pulse of each frequency per frequency hopping burst when working in a reverberation environment. Thus, it has been determined that a frequency hopper should use signal sets with the following properties if working in a reverberation environment:

1. Frequencies of individual pulses should be separated by the reciprocal of the pulse length to minimize ambiguities along the range delay axis.

2. When a burst of pulses is transmitted, the burst should have no more than one pulse of each frequency in the burst.

3. A burst should have only one pulse at a time; i.e., two pulses using different frequencies in the set should not be transmitted simultaneously.

The main remaining question concerns the optimum way to select the order in which frequencies in the set should be sent; i.e., should we send f_1, f_2, f_3 sequentially or f_1, f_3, f_2 sequentially so as to minimize ambiguities along the Doppler shift axis? Costas has shown in his paper that the Welch sequences constructed as described by L. R. Welch [For a history of this development, see the paper by S. W. Golomb and H. Taylor, Proceeding, of IEEE, Vol. 72, No. 9, September 1984, Constructions and Properties of Costas Arrays, pages 1143-1163.] provide an ambiguity plot for the frequency hopping burst that is close to the ideal ambiguity plot, and that is much better than that obtained for a single CW pulse or for a quantized FM burst. The answer then to the question of an optimum way to select the order in which frequencies should be transmitted in a burst (i.e., the firing order) is that the firing order should be picked to minimize velocity shift axis ambiguities. The firing order obtained through use of a Welch sequence is one method of minimizing the velocity shift axis ambiguity.

3.2 WELCH SEQUENCE GENERATION

The frequency-hopping sonar system discussed in the previous section utilizes a uniform pulse train consisting of N distinct

frequencies transmitted over N consecutive time intervals. The optimum frequency-hop patterns with respect to range-Doppler sidelobe peaks can be determined using a special class of permutation matrices known as Costas arrays. Several systematic techniques may be used to generate Costas arrays [Reference Golomb, S. W. and Taylor, H., Construction and Properties of Costas Arrays, Proceedings of the IEEE, Vol. 72, No. 9, September 1984, pages 1143-1163.]

The Costas array is an NxN permutation matrix. The N rows of the Costas array represent the N distinct frequencies $\{f_1, f_2, \ldots, f_i, \ldots, f_N\}$ while the N columns represent the N distinct time intervals $\{t_1, t_2, \ldots, t_j, \ldots, t_N\}$. The sequence of transmitted frequencies or ''firing order'' is chosen so that the ambiguity function of the returned signal and the transmitted signal shifted in time and frequency resembles the ideal ''thumbtack'' response. These optimum firing orders may be determined using a theorem by Welch involving primitive elements of finite fields. We subsequently refer to this firing order of N frequencies as a Welch-N sequence.

3.2.1 GENERATION TECHNIQUE

A Costas array may be constructed using the Welch generation technique by first choosing a finite field GF(p) where p is a prime number greater than two. A Welch-N sequence may be generated for N=p-1, N=p-2 and for certain values of N=p-3. The Costas array is constructed using a log table given a primitive root α of the finite field GF(p). The NxN array has rows numbered i=1,2,...,p-1 while the columns are numbered j=0,1,...,p-2. The (i,j) position of the array grid is filled if and only if $i=\alpha^j$. Figure 3 illustrates the Welch construction of the

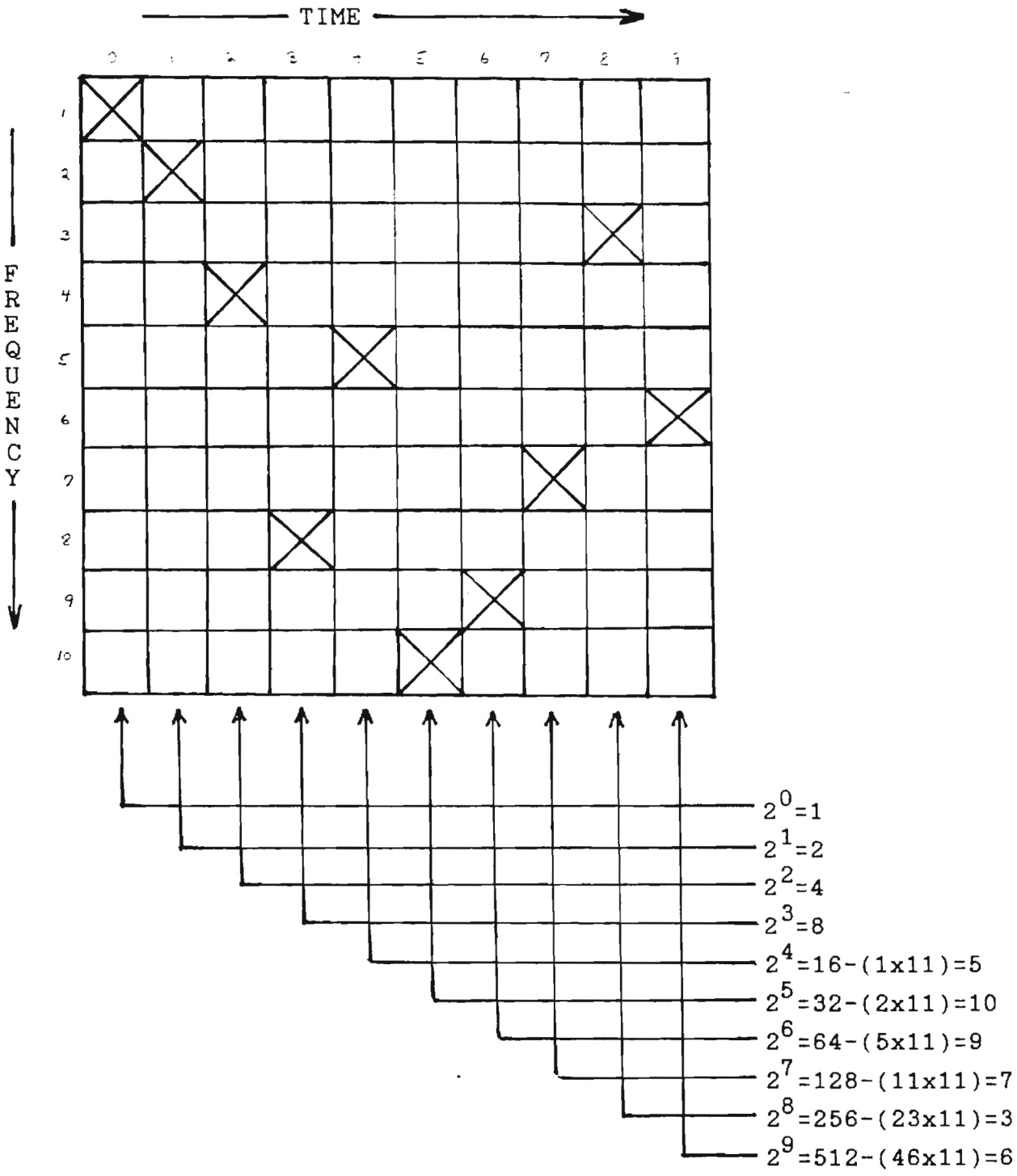

Figure 3. Welch-10 Costas Array Construction.

Costas array for p=11 and α=2. The N=p-1 firing order is obtained directly from the Costas array. The Welch-10 sequence is 1,2,4,8,5,10,9,7,3,6. The Welch-9 sequence (N=p-2) is obtained by first eliminating the first row and column from the N=p-1 array. The rows and columns of the modified array are then renumbered as before. The Welch-9 sequence is 1,3,7,4,9,8,6,2,5. As previously mentioned, the N=p-3 sequence is obtainable only under specific conditions. Namely, the number 2 must be a primitive root of GF(p). Obviously, for p=11, 2 is a primitive root. The technique for obtaining the N=p-3 sequence follows that for N=p-2 in that the first two rows and columns are eliminated from the Costas array. The resulting Welch-8 (N=p-3) sequence is 2,6,3,8,7,5,1,4.

Based on the previous discussion, the Welch construction technique is not applicable for certain choices of N. Considering values of N up to 30, the Welch construction technique does not apply for N of 7, 13, 14, 19, 20, 23, 24 and 25. Yet, other Costas array construction techniques are available for most N where the Welch construction does not apply. Systematic Costas array construction techniques are known for all N up to 50 except for N of 32, 33, 43, 48 and 49.

The Costas array shown in Figure 3 exhibits a special physical characteristic which produces low range-Doppler sidelobe peaks. If the Costas array (A) is compared with the same array shifted in time and frequency (A'), at most one coincidence will occur. Another way of stating this property is illustrated by considering all the lines which connect any two distinct entries in the array. For a Costas array, no two of these lines have the same magnitude and slope. This principle is the basis of the difference triangle approach used by Costas.

The difference triangle for the Welch-10 sequence derived previously is shown in Figure 4. The entries in the first row represent the difference between adjacent elements of the sequence. The second row represents differences between every other element. The third row is the difference between every third element and so on. If each row consists of unique values, then the corresponding array is a Costas array.

3.3.2 A WELCH SEQUENCE BEAMFORMER EXAMPLE

The uniform pulse train of the aforementioned frequency-hopping system consists of N consecutive sub-pulses each of duration T. The frequency of the sub-pulses are determined by the Welch N sequence $\{\theta_0,\theta_1,\ldots,\theta_{N-1}\}$. A simple choice of frequencies is

$$f_n = \frac{\theta_n}{T} \qquad n = 0,1,\ldots,N-1 \qquad (21)$$

where the sub-pulses range from one cycle per pulse to N cycles per pulse. By increasing each element in the Welch sequence by some positive integer K, the number of cycles per pulse may be increased while the sequence still exhibits the proper range-Doppler sidelobe behavior. The frequencies become

$$f_n = \frac{\theta_n + K}{T} \qquad n = 0,1,\ldots,N-1 \qquad (22)$$

where the sub-pulses now range from 1+K cycles per pulse to N+K cycles per pulse. The pulse train $\mu(t)$ may be described in complex envelope notation as

Difference Triangle for N = 10

L \ $\{\theta_m\}$	2	4	8	5	10	9	7	3	6	1
1	2	4	-3	5	-1	-2	-4	3	-5	
2	6	1	2	4	-3	-6	-1	-2		
3	3	6	1	2	-7	-3	-6			
4	8	5	-1	-2	-4	-8				
5	7	3	-5	1	-9					
6	5	-1	-2	-4						
7	1	2	-7							
8	4	-3								
9	-1									

FIGURE 4 WELCH-10 DIFFERENCE TRIANGLE

$$\mu(t) = \sum_{n=0}^{N-1} p_n (t-nT) \tag{23}$$

where

$$p_n(t) = \begin{cases} e^{j2\pi f_n t} & 0 \leq t \leq T \\ 0 & \text{otherwise} \end{cases} \tag{24}$$

The upper limit on the sub-pulse duration T is dictated by the required range resolution of the target. That limit is given by

$$T_{max} = \frac{2R}{c} \tag{25}$$

where R is the range resolution and c is the velocity of propagation. For a range resolution of 20 cm and a speed of sound in water of 1500 m/s, the maximum subpulse period is 267 μs.

The delay-Doppler ambiguity function is a two-dimensional correlation function in delay (time shift) and Doppler (frequency shift). The general formula for the ambiguity function is given in equation (18). The ambiguity function exhibits a symmetric relationship defined by

$$|X(-\tau,-v)| = |X(t,v)| \tag{26}$$

so that only non-negative values of time delay τ are required. The time delay τ may be defined as

$$\tau = kT + \delta \tag{27}$$

where

$$0 \leq \delta \leq T \tag{28}$$

and

$$k = 0,1,\ldots,N-1 \ . \tag{29}$$

Inserting the appropriate pulse train expressions into equation (18) yields

$$X(\tau,v) = \sum_{r=0}^{N-1-k} A + \sum_{\substack{r=0 \\ (r\geq 0)}}^{N-2-k} B \tag{30}$$

where

$$A = \frac{(T-\delta)}{NT} \operatorname{sinc}[\beta(T-\delta)] \exp\{j\pi[\beta(2kT+2rT+T+\delta)-2f_r\delta]\} \tag{31a}$$

$$\beta = f_r - f_{k+r} + v \tag{31b}$$

and

$$B = \frac{\delta}{NT} \operatorname{sinc}[\gamma\delta] \exp\{\sigma\pi[\gamma(2kT+2rT+2T+\delta)-2f_r\delta]\} \tag{32a}$$

$$\gamma = f_r - f_{k+r+1} + v \ . \qquad (32b)$$

Covering the frequency band of 50-250 kHz inclusively with sub-pulse signals that contain an integral number of cycles directly determines the specific N values which are applicable. In other words, given a minimum frequency of operation (50 kHz), choosing the minimum number of cycles per sub-pulse determines the frequency increment Δf and thus the required N. Table 3 summarizes the 13 possible N values that completely cover the 50-250 kHz band assuming a maximum sub-pulse period of 267 μs as defined by a range resolution of 20 cm. Modifying the range resolution from 20 cm to 50 cm would increase the number of possible N values from 13 to 33.

The Welch-5 sequence (N=5 entry) in Table 3 generates frequencies of 50, 100, 150, 200 and 250 kHz. The firing order determined using the Welch construction is 2,1,5,3,4. Figure 5 represents the resulting pulse train and array for this Welch-5 sequence frequency hopping signal. The ambiguity function of the Welch-5 sequence is shown in Figure 6. The ambiguity function of Figure 6 is defined in terms of normalized delay x defined by

$$x = \frac{\tau}{T} \qquad (33)$$

and normalized frequency y given by

$$y = vT \ . \qquad (34)$$

Table 3

Possible N Values for Welch-N Sequences
Which Cover the 50–250 kHz Frequency Range
With 20 cm Range Resolution

Minimum Cycles Per Pulse	T (μs)	Δf (kHz)	N
1	20	50.0	5
2	40	25.0	9
3	60	16.7	13
4	80	12.5	17
5	100	10.0	21
6	120	8.33	25
7	140	7.14	29
8	160	6.25	33
9	180	5.55	37
10	200	5.00	41
11	220	4.54	45
12	240	4.17	49
13	260	3.85	53

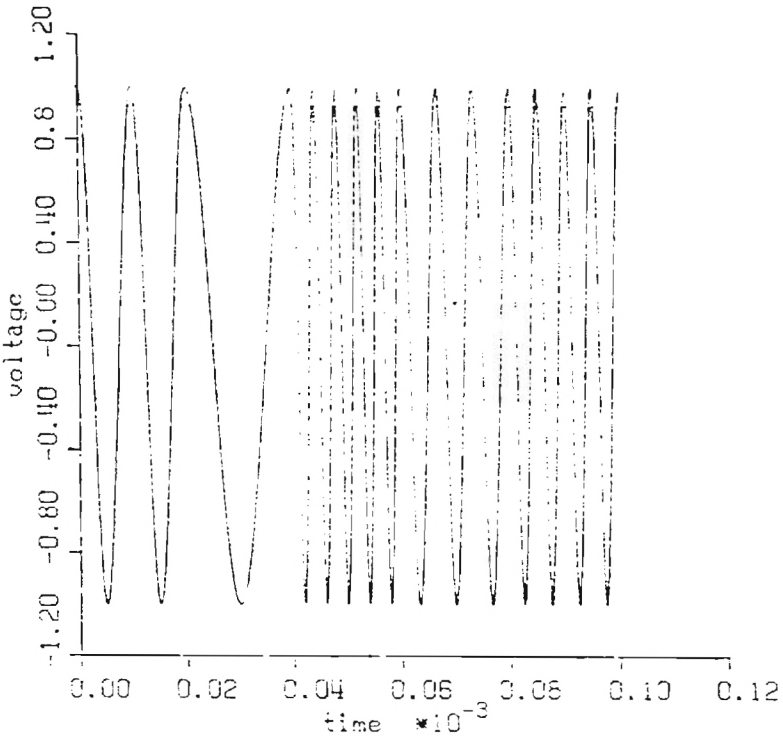

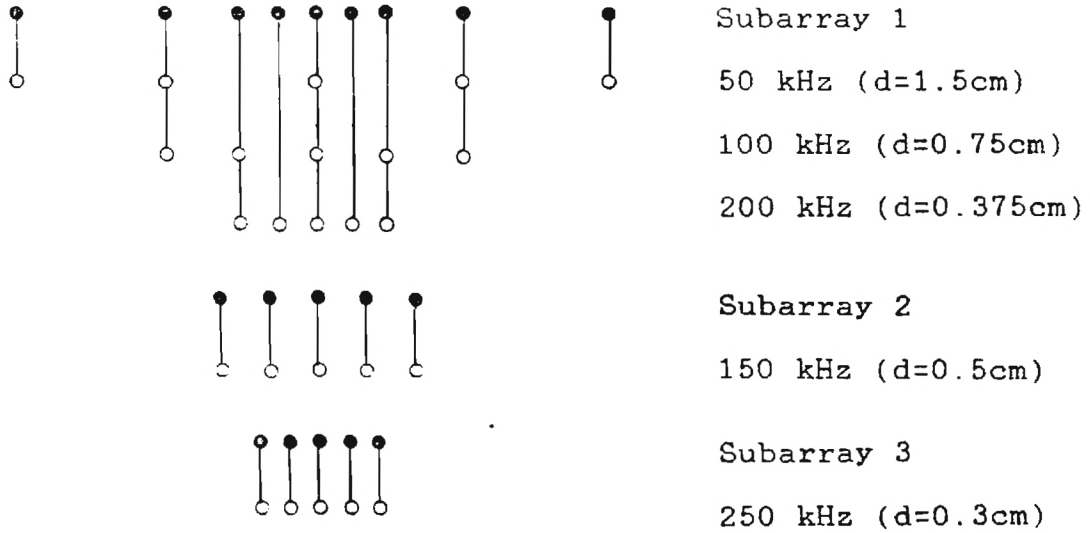

Figure 5. Welch-5 Frequency Hopping Beamformer Implementation (3 Subarrays, 5 active elements per frequency, d=λ/2 spacing).

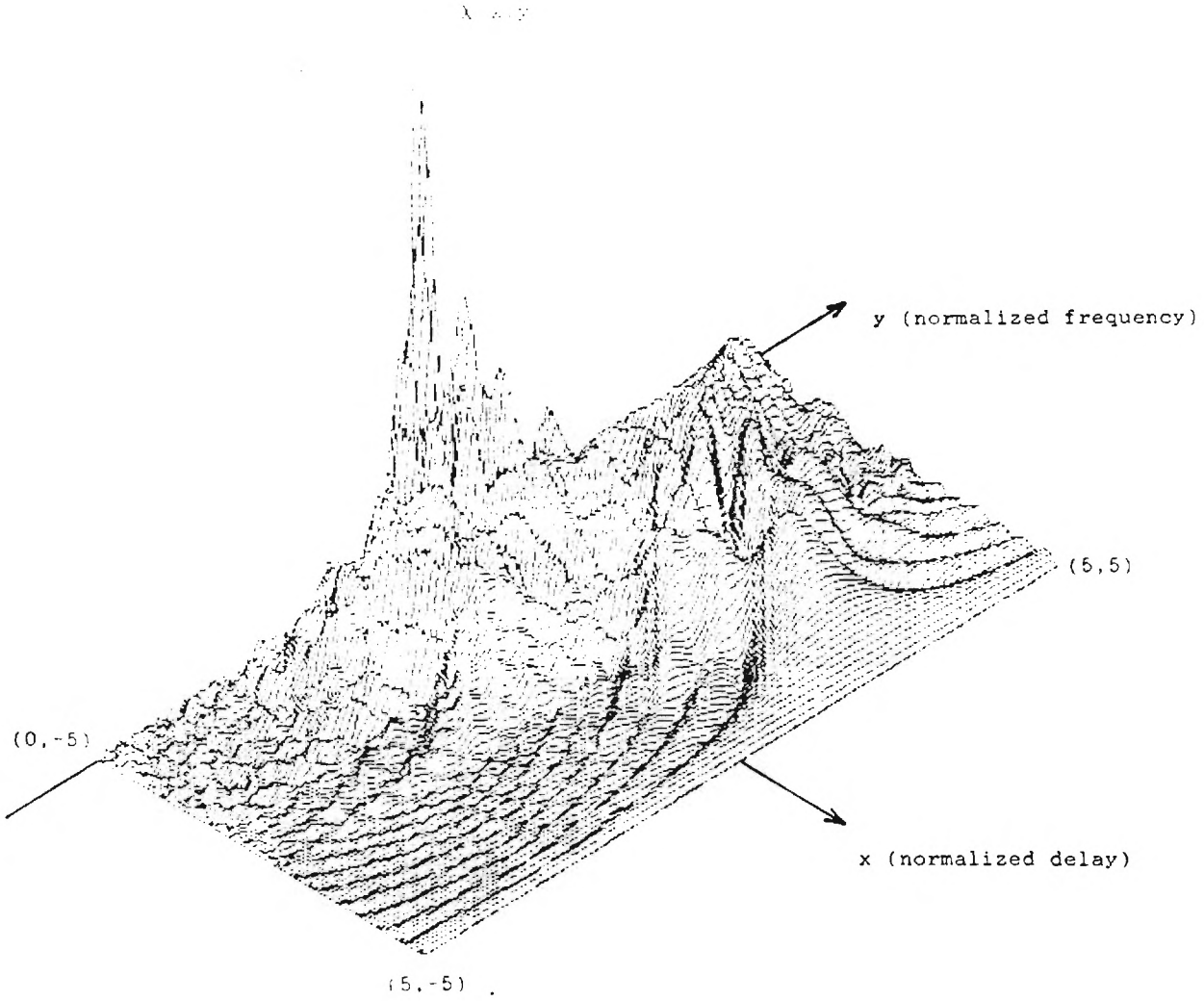

Figure 6. Welch-5 Ambiguity Function (Sequence- 2,1,5,3,4)

As expected, the Welch-5 sequence exhibits the desired range-Doppler sidelobe peak behavior in that the map approximates the ideal thumbtack diagram shown in Figure 2.

The frequency spectral content of the Welch-N sequence is also of interest. The energy spectral density of a single burst Welch-N sequence may be determined using the Fourier transform of the pulse train given by

$$F\{\mu(t)\} = U(f) = \int_{-\infty}^{\infty} \mu(t)\ e^{j2\pi ft}\ dt\ . \tag{35}$$

The energy spectral density function E(f) is related to U(f) by

$$E(f) = U(f)\ U^*(f) = |U(f)|^2\ . \tag{36}$$

For the Welch-N sequence, the energy spectral density function becomes

$$E(f) = \frac{T^2}{4} \sum_{n=0}^{N-1} \sum_{m=0}^{N-1} (-1)^{(\theta_m + \theta_n)} \cos[2\pi f(n-m)T]$$
$$\{\mathrm{sinc}(fT+\theta_m) + \mathrm{sinc}(fT-\theta_m)\}\ \{\mathrm{sinc}(fT+\theta_n) + \mathrm{sinc}(fT-\theta_n)\}\ . \tag{37}$$

The Welch-5 sequence considered previously consists of sub-pulses which contain 1, 2, 3, 4 and 5 cycles per pulse at 50, 100, 150, 200 and 250 kHz, respectively. The energy spectral density of this pulse train assuming phase coherent reception is shown in Figure 7. The energy is

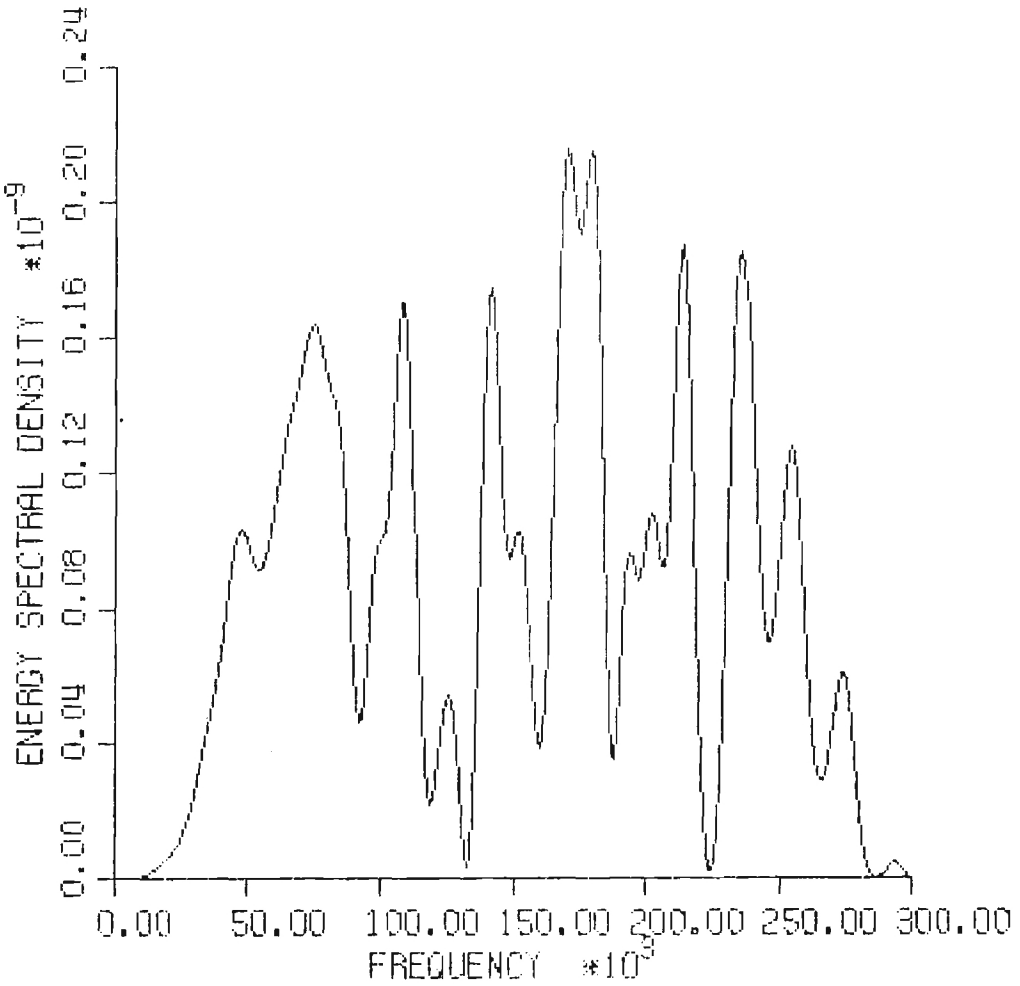

Figure 7. ESD for Welch-5 Sequence (2,1,5,3,4)

not localized at the five transmission frequencies due to the small number of cycles per pulse. The energy is ''spread'' when a small number of cycles per pulse are used due to the sinc function dependence of the energy spectral density function. By increasing the number of cycles per pulse for the Welch-5 sequence to 5, 10, 15, 20 and 25 at the respective frequencies of transmission (effectively multiplying the Welch sequence by a constant), the energy distribution is altered significantly. The energy spectral density function of the Welch-5 sequence with a minimum of 5 cycles per pulse is shown in Figure 8. Clearly, the energy of the Welch sequence with several cycles per pulse is concentrated at the transmission frequencies.

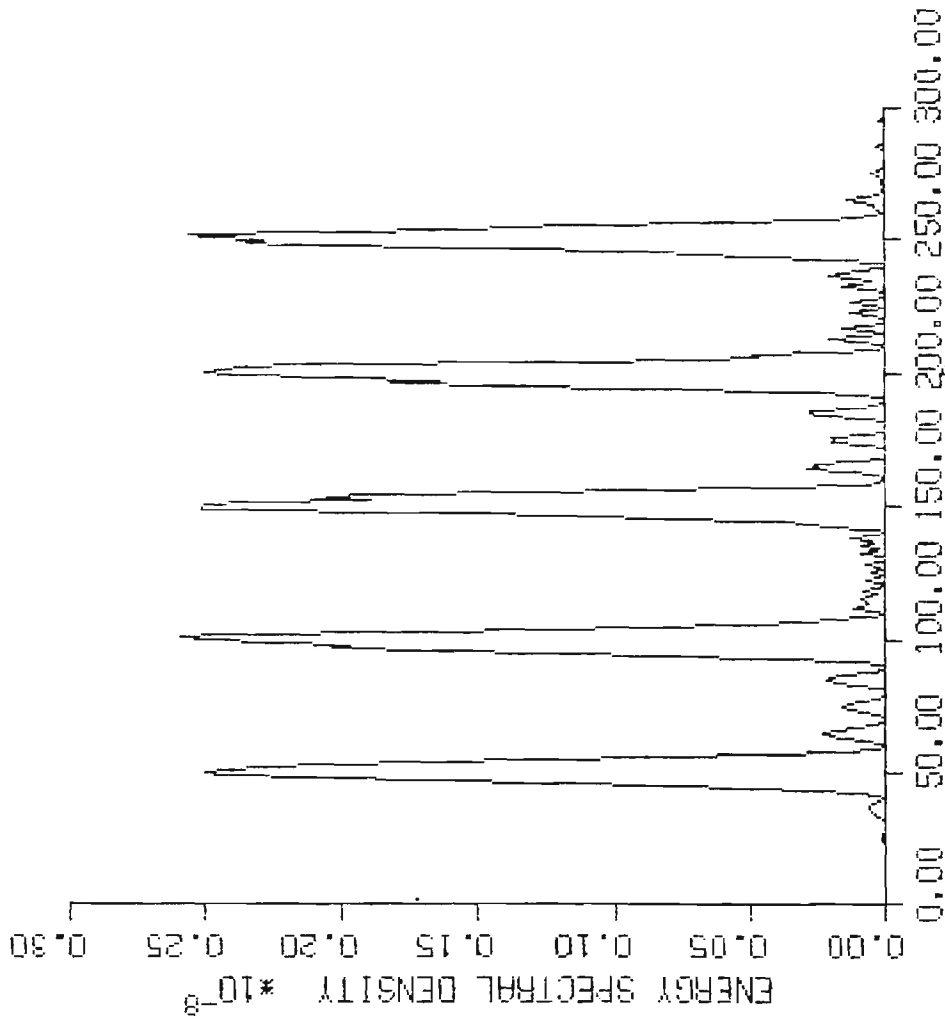

Figure 8. ESD for Welch-5 Sequence (10,5,25,15,20)

4.0 SUMMARY OF WORK TO DATE

The design of an array signal scheme which has properties lending itself to a low probability of intercept transmission has been initiated. At the same time, the array has a signal design that has good tolerance to range delay and Doppler shift of the return signal.

As an example of the technique, a Welch-5 frequency set composed of five frequencies to be used for frequency-hopping is illustrated in Figure 5. The array that would be designed to accommodate this frequency-hopping signal set is also illustrated in Figure 5 and may be observed to consist of three subarrays. Each frequency would drive five active elements in the example illustrated. The selection of the frequencies and the order in which the frequencies are chosen are also indicated in Figure 5. The ambiguity diagram of Figure 6 illustrates good range delay-Doppler shift tolerance with close to the ideal thumbtack response. This means accurate range estimation would be possible even with Doppler shifted returns.

The extension of the three subarrays to a larger number of active elements per frequency is a matter of adding elements to the array, thereby increasing the length of the arrays. The next item of consideration is that of encoding the Welch frequency subpulses with a faster code to achieve spectral spreading. The limitations on this will be set by the sensor element and transducer element Q factors.

5.0 BUDGET STATEMENT

As of December 1, 1987, there has been a total expenditure of 16,204 dollars spent out of the contract total of 44,026 dollars, leaving a balance of 28,002 dollars. There are sufficient funds remaining to finish the contract.

FREQUENCY AGILE BEAMFORMER

FINAL REPORT

31 March 1988

Contract No. E-21-J33-S1 (Ga. Tech Omnibus)
Naval Contract N61331-85-D-0025; D.O. 0033

Deliver To:

Dr. Larry Howell
Code 4230
Naval Coastal System Laboratory
Panama City, FL 32407-5000

P. Donohoe
F. Ingels
Department of Electrical Engineering
Mississippi State University
Drawer EE
Miss. State, MS 39762
601+325-3912

LIST OF TABLES

		Page
TABLE 1	INTERCEPTOR RANGE VERSUS USER RANGE, LOW SNR.....	14
TABLE 2	INTERCEPTOR RANGE VERSUS USER RANGE, HIGH SNR.....	16
TABLE 3	MASTER SEQUENCES WHICH YIELD UNIFORM COVERAGE OF THE 50 - 250 kHz BAND FOR N = 2 THROUGH 10.....	39
TABLE 4	COSTAS ARRAY GENERATED SEQUENCES WHICH COVER THE 50 - 250 kHz BAND ASSUMING A RANGE RESOLUTION OF 20 cm (T_{max} = 267 μs).....	41
TABLE 5	MINIMUM FREQUENCY SPACINGS FOR VARIOUS SUB-PULSE DURATIONS ASSUMING F_H = 250 kHz WITH v = 10 KNOTS AND v = 20 KNOTS.....	67
TABLE 6	CHARACTERISTICS OF THE SUB-ARRAYS USED TO IMPLEMENT THE DESIGN EXAMPLE (N = 17, T = 240 μs, ELEMENT Q = 2).....	73
TABLE 7	DESIGN EXAMPLE STEERED BEAM COVERAGE.....	75

LIST OF FIGURES

1. ACOUSTIC SIGNALS..... 2
2. NARROWBAND ENERGY DETECTOR RECEIVER STRUCTURE..... 3
3. MINIMUM FREQUENCY SPACING TO ACCOUNT FOR MAXIMUM DOPPLER SHIFT IN ONE DIRECTION..... 25
4. IDEAL ''THUMB TACK'' AMBIGUITY FUNCTION..... 28
5. SINGLE CW PULSE AMBIGUITY FUNCTION..... 29
6. WELCH-10 COSTAS ARRAY CONSTRUCTION ($p = 11$, $\alpha = 2$)..... 33
7. WELCH-11 DIFFERENCE TRIANGLE..... 35
8. N = 5 COSTAS ARRAY SEQUENCE (1,3,4,2,5) AMBIGUITY FUNCTION..... 45
9. N = 9 COSTAS ARRAY SEQUENCE (1,2,6,4,9,8,5,7,3) AMBIGUITY FUNCTION..... 46
10. N = 13 COSTAS ARRAY SEQUENCE (1,2,4,9,13,6,12,11,7,5,8,3,10) AMBIGUITY FUNCTION..... 47
11. N = 5 COSTAS ARRAY SEQUENCE (1,3,4,2,5) AMBIGUITY FUNCTION SIDELOBE PRESENTATION..... 48
12. N = 9 COSTAS ARRAY SEQUENCE (1,2,6,4,9,8,5,7,3) AMBIGUITY FUNCTION SIDELOBE PRESENTATION..... 49
13. N = 13 COSTAS ARRAY SEQUENCE (1,2,4,9,13,6,12,11,7,5,8,9,10) AMBIGUITY FUNCTION SIDELOBE PRESENTATION..... 50
14. FREQUENCY-HOPPED SIGNAL WITH N = 5, F_L = 50 KHZ, F_H = 250 KHZ AND FIRING ORDER OF (1,3,4,2,5)..... 51
15. BEAMFORMER/RECEIVER STRUCTURE..... 54
16. FREQUENCY RESPONSE OF THE SUB-ARRAY SENSORS IN TERMS OF THE HOPPED FREQUENCIES..... 57

LIST OF FIGURES (continued)

17. ENERGY SPECTRAL DENSITY OF AN N = 5 SEQUENCE WITH A MINIMUM OF ONE CYCLE PER SUB-PULSE (1,3,4,2,5), T = 20 μs..... 63

18. ENERGY SPECTRAL DENSITY OF AN N = 5 SEQUENCE WITH A MINIMUM OF TWO CYCLES PER SUB-PULSE (2,6,8,4,10), T = 40 μs..... 64

19. ENERGY SPECTRAL DENSITY OF AN N = 5 SEQUENCE WITH A MINIMUM OF THREE CYCLES PER SUB-PULSE (3,9,12,6,15), T = 60 μs... 65

20. ENERGY SPECTRAL DENSITY OF AN N = 5 SEQUENCE WITH A MINIMUM OF TWELVE CYCLES PER SUB-PULSE (12,36,48,24,60), T = 240 μs..... 66

21. ENERGY SPECTRAL DENSITY OF THE DESIGN EXAMPLE SIGNAL: N = 17, (12,18,30,54,45,27,48,33,60,57,51,39,15,24,42,21,36), T = 240 μs..... 69

22. SENSOR FREQUENCY RESPONSE PARAMETERS..... 70

23. AMBIGUITY FUNCTION OF THE DESIGN EXAMPLE SEQUENCE (N = 17)..... 92

24. AMBIGUITY FUNCTION SIDELOBE PRESENTATION OF THE DESIGN EXAMPLE SEQUENCE (N = 17)..... 93

A.1 BANDLIMITED, SQUARE LAW, FINITE TIME INTEGRATOR DETECTOR..... 98

TABLE OF CONTENTS

Section		Page
LIST OF TABLES		i
LIST OF FIGURES		ii
1.0	PROBABILITY OF INTERCEPT	1
1.1	SIGNAL-TO-NOISE RATIO OF ENERGY DETECTOR	1
1.2	SIGNAL POWER	5
1.3	SIGNAL-TO-NOISE RATIO VERSUS SIGNAL DETECTION OR SIGNAL INTERCEPTION	6
1.4	INTERCEPTOR RANGE VERSUS USER DETECTION RANGE	7
1.5	SIGNAL DESIGN VERSUS SONAR PARAMETERS	17
2.0	FREQUENCY HOP PATTERN	23
2.1	RANGE-VELOCITY AMBIGUITY	23
2.2	GENERATION OF SEQUENCES BASED ON COSTAS ARRAYS	31
2.2.1	THE WELCH SEQUENCE GENERATION TECHNIQUE	32
2.2.2	A WELCH SEQUENCE SIGNALLING EXAMPLE	34
3.0	PROPERTIES OF THE ARRAY, BEAMFORMER AND RECEIVER	53
3.1	RECEIVER STRUCTURE	53
3.2	BEAMFORMER AND ARRAY STRUCTURES	56
3.2.1	SUB-ARRAY SENSOR CHARACTERISTICS	56
3.2.2	SUB-ARRAY DESIGN CONCERNING THE FIELD OF VIEW COVERAGE	58
4.0	DESIGN EXAMPLE	61

TABLE OF CONTENTS (continued)

5.0 CONCLUSIONS..... 94

5.1 COMMENTS..... 94

5.2 OPERATIONAL SUGGESTIONS..... 94

6.0 REFERENCES..... 102

1.0 PROBABILITY OF INTERCEPT

1.1 SIGNAL-TO-NOISE RATIO OF ENERGY DETECTOR

The intercept range for an observer of a radiated sonar signal which is obeying spherical spreading may be estimated in terms of the detection range for the user transmitting the sonar signal. Two possible signal types are shown in Figure 1. Figure 1a illustrates a single frequency per pulse acoustic signal where each pulse contains only one frequency. Figure 1b illustrates a multiple frequency per pulse acoustic signal where each pulse contains N sub-pulses of distinct frequencies.

The type of receiver used by the interceptor is a predominant factor in the comparison of the two ranges. For this analysis a narrowband energy detector (equivalent to envelope detection) receiver, as illustrated in Figure 2, is assumed to be the basic receiver for both the user and the interceptor. If the interceptor utilizes a wideband receiver, then the performance would typically be reduced by the ratio of the bandwidth of the signal to the receiver bandwidth. If the SNR of the received signal is more than 10 dB, the performance of energy detectors (and envelope detectors) are approximately equivalent to the performance of coherent detectors. For low SNR received signals, the energy detector (and the envelope detector) operate inferior to a coherent detector. In view of these facts the analysis presented is a conservative approach.

For the receiver structure of Figure 2, the output signal-to-noise ratio, SNR, for any channel may be computed assuming a rectangular filter of width β, noise power spectral density of N_o and signal power P_s. At the output of the filter, the signal-to-noise ratio is

$$SNR_F = \frac{S_s(f)\ |H(f)|^2}{S_n(f)\ |H(f)|^2} = \frac{P_s}{N_o \beta} \qquad (1)$$

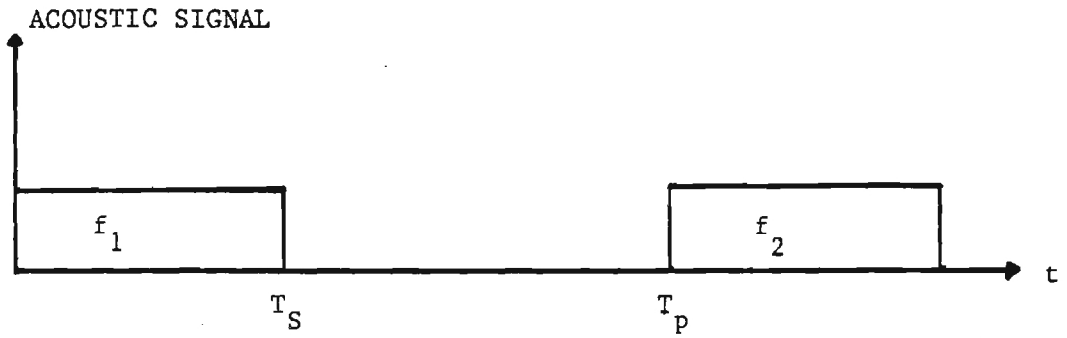

a) Single Frequency Per Pulse Acoustic Signal

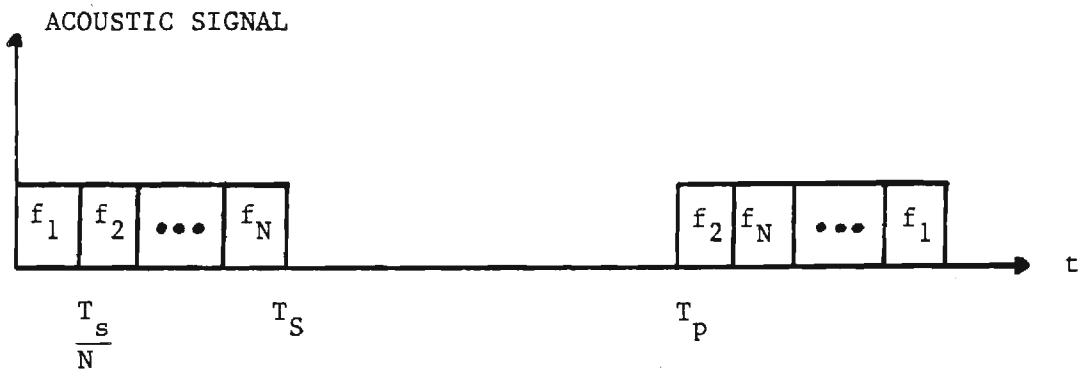

b) Multiple Frequency Per Pulse (Multiple Sub-Pulse) Acoustic Signal

Figure 1 Acoustic Signals

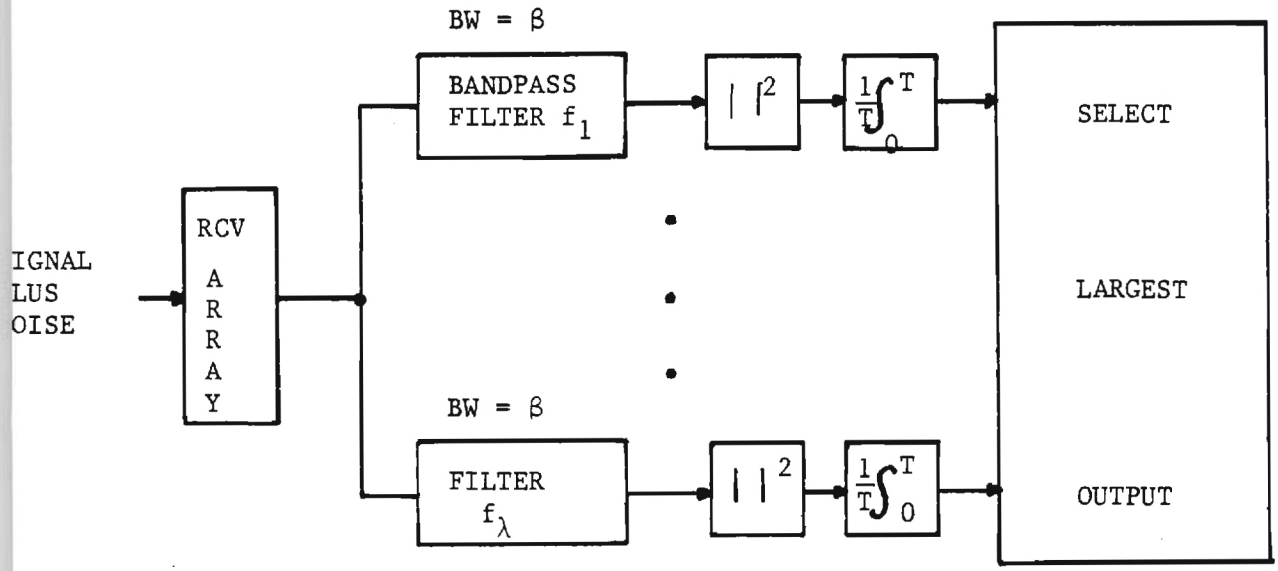

a) Typical Narrowband Receiver, Single Pulse Single Frequency

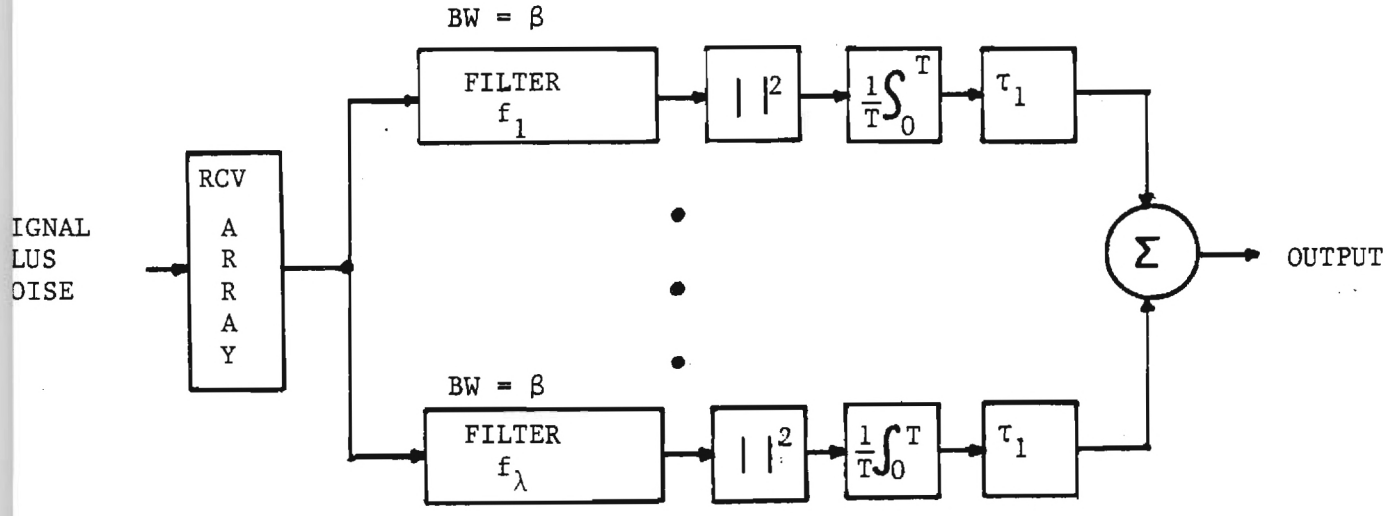

b) Narrowband Receiver, Multiple Pulse, Multiple Frequency Sequence

Figure 2 NARROWBAND ENERGY DETECTOR
RECEIVER STRUCTURE

The signal-to-noise ratio out of the square-law device is equal to the square of the signal-to-noise ratio of the input if the double frequency components are assumed removed by the detector [1]. If we note the integrator is actually equivalent to a low-pass filter and that the finite time integrator has a normalized impulse response of $h(t) = \frac{1}{T}\Pi(t/T)$, the signal-to-noise ratio of the output of the integrator (assuming a low SNR input) is [2]

$$SNR_{channel} = T\beta\left[\frac{P_s}{N_o\beta}\right]^2 = \frac{T}{\beta}\left[\frac{P_s}{N_o}\right]^2 \quad . \quad \underline{\text{LOW SNR INPUT}} \qquad (2)$$

Equation (2) will be the reference benchmark for analyzing the interception detection range versus the user detection range for low SNR received signals.

In general the signal-to-noise at the output of the squaring circuit of an energy detector (also equivalent to envelope detectors) is [2]

$$SNR_{Channel} = \frac{(SNR_I)^2}{1 + 2SNR_I} \quad . \qquad (3)$$

Thus for values of input SNR of about 10 or more the output SNR is effectively one half of the input SNR, whereas for a coherent detector the output SNR is effectively twice the input SNR [reference 3 or 4]. For high SNR inputs the following equation will be the benchmark for analyzing the interception detection range versus the user detection range (assuming a filtered finite time integrator following the output of the squaring circuit of an energy detector):

$$SNR_{channel} = \frac{T\beta}{2} SNR_I = \frac{T\beta}{2}\left[\frac{P_s}{N_o\beta}\right] \quad . \quad \underline{\text{HIGH SNR INPUT}} \qquad (4)$$

Before proceeding, it is necessary to determine the relationship for the signal power, P_s, versus the spherical spreading range factor, R, and the various array and target parameters.

1.2 SIGNAL POWER

For spherical wave spreading the acoustic intensity in watts per unit area, I, is related to the distance from the sound source, R, the speed of propagation, c, the root mean square amplitude of the real pressure waveform, P_{rms}, at R = 1 and the density, ρ, of the medium (water) by [5]

$$I = \frac{1}{R^2}\left[\frac{P^2_{rms}}{\rho c}\right] \quad . \qquad (5)$$

The total power at range R for an omniradiating source (assuming a lossless medium) is

$$P = 4\pi R^2 I \qquad (6)$$

If directional sound projectors are used, then the directivity factor (gain along the main axis) must be factored in to determine the power at a range R.

The power reflected at a target range, R_U, from the user is

$$P_{\substack{\text{target}\\ \text{reflection}}} = \frac{1}{R_U^2}\left[\frac{P^2_{rms}}{\rho c}\right] D_S\, A_T\, RF_T = P_{TR} \qquad (7)$$

where A_T is the target equivalent area, RF_T is the target reflection coefficient and D_S is the source directivity factor. The power received by the user, P_U, as a reflected echo is thus,

$$P_U = P_{TR} \frac{1}{R_U^2} A_U = \left[\frac{P^2_{rms}}{\rho c}\right] \frac{D_S A_T A_U RF_T}{R_U^4} \tag{8}$$

where A_U is the effective receiver array area. For an interceptor the power received, P_I, at range R_I from the user source is

$$P_I = \left[\frac{P^2_{rms}}{\rho c}\right] \frac{D_S A_I}{R_I^2} \tag{9}$$

where A_I is the effective intercepter array area.

1.3 SIGNAL-TO-NOISE RATIO VERSUS SIGNAL DETECTION OR SIGNAL INTERCEPTION

The signal-to-noise ratio per channel of the receiver for the user (detection) and the interceptor is respectively:

$$SNR_U = \frac{T_U}{\beta_U}\left[\left[\frac{P^2_{rms}}{\rho c}\right] \frac{D_S A_T A_U RF_T}{R_U^4 N_o}\right]^2 \quad \underline{\text{LOW SNR INPUT}} \tag{10}$$

and

$$SNR_I = \frac{T_I}{\beta_I}\left[\left[\frac{P^2_{rms}}{\rho c}\right] \frac{D_S A_I}{N_o R_I^2}\right]^2 \quad \underline{\text{LOW SNR INPUT}} \tag{11}$$

Equations (10) and (11) do not reflect possible parameters of the signal structure versus the receiver bandwidths and integration times. These parameters are illustrated in Figure 2.

The ratio of signal time, T_S, to integrator time T_U or T_I must be included in Equations (10) and (11) for SNR. This effect can be illustrated for the normalized finite time integrator by inspecting the integral form as

$$\frac{1}{T}\int_0^T [U(t) - U(t-T_S)]P_S dt = \frac{P_S T_S}{T} \quad , \quad T \geq T_S \quad . \tag{12}$$

The ratio T_S to T represents the penalty incurred by integrating over a period T longer than the signal period, T_S. The integrator output is maximized for the case where the integrate time T is matched to the signal time T_S. This effect can be included in Equations (10) and (11) as

$$SNR_U = \frac{T_U}{\beta_U}\left[\left[\frac{P^2_{rms}}{\rho c}\right] \frac{D_S A_T A_U RF_T}{R_U^4 N_o} \frac{T_S}{T_U}\right]^2 \qquad \frac{\text{LOW SNR INPUT}}{T_U \geq T_S} \tag{13}$$

and

$$SNR_I = \frac{T_I}{\beta_I}\left[\left[\frac{P^2_{rms}}{\rho c}\right] \frac{D_S A_I}{N_o R_I^2} \frac{T_S}{T_I}\right]^2 \qquad \frac{\text{LOW SNR INPUT}}{T_I \geq T_S} \quad . \tag{14}$$

1.4 INTERCEPTER RANGE VERSUS USER DETECTION RANGE

Using Equations (13) and (14), the relationship for the interceptor range may be solved in terms of the user detection range and the receiver parameters. If it is assumed that both user and interceptor require the same SNR to detect a signal, then equating Equations (13) and (14) and

solving for R_I (assuming the intercepter is on the main directivity axis of the user source projector) yields

$$R_I = \left[\frac{T_I \beta_U}{T_U \beta_I}\right]^{1/4} \left[A_I \frac{T_S}{T_I} \cdot \frac{T_U}{T_S} \frac{R_U^4}{RF_T A_U A_T}\right]^{1/2} \quad \underline{\text{LOW SNR INPUT}} \quad (15)$$

$$R_I = \left[\frac{T_U \beta_U}{T_I \beta_I}\right]^{1/4} K R_U^2 \quad \underline{\text{LOW SNR INPUT}} \quad (16)$$

where K relates the various target and array parameters.

The user knows the parameters of the signal and hence can match T_U and β_U to the signal to achieve the optimum time bandwidth product, given by

$$T_U = T_S \quad , \quad (17)$$

$$\beta_U = \frac{1}{T_S} \quad , \quad (18)$$

or

$$T_U \beta_U = 1.0 \quad . \quad (19)$$

The interceptor will not know the signal structure and hence will not be able to optimize the integration time and the bandwidth. As a result, the interception range for the signal structure of Figure 1a and receiver structure of Figure 2a for both user and integrator is:

$$R_I = K R_U^2 \left[\frac{\beta_U T_U}{T_I \beta_I}\right]^{1/4} \quad \underline{\text{INTERCEPTOR RANGE SINGLE PULSE}} \quad \underline{\text{LOW SNR INPUT}} \quad (20)$$

For a signal structure as in Figure 1b, the SNR for the user will be the same as in the previous case when integrated and summed over N pulses as in the Figure 1b receiver structure. Modifying Equation (13) to reflect the smaller pulse time, we have after summing N sub-pulses as in Figure 1b:

$$\underset{\text{LOW SNR INPUT}}{SNR_U\ (N\ \text{Sub-pulses})} = N\left[\frac{(T_S/N)^2\ T_U}{\beta_U T_U^{\,2}}\right]\left[\left[\frac{P^2_{rms}}{\rho c}\right]\ \frac{D_S\ A_T\ A_U\ RF_T}{R_U^{\,4}\ N_o}\right]^2 \quad . \quad (21)$$

The interceptor SNR will be affected by the lower energy due to the smaller pulse time and inability to properly delay and sum the various sub-pulses. The interceptor will see the energy of one sub-pulse averaged over a much longer time than the sub-pulse. If in fact the interceptor is covering the frequency band, the interceptor will see very little difference in the various outputs of a receiver structured as in Figure 2a and will also be less likely to detect the signal over the noise. The interceptor SNR is from modification of Equation (13),

$$\underset{\text{LOW SNR INPUT}}{SNR_I\ (N\ \text{Sub-pulses})} = \frac{(T_S/N)^2\ T_I}{\beta_I T_I^{\,2}}\left[\left[\frac{P^2_{rms}}{\rho c}\right]\ \frac{D_S A_I}{N_o R_I^{\,2}}\right]^2 \quad . \quad (22)$$

Notice that SNR_I (N sub-pulses) does not include the multiplying factor of N due to the interceptor's inability to sum the signals in time. The interceptor detection range for the N sub-pulse signal is,

$$R_I = \left[\frac{(T_S/N)^2\ T_I}{\beta_I T_I^{\,2} N}\right]^{1/4}\left[\frac{\beta_U T_U^{\,2}}{(T_S/N)^2 T_U}\right]^{1/4}\left[\frac{D_S A_I}{D_S A_T A_U RF_T}\right]^{1/2} R_U^{\,2} \quad (23)$$

$$R_I = \left[\frac{\beta_U T_U}{\beta_I T_I N}\right]^{1/4} K R_U^2 \quad \begin{array}{l}\underline{\text{INTERCEPTOR}}\\ \underline{\text{RANGE}}\\ \underline{\text{MULTIPLE FREQUENCY}}\\ \underline{\text{N SUB-PULSES}}\end{array} \quad . \quad \underline{\text{LOW SNR INPUT}} \quad (24)$$

If the sub-pulses are encoded with a pseudo random sequence, such as a Barker sequence, the energy density is reduced for both interceptor and user. However, the user can utilize the knowledge of the spreading code to despread the received signal and gain all of the signal energy. The interceptor, on the other hand, will not have this capability and will suffer a loss of energy equal to the ratio of the unspread to spread bandwidth termed the spreading factor, SF.

Equation (22) modified to reflect spreading is

$$\underline{\text{SNR}_I \text{ (N Sub-pulses, Spread)}} = \frac{(T_S/N)^2 T_I}{\beta_I T_I^2} \left[\left[\frac{P^2_{rms}}{\rho c}\right] \frac{D_S A_I \beta_I}{N_o R_I^2 \beta_S}\right]^2 \quad (25)$$
$$\underline{\text{LOW SNR INPUT}}$$

and the interceptor range for the spread N sub-pulse signal is,

$$R_I = \left[\frac{B_U T_U}{\beta_I T_I N SF^2}\right]^{1/4} K R_U^2 \quad \begin{array}{l}\underline{\text{INTERCEPTOR RANGE}}\\ \underline{\text{MULTIPLE FREQUENCY}}\\ \underline{\text{N SUB-PULSES}}\\ \underline{\text{SPREADING FACTOR, SF}}\\ \underline{\text{LOW SNR INPUT}}\end{array} \quad . \quad (26)$$

The constant K in Equations (20), (24) and (26) relate the parameters of array gain and target.

$$K = \left[\frac{D_S A_I}{D_S A_T A_U R F_T}\right]^{1/2} \quad (27)$$

where D_S is the directivity index or radiation pattern gain of the user's acoustic projector, A_I is the interceptor receiver array gain factor, A_T is the target effective area, A_U the user receiver array gain and RF_T is the target reflection coefficient.

These parameters are unique to each system. For illustrative purposes, the parameters are estimated for a possible system environment. Equation (8) relates the power received by the user as a reflected echo and is

$$P_U = \left[\frac{P^2_{rms}}{\rho c}\right] \frac{D_S A_T A_U RF_T}{R_U^4} = \frac{I_o D_S A_T A_U RF_T}{R_U^4} \quad . \tag{28}$$

In sonar work the term received echo level, EL, is generally used. This term is the acoustic intensity of the echo at the receiver location and for a co-located transducer receiver (monostatic system) it is (spherical spreading assumed)

$$I_R = \frac{I_r}{R_U^2} = t_s \left[\frac{I_o}{R_U^4}\right] \tag{29}$$

where I_o is the source intensity measured at 1 meter from the source, R_U is the distance or range from the source to the target, and t_s is the target strength. The target strength, t_s, is defined as the ratio of the reflected intensity, I_r, in the direction of the receiver, measured 1 meter from the effective target center, to the incident intensity. Thus

$$t_s = \frac{I_r}{I_i} = \text{TS in db} \quad . \tag{30}$$

In decibels (monostatic system) Equation (29) is

$$EL = SL + TS - 2TL \tag{31}$$

where

$$TS = 10Log_{10}\left[\frac{I_r}{I_i}\right] = 10Log_{10}\left[\frac{I_r}{I_o} R_U^2\right] \tag{32}$$

$$TL = 20Log_{10}\left[\frac{R}{R_{REF}}\right] = \text{one way spreading loss} \tag{33}$$

and

$$SL = 10Log_{10}\left[\frac{I(1\ meter)}{I_{REF}}\right] = 170.77dB + 10Log_{10}P \tag{34}$$

when using meters and micropascal units.

Equation (28) contains the same basic terms as Equation (31) and may be written as

$$\frac{I_O D_S A_T A_U RF_T}{R_U^4} = I_R D_S A_U RF_T A_T = I_R D_S A_U TS \quad . \tag{35}$$

Thus

$$TS = A_T RF_T \quad . \tag{36}$$

For a perfect rigid sphere, A_T, the effective area is $a^2/4$ and RF_T, the reflection coefficient is assumed to be one [6].

The term D_S in Equation (28) is the directivity index, DI (roughly the ratio of the noise gain of a receiving array to the gain of an omnidirectional receiver element). The term A_U is the effective receiver array gain and is equivalent to the directivity index for the receiver array, DI_U. Thus, Equation (27) for K may be written as

$$2K(dB) = DI_I - DI_U - TS \quad . \tag{37}$$

For a system environment where the user is receiving with a 50-wavelength line array of half wavelength spaced elements, the directivity index is approximately N = 100. Assuming the interceptor uses an omnidirectional receiving element, the directivity index is 1. For an obstacle of the shape of a typical mine, the beam aspect target strength is approximately 10 dB (for comparison target strengths of seamounts vary from 30 to 60 dB and submarines vary from 10 to 25 dB [7]). For this assumed system environment, the parameter K is

$$K = \frac{1}{2}[0 - 10Log_{10}(100) - TS] = -15 \text{ dB} = .0316 \quad . \tag{38}$$

Table 1.0 illustrates the interceptor range as a function of the parameters K (as estimated in Equation (38)) and the energy receiver processor parameters for low received SNR signals for both the user and the interceptor. The data in Table 1.0 assumes the interceptor is an end on submarine target and is located on the main directivity axis of the user's source projector. This likelihood is reduced as the directivity index of the source projector increases.

TABLE 1.0

K assumed to be -15 dB = .0316 as determined in text and Equation 38. LOW SNR ASSUMED.

User receiver is assumed to be optimized with $\beta_U T_U = 1.0$.

Interceptor receiver is assumed to have non-optimized parameters with $\beta_I T_I = 10.0$. (Receiver could be set up for wideband and short integration period or vice versa or in the middle ground.)

R_U is the user maximum detection range.

SIGNAL STRUCTURE	INTERCEPTION RANGE VERSUS USER RANGE ASSUMING INTERCEPTOR ON MAIN DZ AXIS OF USER SOURCE	INTERCEPTION RANGE FOR R_U = 100 METERS ASSUMING INTERCEPTOR ON MAIN DI AXIS OF USER SOURCE	INTERCEPTION RANGE FOR R_U = 300 METERS ASSUMING INTERCEPTOR ON MAIN DI AXIS OF USER SOURCE
Single Frequency, Single Pulse (Equation 16)	$R_I = K\left[\frac{T_U\beta_U}{T_I\beta_I}\right]^{1/4} R_U^2 = (.0316)\left[\left(\frac{1}{10}\right)\right]^{1/4} R_U^2$	R_I = 177.7 km	R_I = 1.6 km
Multiple Freq., N Sub-pulses (Equation 24)	$R_I = K\left[\frac{T_U\beta_U}{T_I\beta_I N}\right]^{1/4} R_U^2 = \frac{.01777}{(N)^{1/4}} R_U^2$	For N = 5 Sub-pulses R_I = 118.8 m	For N = 5 Sub-pulses R_I = 1070 m
		For N = 13 Sub-pulses R_I = 93.6 m	For N = 13 Sub-pulses R_I = 843 m
		For N = 17 Sub-pulses R_I = 87.5 m	For N = 17 Sub-pulses R_I = 788 m
Multiple Freq., N Sub-pulses, Spreading Factor= SF, (Equation 26)	$R_I = K\left[\frac{T_U\beta_U}{T_I\beta_I N\ SF^2}\right]^{1/4} R_U^2 = \frac{.01777}{(N(SF)^2)^{1/4}} R_U^2$	For N = 5 Sub-pulses, SF=5 R_I = 53 m	For N = 5 Sub-pulses, SF=5 R_I = 478 m
		For N = 5 Sub-pulses, SF=10 R_I = 37.5 m	For N = 5 Sub-pulses, SF=10 R_I = 337 m
		For N = 13 Sub-pulses, SF=6 R_I = 38.2 m	For N = 13 Sub-pulses, SF=6 R_I = 344 m
		For N = 13 Sub-pulses, SF=12 R_I = 27 m	For N = 13 Sub-pulses, SF=12 R_I = 243
		For N = 17 Sub-pulses, SF=12 R_I = 25.3 m	For N = 17 Sub-pulses, SF=12 R_I = 227 m

Using the equations for the high SNR case derived in Appendix 1, the interception range versus user range for the high SNR input situations are:

SINGLE PULSE FREQUENCY

$$R_I = \sqrt{\frac{T_U \beta_U}{T_I \beta_I}} \; K \; R_U^2 \quad , \text{ HIGH SNR} \tag{39}$$

MULTIPLE FREQUENCY, N SUB-PULSES

$$R_I = \sqrt{\frac{T_U \beta_U}{T_I \beta_I \; N}} \; K \; R_U^2 \quad , \text{ HIGH SNR} \tag{40}$$

MULTIPLE FREQUENCY, N SUB-PULSES SPREADING FACTOR, SF

$$R_I = \sqrt{\frac{T_U \beta_U}{T_I \beta_I \; N \; (SF)}} \; K \; R_U^2 \quad . \text{ HIGH SNR} \tag{41}$$

Table 2.0 illustrates the interceptor range as a function of the parameters K as estimated in Equation (38) and the energy receiver processor parameters for the high SNR signals for both the user and the interceptor. Again, it is assumed the interceptor is an end on submarine target and is located on the main directivity axis of the user's source projector.

The data in Tables 1.0 and 2.0 indicate that for the system environment assumed, it is feasible for close-in ranges (less than 300 meters) to reduce the range of interception to be equal to or less than that of the user's detection range. It should be noted that, unless the interceptor is fortunate, the probability is low that the interceptor is both on the main directivity axis of the sound projector and simultaneously has a fairly good match of receiver integration time and bandwidth. Thus, it is unlikely that the interceptor's detection range will be as good as indicated in Table 1.0 and Table 2.0.

TABLE 2.0

K assumed to be -15 dB = .0316 as determined in text and Equation 38. HIGH SNR ASSUMED.

User receiver is assumed to be optimized with $\beta_U T_U = 1.0$ and $T_U = T_S$ and $\beta_U = 1/T_S$.

Interceptor receiver is assumed to have non-optimized parameters with $\beta_I T_I = 10.0$, (Receiver could be set up for wideband and short integration period or vice versa or in the middle ground.), $T_I = 5T_S$ and $\beta_I = 2\beta_U$.

R_U is the user maximum detection range.

SIGNAL STRUCTURE	INTERCEPTION RANGE VERSUS USER RANGE ASSUMING INTERCEPTOR ON MAIN DZ AXIS OF USER SOURCE	INTERCEPTION RANGE FOR R_U = 100 METERS ASSUMING INTERCEPTOR ON MAIN DI AXIS OF USER SOURCE	INTERCEPTION RANGE FOR R_U = 300 METERS ASSUMING INTERCEPTOR ON MAIN DI AXIS OF USER SOURCE
Single Frequency, Single Pulse (Equation 39)	$R_I = K\sqrt{\frac{T_U\beta_U}{T_I\beta_I}}\ R_U^2$	R_I = 100 m	R_I = 900 m
Multiple Freq., N Sub-pulses (Equation 40)	$R_I = K\sqrt{\frac{T_U\beta_U}{T_I\beta_I\ N}}\ R_U^2$	For N = 5 Sub-pulses R_I = 45 m	For N = 5 Sub-pulses R_I = 403 m
		For N = 13 Sub-pulses R_I = 28 m	For N = 13 Sub-pulses R_I = 250 m
		For N = 17 Sub-pulses R_I = 24 m	For N = 17 Sub-pulses R_I = 218 m
Multiple Freq., N Sub-pulses, Spreading Factor= SF, (Equation 41)	$R_I = K\sqrt{\frac{T_U\beta_U}{T_I\beta_I\ N\ (SF)}}\ R_U^2$	For N = 5 Sub-pulses, SF=5 R_I = 20 m	For N = 5 Sub-pulses, SF=5 R_I = 180 m
		For N = 5 Sub-pulses, SF=10 R_I = 14 m	For N = 5 Sub-pulses, SF=10 R_I = 129 m
		For N = 13 Sub-pulses, SF=6 R_I = 11 m	For N = 13 Sub-pulses, SF=6 R_I = 102 m
		For N = 13 Sub-pulses, SF=12 R_I = 8 m	For N = 13 Sub-pulses, SF=12 R_I = 72 m
		For N = 17 Sub-pulses, SF=12 R_I = 7 m	For N = 17 Sub-pulses, SF=12 R_I = 63 m

1.5 SIGNAL DESIGN VERSUS SONAR PARAMETERS

Equations (20), (24), (26) and (39), (40), (41) and Tables 1.0 and 2.0 illustrate the relative benefits of using multiple frequency sub-pulses within a master pulse (Figure 1b) and also using a spectral spreading factor. The construction of the multiple frequency sub-pulses may be done in a variety of ways. Factors for consideration in such a design are:

1) What is the best frequency hopping sequence to use from a range/Doppler ambiguity point of view?
2) What are reasonable bandwidth spreading factors that can be obtained from state-of-the-art acoustic transmitter and receiver sensors?
3) What type of wide frequency band constant beamwidth arrays could be designed with the above techniques?
4) What are the tradeoffs for range resolution and acoustic sensor Q versus the number of sub-pulses, N, and the spreading factor, SF?

The relationship between the signal waveform of Figure 1b and the sonar range resolution is a tradeoff parameter that must be considered. To signal with N sub-pulses within a master pulse is to allow a range resolution determined by T_S/N. The basic range resolution of the single frequency pulse of Figure 1, which is T_S seconds long, is

$$RR = \text{Range Resolution} = \frac{c\ T_S}{2} \quad . \tag{42}$$

For a single pulse and a desired range resolution of 20 cm the maximum value T_S can take on is 266.6 microseconds.

When signalling with sub-pulses, the range resolution is still determined by the minimum identifiable feature which is T_S/N. Thus the

longest sub-pulse that can be utilized is determined by the desired range resolution and this pulse length is

$$T_{SP} = T_{\substack{\text{SUB-PULSE} \\ \text{MAX}}} = \frac{2(RR)}{c} \quad . \tag{43}$$

At this point the next parameter which should be considered is the allowable bandwidth versus frequency spacing and the number of sub-pulses, N. The desired operating frequency band is determined by the upper and lower frequencies. Thus if the sonar is desired to operate over a wide frequency range with discrete frequencies, the spacing between frequencies is equal to

$$\Delta f = \frac{F_H - F_L}{N - 1} \quad . \tag{44}$$

The minimum useable sub-pulse width is determined by the number of cycles of the frequency being transmitted. Thus a single cycle of the lowest frequency in the frequency range will determine the minimum sub-pulse width or,

$$\frac{n}{F_L} \leq T_{SP} \leq \frac{2(RR)}{c} \quad , \tag{45}$$

where the parameter n is the number of cycles per sub-pulse of the frequency F_L.

For N sub-pulses with n cycles in the sub-pulse of lowest frequency, F_L, the total length of the master ping pulse, T_S, is

$$T_S = N(\frac{n}{F_L}) \quad . \tag{46}$$

The minimum acoustic sensor Q required is related to the frequency being transmitted by a sub-pulse and to the bandwidth required by the sub-pulse width T_{SP}. If the bandwidth (BW) utilized is chosen as twice the reciprocal of the sub-pulse width, then approximately 90% of the pulse energy is contained in this bandwidth. (This energy is then reduced somewhat by the acoustic sensor bandwidth as the pulse is transmitted).

The factor Q is defined as

$$Q = \frac{F_o}{BW} \tag{47}$$

where F_o is the center frequency and hence the minimum Q required will be determined by sub-pulses transmitting at frequency F_L and the number of cycles contained in that sub-pulse, n:

$$Q_{minimum} = \frac{F_L}{BW} = \frac{F_L}{2/T_{SP}} = \frac{F_L\, n}{2\, F_L} = \frac{n}{2} \quad . \tag{48}$$

Thus, for F_L = 50 KHz and n cycles per 50 KHz sub-pulse, the Q required is:

n	Q required
1	0.5
2	1.0
3	1.5
4	2.0

A minimum Q of 2.0 has been specified as the lowest Q which can be constructed for deployable equipment.

Since T_{SP} cannot exceed the length bounded by range resolution, as noted in Equation (45), the upper bound on the number of carrier cycles per sub-pulse, n, is

$$n \leq \frac{2(RR)\ F_L}{c} \tag{49}$$

and if Q is lower bounded by 2, then n would be lower bounded by 4 and hence

$$2\ Q_{min} \leq n \leq \frac{2(RR)}{c} \quad . \tag{50}$$

The spreading factor, SF, is upper bounded by n

$$SF \leq n \quad . \tag{51}$$

The bandwidth for any sensor element cannot exceed the spacing between frequencies, ΔF, which is determined by N, the number of sub-pulses to be used in the frequency band F_L to F_H (this does not consider the additional spacing necessary to accommodate Doppler shift). Thus

$$BW \leq \frac{F_H - F_L}{N - 1} = \Delta F \quad . \tag{52}$$

A simplified procedure for design of the master pulse structure may now be outlined as (this simplified procedure does not include Doppler effects):

1) Set the desired operating parameters:

Range Resolution, F_H, F_L, Q_{min}

2) Pick a desired number of sub-pulses, N and calculate ΔF

$$\Delta F = \frac{F_H - F_L}{N - 1}$$

3) Calculate the bounds on the number of cycles per sub-pulse by

$$\frac{2F_L}{\Delta F} < n < \frac{2(RR)F_L}{c}$$

and $n > 2\, Q_{min}$

4) Note $SF_{max} = n_{max}$.

For example, for the following parameters

Range Resolution = 20 cm, F_H = 250 KHz, F_L = 50 KHz, Q_{min} = 2.0.

If N is selected as 21, then

$$\Delta F = \frac{200\ KHz}{20} = 10\ KHz$$

and $10\, n < 13.33$

and $n > 4$ is satisfied.

At this point the type of frequency hopping sequence to be used must be chosen. If a standard frequency hopping scheme is utilized, then n could vary from 10 to 13. However, such a choice could likely be sensitive to Doppler shifts of the return pulses. If a Welch sequence is used to

determine the choice of frequencies, then the bounds on n are restricted. As will be determined in the following sections, to achieve maximum Doppler tolerance, n will be restricted to 10 for the above system designs. Thus the spreading factor will be upper bounded by 10, and the system design will allow (assuming no Doppler shift)

$$N = 21 \quad \text{and} \quad SF = 10 \quad .$$

The next sections of the report will describe a sequence for selecting the frequencies to be transmitted. This sequence will provide a signal highly tolerant to Doppler shifts. A variety of allowable choices of N and SF will be given and the beamformer structure detailed. Other factors of importance, such as energy spectral density, bandwidth choices, Doppler effects and the number of different sequences of the same length, will be discussed.

2.0 FREQUENCY HOP PATTERN

2.1 RANGE-VELOCITY AMBIGUITY

Although Doppler shifts are small for sea surface reverberation due to a rough-moving sea surface, (typically 25 Hz or less for 85 KHz signals and 10 Hz for 60 KHz signals [8]), the Doppler shift for a moving target is more significant. The Doppler shift δF is easily calculated by

$$\delta F = \frac{2vF}{c} = \frac{vF}{1456 \text{ kts}} .$$

Thus for a relative speed of 10 knots and a 250 KHz signal frequency, the Doppler shift expected is 1.72 KHz. If the platform and target are both traveling at 10 knots in opposite directions, the relative speed between the two is 20 knots, and the resulting Doppler shift is 3.44 KHz for a 250 KHz signal.

The Doppler shift for a 250 KHz signal with a relative velocity of 20 knots is seen to be significant compared to the possible signal bandwidth of 200 KHz (50-250 KHz). A shift of 3.44 KHz in the signal carrier would, in fact, move the signal out of a typical non-Doppler compensating bandpass filter with a 5 KHz bandwidth (2% bandwidth, $\pm$2.5 KHz about the carrier frequency).

Another effect which must be accounted for is the possibility of return echo elongation due to target length. For a target length L at an aspect angle θ, the return echo is lengthened by an approximate factor

$$\frac{2L \cos\theta}{c} . \qquad (53)$$

The signal processing of the return echo data should be designed to accommodate the echo elongation. For mines the echo elongation is not the

severe problem it can be for submarine detection. This phenomena will not be considered for this specific contract.

The Doppler shift of the return echo is a critical factor in the choice of frequency spacing for the frequency hopping system. The frequencies must be spaced such that the Doppler shifted returned signal does not lie outside the passband of the receiver filter associated with the transmitted frequency. The absolute minimum spacing between adjacent frequencies is defined such that the largest Doppler shift of the highest frequency (δF_H) is equal to the minimum frequency spacing ΔF_{min} minus the signal bandwidth (2/T) as shown in Figure 3. This situation is described by

$$\Delta F_{min} = \delta F_H + \frac{2}{T} = 2\left[\frac{vF_H}{c} + \frac{1}{T}\right] \quad . \tag{54}$$

The Doppler shift for a 250 KHz signal and a 20 knot relative speed has been previously calculated to be 3.45 KHz. The signal bandwidth must be held low to keep the frequency spacing small so the sub-pulse period must in turn be long. A 20 μsec sub-pulse adds 100 KHz to the required frequency spacing (ΔF_{min} = 103.45 kHz) while a 200 μsec pulse adds only 10 KHz (ΔF_{min} = 13.45 kHz). The previous discussion is based on the assumption that the receiver filters must account for Doppler shifts in only one direction. If a bank of ''up-Doppler'' filters are used in conjunction with a bank of ''down-Doppler'' filters, then the filters would be required to detect Doppler shifts in only one direction. This situation would require processing logic for the received signals to determine whether the signal was shifted up or down in frequency since the filter responses from the two banks would overlap. A more conservative design would account for Doppler shifts in both directions with one bank of filters. The absolute minimum frequency

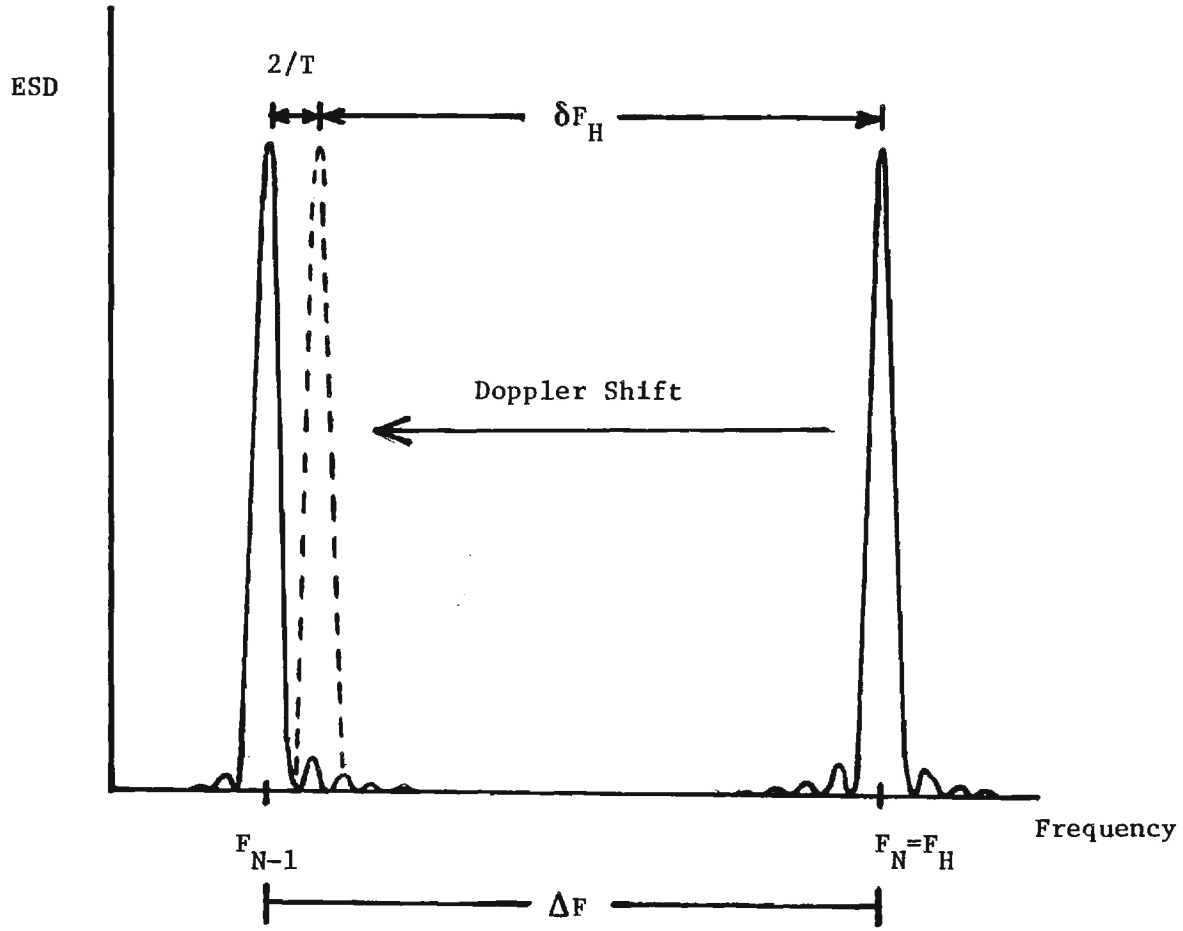

Figure 3. Minimum Frequency Spacing to Account for Maximum Doppler Shift in One Direction.

spacing between adjacent frequencies for this case is equal to the sum of the largest down-Doppler shift of the highest frequency ($F_H = F_N$) plus the largest up-Doppler shift of the next highest frequency (F_{N-1}) plus the signal bandwidth. This situation is described by

$$\Delta F_{min} = \delta F_N + \delta F_{N-1} + 2/T$$

or

$$\Delta F_{min} = F_N - F_{N-1} = 2\left[\frac{v(F_N + F_{N-1})}{c} + \frac{1}{T}\right] . \qquad (54)$$

Solving (54) for F_{N-1} in terms of F_N and re-inserting the result into (54) yields ΔF_{min} in terms of F_N:

$$\Delta F_{min} = \frac{2\left[F_N\left(\frac{2v}{c}\right) + \frac{1}{T}\right]}{1 + \frac{2v}{c}} . \qquad (55)$$

Assuming F_N = 250 kHz and v = 20 knots, a 20 μsec sub-pulse would require a minimum spacing of ΔF_{min} = 105.2 kHz while a 200 μsec sub-pulse would require a spacing of ΔF_{min} = 16.6 kHz.

Correct ordering of the pulse frequencies in terms of transmission is also an important design consideration in a frequency hopping system. This problem has been addressed by radar designers for many years. The use of a range/velocity ambiguity function, which is in effect a two-dimensional correlation equation, has been the typical figure of merit for investigating signal waveforms that exhibit good range/velocity ambiguities.

The ideal signal shape with regards to producing unambiguous returns due to range timing shifts or velocity induced frequency shifts is a signal whose two-dimensional correlation function is a ''thumb tack'' or impulse shape, as illustrated in Figure 4. The delay-Doppler ambiguity function is defined as

$$X(\tau,v) = \frac{1}{2E}\int_{-\infty}^{\infty} \mu^*(\sigma)\mu(\sigma-\tau)e^{j2\pi v\sigma}d\sigma \qquad (56)$$

where E is the total energy of the signal pulse $\mu(t)$. Consider a pulsed sinusoid

$$\mu(t) = \prod\left(\frac{t}{T}\right)\cos\omega_o t$$

where T is the pulse duration and ω_o is the carrier radian frequency. For this signal shape, the energy E is

$$E = \int_{-\infty}^{\infty} \mu(t)\ \mu^*(t)\ dt = \int_0^T \cos^2\omega_o t\ dt = \frac{T}{2} \qquad (57)$$

and for N contiguous pulses, the total energy is $\frac{NT}{2}$.

The ambiguity response for a single CW pulse, such as the pulsed sinusoid signal used previously, is shown in Figure 5. The ridges on the plot are areas of high response due to time delay and frequency shift. Strong return echoes with certain normalized frequency values would produce a correlator output that could indicate a false return in terms of range delay and Doppler shift.

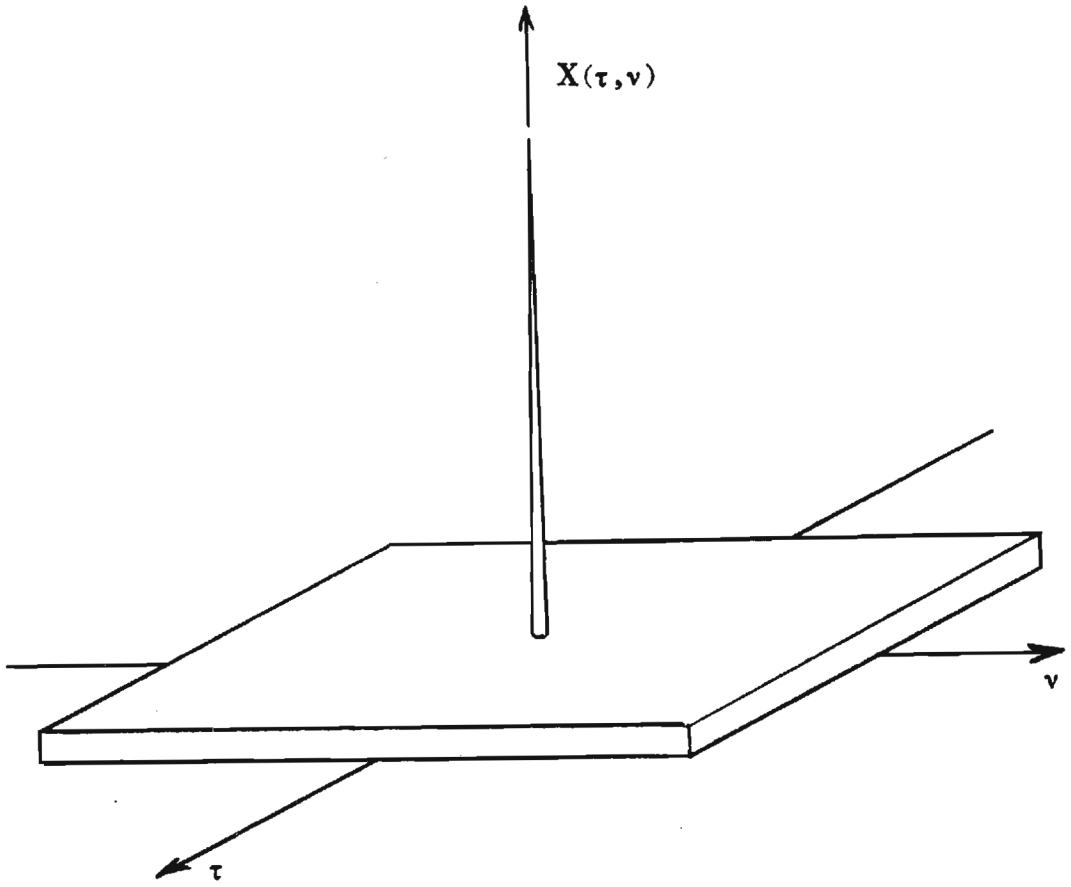

Figure 4. Ideal "Thumb Tack" Ambiguity Function.

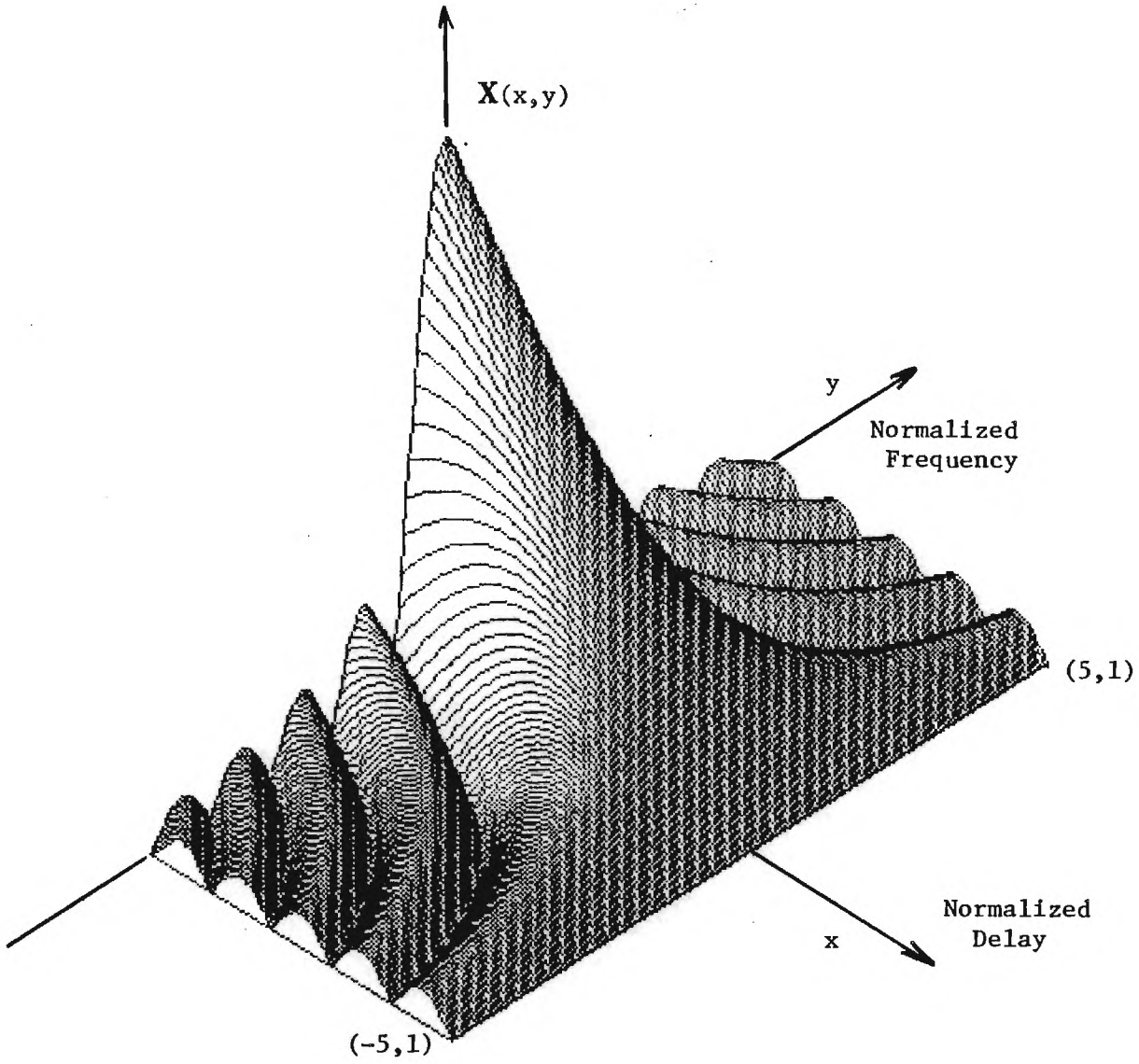

Figure 5. Single CW Pulse Ambiguity Function.

A paper by John P. Costas [9] has investigated a signalling set for frequency hopping using a ''Welch'' sequence to determine the order of transmission of the various frequencies. Costas also has made use of the fact previously determined by others that the frequency differences of the signals should be equal to the reciprocal of the pulse length to prevent ambiguities along the range delay axis.

Furthermore Costas, in this paper, has made a good argument for one pulse per time period and no more than one pulse of each frequency per frequency hopping burst when working in a reverberation environment. Thus, it has been determined that a frequency hopper should use signal sets with the following properties if working in a reverberation environment:

1. Frequencies of individual pulses should be separated by the reciprocal of the pulse length to minimize ambiguities along the range delay axis.

2. When a burst of pulses is transmitted, the burst should have no more than one pulse of each frequency in the burst.

3. A burst should have only one pulse at a time; i.e., two pulses using different frequencies in the set should not be transmitted simultaneously.

The main remaining question concerns the optimum way to select the order in which frequencies in the set should be sent; i.e., should we send f_1, f_2, f_3 sequentially or f_1, f_3, f_2 sequentially so as to minimize ambiguities along the Doppler shift axis? Costas has shown in his paper that the Welch sequences constructed as described by L. R. Welch [10]

provide an ambiguity plot for the frequency hopping burst that is close to the ideal ambiguity plot, and that is much better than that obtained for a single CW pulse or for a quantized FM burst. The answer then to the question of an optimum way to select the order in which frequencies should be transmitted in a burst (i.e., the firing order) is that the firing order should be picked to minimize velocity shift axis ambiguities. The firing order obtained through use of a Welch sequence is one method of minimizing the velocity shift axis ambiguity.

2.2 GENERATION OF SEQUENCES BASED ON COSTAS ARRAYS

The frequency hopping sonar system discussed in the previous section utilizes a uniform pulse train consisting of N distinct frequencies transmitted over N consecutive time intervals. The optimum frequency hop patterns with respect to range-Doppler sidelobe peaks can be determined using a special class of permutation matrices known as Costas arrays. Several systematic techniques may be used to generate Costas arrays [10].

The Costas array is an NxN permutation matrix. The N rows of the Costas array represent the N distinct frequencies $\{f_1, f_2, \ldots, f_i \ldots, f_N\}$ while the N columns represent the N distinct time intervals $\{t_1, t_2, \ldots, t_j \ldots, t_N\}$. The sequence of transmitted frequencies or ''firing order'' is chosen so that the ambiguity function of the returned signal and the transmitted signal shifted in time and frequency resembles the ideal ''thumbtack'' response. For certain values of N, these optimum firing orders may be determined using a theorem by Welch involving primitive elements of finite fields. We subsequently refer to this firing order of N frequencies as a Welch-N sequence. The Welch construction technique is only one of several techniques used to generate Costas arrays.

2.2.1 THE WELCH SEQUENCE GENERATION TECHNIQUE

A Costas array may be constructed using the Welch generation technique by first choosing a finite field GF(p) where p is a prime number greater than two. A Welch-N sequence may be generated for N=p-1, N=p-2 and for certain values of N=p-3. The Costas array is constructed using a log table given a primitive root α of the finite field GF(p). The NxN array has rows numbered i=1,2,...,p-1 while the columns are numbered j=0,1,...,p-2. The (i,j) position of the array grid is filled if and only if $i=\alpha^j$. Figure 6 illustrates the Welch construction of the Costas array for p=11 and α=2. The N=p-1 firing order is obtained directly from the Costas array. The Welch-10 sequence is 1,2,4,8,5,10,9,7,3,6. The Welch-9 sequence (N=p-2) is obtained by first eliminating the first row and column from the N=p-1 array. The rows and columns of the modified array are then renumbered as before. The corresponding Welch-9 sequence is 1,3,7,4,9,8,6,2,5. As previously mentioned, the N=p-3 sequence is obtainable only under specific conditions. Namely, the number 2 must be a primitive root of GF(p). Obviously, for p=11, 2 is a primitive root. The technique for obtaining the N=p-3 sequence follows that for N=p-2 in that the first two rows and columns are eliminated from the Costas array. The resulting Welch-8 (N=p-3) sequence is 2,6,3,8,7,5,1,4.

Based on the previous discussion, the Welch construction technique is not applicable for certain choices of N. Considering values of N up to 30, the Welch construction technique does not apply for N of 7,13,14,19,20,23,24 and 25. Yet, other Costas array construction techniques are available for most N where the Welch construction does not apply. Systematic Costas array construction techniques are known for all N up to 50 except for N of 32,33,43,48 and 49.

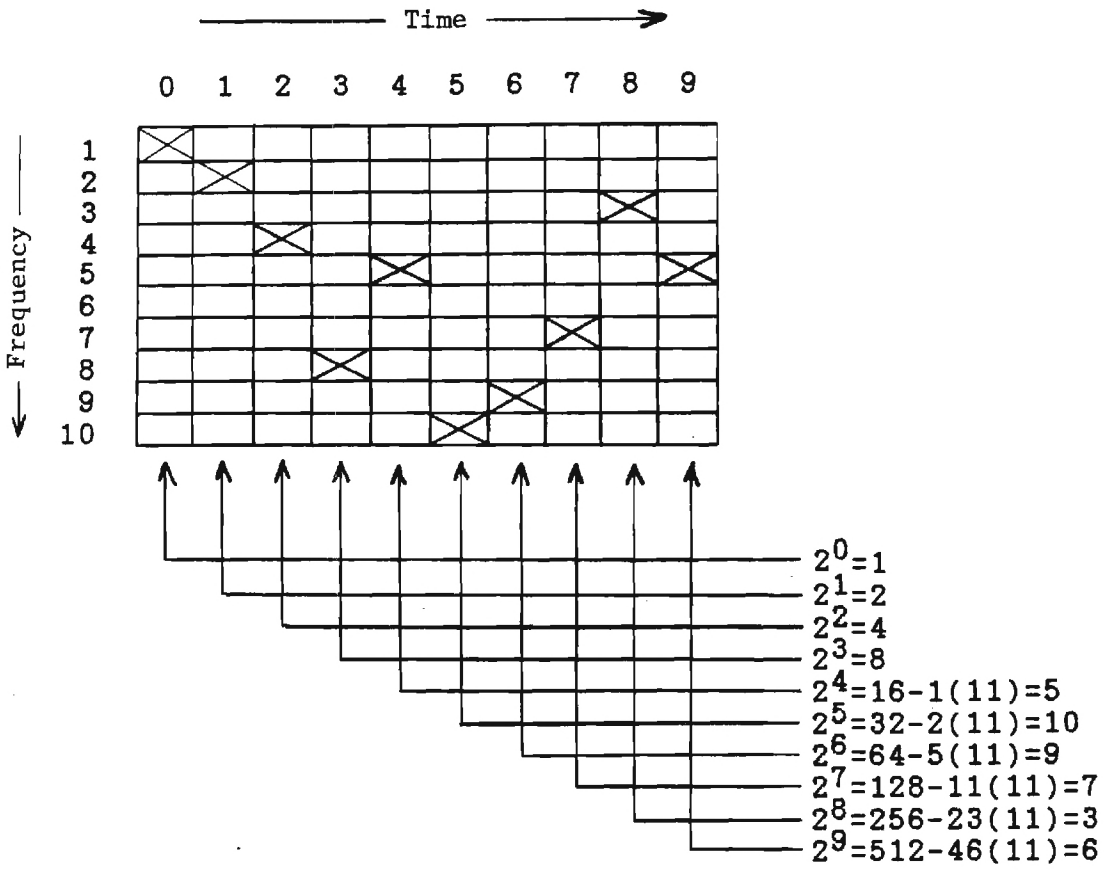

Figure 6. Welch-10 Costas Array Construction (p=11, α=2).

The Costas array shown in Figure 6 exhibits a special physical characteristic which produces low range-Doppler sidelobe peaks. If the Costas array (A) is compared with the same array shifted in time and frequency (A'), at most one coincidence will occur. Another way of stating this property is illustrated by considering all the lines which connect any two distinct entries in the array. For a Costas array, no two of these lines have the same magnitude and slope. This principle is the basis of the difference triangle approach used by Costas.

The difference triangle for the Welch-10 sequence derived previously is shown in Figure 7. The entries in the first row represent the difference between adjacent elements of the sequence. The second row represents differences between every other element. The third row is the difference between every third element and so on. If each row consists of unique values, then the corresponding array is a Costas array. Costas states that the number of sequences which satisfy the difference triangle requirement for N = 3,4,5,6,7,8,9,10,11 and 12 are 4,12,40,116,200,444,760,2160,4368 and 7852 respectively.

2.2.2 A WELCH SEQUENCE SIGNALING EXAMPLE

The uniform pulse train of the aforementioned frequency-hopping system consists of N consecutive sub-pulses each of duration T. The frequency of the sub-pulses are determined by the Welch N sequence $\{\theta_0,\theta_1,\ldots,\theta_{N-1}\}$. As previously discussed, each sub-pulse must contain an integral number of cycles. The simplest choice of frequencies is

$$f_n = \frac{\theta_n}{T} \qquad n = 0,1,\ldots,N-1 \tag{58}$$

	1	2	4	8	5	10	9	7	3	6
1	1	2	4	-3	5	-1	-2	-4	3	
2	3	6	1	2	4	-3	-6	-1		
3	7	3	6	1	2	-7	-3			
4	4	8	5	-1	-2	-4				
5	9	7	3	-5	1					
6	8	5	-1	-2						
7	6	1	2							
8	2	4								
9	5									

Figure 7. Welch-10 Difference Triangle.

where T is the sub-pulse period. The sequence values (θ_n's) represent the number of cycles per sub-pulse period. Thus, for a sequence ranging from 1 to N, the lowest frequency of transmission would consist of 1 cycle per sub-pulse while the highest frequency of transmission would contain N cycles per sub-pulse.

The integral values in any sequence generated from a Costas array may be modified in order to increase the number of cycles per sub-pulse. If one were to add some positive integer K, to each element of the sequence, the elements of the resulting sequence would range from 1+K to N+K. Yet, the difference triangle of the new sequence would be identical to that of the original sequence. Thus, the new sequence would exhibit the proper behavior in terms of range-Doppler sidelobe suppression. The frequencies of transmission using the new sequence would be

$$f_n = \frac{\theta_n + K_1}{T} \quad . \quad n = 0,1,\ldots,N-1 \tag{59}$$

The lowest frequency of transmission would contain $1+K_1$ cycles per sub-pulse [$T = (1+K_1)/F_L$] while the highest transmitted frequency would contain $N+K_1$ cycles per sub-pulse.

Another method of increasing the number of cycles per sub-pulse is to multiply the sequence generated from a Costas array by some positive integer K_2. The new sequence ranges from K_2 to NK_2 in multiples of K_2. This procedure has the effect of multiplying each element in the difference triangle of the original sequence by K_2. Therefore, this new sequence will also exhibit the proper behavior in terms of range-Doppler sidelobe suppression. The frequencies of transmission using this new sequence are

$$f_n = \frac{K_2 \theta_n}{T} \quad . \quad n = 0,1,\ldots,N-1 \tag{60}$$

The lowest transmitted frequency contains K_2 cycles per sub-pulse ($T = K_2/F_L$) while the highest transmitted frequency contains NK_2 cycles per sub-pulse.

The pulse train $\mu(t)$ may be described in complex envelope notation as

$$\mu(t) = \sum_{n=0}^{N-1} p_n (t-nT) \tag{61}$$

where

$$p_n(t) = \begin{cases} e^{j2\pi f_n t} & 0 \leq t \leq T \\ 0 & \text{otherwise} \end{cases} \quad . \tag{62}$$

The upper limit on the sub-pulse duration T is dictated by the required range resolution of the target. That limit is given by

$$T_{max} = \frac{2R}{c} \tag{63}$$

where R is the range resolution and c is the velocity of propagation. For a range resolution of 20 cm and a speed of sound in water of 1500 m/s, the maximum sub-pulse period is 267 μs.

The frequency band over which the hopped frequencies are chosen ranges from F_L to F_H. If the transmitted frequencies are chosen with a uniform spacing over the frequency band, the increment between frequencies is given by

$$\Delta F = \frac{F_H - F_L}{N - 1} \tag{64}$$

where N is the number of hopped frequencies. The set of transmitted frequencies becomes $\{F_n\} = F_L, F_L + \Delta F, F_L + 2\Delta F, \ldots, F_L + (N-1)\Delta F = F_H$. The method by which one may determine sequence values which produce the appropriate frequency coverage over a certain band is illustrated in Table 3. Assuming F_L = 50 KHz and F_H = 250 KHz, the sequence values which produce a uniform coverage of the 200 KHz band are determined as N ranges from 2 to 10. The final column in Table 3 are sequence values associated with what is called the ''master sequence''. The master sequence is the lowest integral value sequence which produces the given frequency coverage. The ''rational sequence'' shown in Table 3 represents the ratio of each of the transmitted frequencies to F_L. For certain values of N, the rational sequence is a non-integral sequence which must be multiplied by some constant to obtain the master sequence.

The master sequences in Table 3 which skip integer values are unobtainable through standard Costas array construction techniques. These sequences may be arranged to exhibit the required range-Doppler sidelobe suppression, but only through trial and error. The master sequences which are continuous over a certain range of integers (N=5, N=9 in Table 3) may be determined using the standard techniques of Costas array construction. For instance, the N=5 example may be implemented with a Welch-5 sequence while the N=9 example may be implemented by adding one to each element of a Welch-9 sequence.

. The master sequence values represent the number of cycles per sub-pulse at the respective frequencies. Thus, given a specific range resolution, the

N	ΔF(kHz)	F's (kHz)	RATIONAL SEQUENCE VALUES	MASTER SEQUENCE VALUES	T (μs)
2	200.0	50,250	$\frac{1}{1}, \frac{5}{1}$	1,5	20
3	100.0	50,150,250	$\frac{2}{2}, \frac{6}{2}, \frac{10}{2}$	1,3,5	20
4	66.67	50,116.67,183.33,250	$\frac{3}{3}, \frac{7}{3}, \frac{11}{3}, \frac{15}{3}$	3,7,11,15	60
5	50.0	50,100,150,200,250	$\frac{4}{4}, \frac{8}{4}, \frac{12}{4}, \frac{16}{4}, \frac{20}{4}$	1,2,3,4,5	20
6	40.0	50,90,130,170,210, 250	$\frac{5}{5}, \frac{9}{5}, \frac{13}{5}, \frac{10}{5}, \frac{21}{5}, \frac{25}{5}$	5,9,13,17,21,25	100
7	33.3	50,83.33,116.67, 183.33, 216.67,250	$\frac{6}{6}, \frac{10}{6}, \frac{14}{6}, \frac{18}{6}, \frac{22}{6}, \frac{26}{6}, \frac{30}{6}$	3,5,7,9,11,13,15	60
8	28.57	50,78.57,107.14,135.71 164.28,192.85,221.42 250	$\frac{7}{7}, \frac{11}{7}, \frac{15}{7}, \frac{19}{7}, \frac{23}{7}, \frac{27}{7}, \frac{31}{7}, \frac{35}{7}$	7,11,15,19,23,27,31,35	140
9	25.0	50,75,100,125,150,175, 200,225,250	$\frac{8}{8}, \frac{12}{8}, \frac{16}{8}, \frac{20}{8}, \frac{24}{8}, \frac{28}{8}, \frac{32}{8}, \frac{36}{8}, \frac{40}{8}$	2,3,4,5,6,7,8,9,10	40
10	22.22	50,77.22,94.44,116.67 138.88,161.10,183.32, 205.54,227.76,250	$\frac{9}{9}, \frac{13}{9}, \frac{17}{9}, \frac{21}{9}, \frac{25}{9}, \frac{29}{9}, \frac{33}{9}, \frac{37}{9}, \frac{41}{9}, \frac{45}{9}$	9,13,17,21,25,29,33,37,41,45	180

TABLE 3. MASTER SEQUENCES WHICH YIELD UNIFORM COVERAGE OF THE 50-250 kHz BAND FOR N=2 THROUGH 10

maximum sub-pulse duration limits the number of cycles per sub-pulse. For a range resolution of 20 cm, the maximum sub-pulse duration is 267 μs so that a maximum of 13 cycles at 50 KHz (20 μsec/cycle) are allowed. There are therefore only 13 possible values of N which produce continuous master sequences given a range resolution of 20 cm. These values of N are shown in Table 4 along with the corresponding sequences. The first sequence in each group is the master sequence while the following sequences are simply multiples of the master sequence (obtained by multiplying the master sequence by a positive integer).

The delay-Doppler ambiguity function is a two-dimensional correlation function in delay (time shift) and Doppler (frequency shift). The general formula for the ambiguity function is given in equation (56). The ambiguity function exhibits a symmetric relationship defined by

$$|X(-\tau,-v)| = |X(\tau,v)| \tag{65}$$

so that only non-negative values of time delay τ are required. The time delay τ may be defined as

$$\tau = kT + \delta \tag{66a}$$

where

$$0 \leq \delta \leq T \tag{66b}$$

and

$$k = 0,1,\ldots,N-1 \quad . \tag{66c}$$

TABLE 4. COSTAS ARRAY GENERATED SEQUENCES WHICH COVER THE 50-250 KHz BAND ASSUMING A RANGE RESOLUTION OF 20 cm (T_{max} = 267 μs).

	Min. Cycles	Sequence Values	T (μs)	NT (μs)	BW (2/T) (kHz)
N=5	1	1,2,3,4,5	20	100	100.00
ΔF=50.0 kHz	2	2,4,6,8,10	40	200	50.00
	3	3,6,9,12,15	60	300	33.33
	4	4,8,12,16,20	80	400	25.00
	5	5,10,15,20,25	100	500	20.00
	6	6,12,18,24,30	120	600	16.67
	7	7,14,21,28,35	140	700	14.29
	8	8,16,24,32,40	160	800	12.50
	9	9,18,27,36,45	180	900	11.11
	10	10,20,30,40,50	200	1000	10.00
	11	11,22,33,44,55	220	1100	9.09
	12	12,24,36,48,60	240	1200	8.33
	13	13,26,39,52,65	260	1300	7.69
N=9	2	2,3,4,5,6,7,8,9,10	40	360	50.00
ΔF=25.0 kHz	4	4,6,8,10,12,14,16,18,20	80	720	25.00
	6	6,9,12,15,18,21,24,27,30	120	1080	16.67
	8	8,12,16,20,24,28,32,36,40	160	1440	12.50
	10	10,15,20,25,30,35,40,45,50	200	1800	10.00
	12	12,18,24,30,36,42,48,54,60	240	2160	8.33
N=13	3	3,4,5,6,7,8,9,10,11,12,13, 14,15	60	780	33.33
ΔF=16.67 kHz	6	6,8,10,12,14,16,18,20,22, 24,26,28,30	120	1560	16.67
	9	9,12,15,18,21,24,27,30,33, 36,39,42,45	180	2340	11.11
	12	12,16,20,24,28,32,36,40,44, 48,52,56,60	240	3120	8.33
N=17	4	4,5,6,7,8,9,10,11,12,13, 14,15,16,17,18,19,20	80	1360	25.00
ΔF=12.5 kHz	8	8,10,12,14,16,18,20,22,24, 26,28,30,32,34,36,38,40	160	2720	12.50
	12	12,15,18,21,24,27,30,33,36, 39,42,45,48,51,54,57,60	240	4080	8.33
N=21	5	5,6,7,8,9,10,11,12,13,14,15, 16,17,18,19,20,21,22,23,24 25	100	2100	20.00
ΔF=10.0 kHz	10	10,12,14,16,18,20,22,24,26, 28,30,32,34,36,38,40,42,44 46,48,50	200	4200	10.00
N=25	6	6,7,8,9,10,11,12,13,14,15, 16,17,18,19,20,21,22,23,24 25,26,27,28,29,30	120	3000	16.67
ΔF=8.33 kHz	12	12,14,16,18,20,22,24,26,28, 30,32,34,36,38,40,42,44,46, 48,50,52,54,56,58,60	240	6000	8.33

TABLE 4. (Continued)

N=29 ΔF=7.14 kHz	7	7 through 35	140	4060	14.29
N=33 ΔF=6.25 kHz	8	8 through 40	160	5280	12.50
N=37 ΔF=5.55 kHz	9	9 through 45	180	6660	11.11
N=41 ΔF=5.0 kHz	10	10 through 50	200	8200	10.00
N=45 ΔF=4.54 kHz	11	11 through 55	220	9900	9.09
N=49 ΔF=4.17 kHz	12	12 through 60	240	11760	8.33
N=53 ΔF=3.85 kHz	13	13 through 65	260	13780	7.69

Inserting the appropriate pulse train expressions into equation (56) yields

$$X(\tau,v) = \sum_{r=0}^{N-1-k} A \quad + \sum_{\substack{r=0 \\ (r\geq 0)}}^{N-2-k} B \tag{67}$$

where

$$A = \frac{(T-\delta)}{NT} \operatorname{sinc}[\beta(T-\delta)] \exp\{j\pi[\beta(2kT+2rT+T+\delta)-2f_r\delta]\} \tag{68a}$$

$$\beta = f_r - f_{k+r} + v \tag{68b}$$

and

$$B = \frac{\delta}{NT} \operatorname{sinc}[\gamma\delta] \exp\{\sigma\pi[\gamma(2kT+2rT+2T+\delta)-2f_r\delta]\} \tag{68c}$$

$$\gamma = f_r - f_{k+r+1} + v \tag{68d}$$

The ambiguity function may be redefined in terms of a normalized delay x given by

$$x = \frac{\tau}{T} \tag{69}$$

and a normalized Doppler shift y given by

$$y = vT \ . \tag{70}$$

The normalized ambiguity functions for selected sequences with N=5, 9 and 13 are shown in Figures 8 through 13. The standard three-dimensional presentation of the respective ambiguity functions is shown in Figures 8, 9 and 10. Figures 11, 12 and 13 exhibit the ambiguity surfaces from a reference point on the normalized delay axis so that the range-Doppler sidelobe magnitudes may be clearly referenced to the main peak. The peak sidelobe levels may be approximated by 2/N as shown by Costas so that the ratio of maximum sidelobe response to the main peak is approximately -8.0, -13.1 and -16.3 dB for N=5, 9 and 13, respectively. Figure 14 represents the frequency-hopped signal for N=5 with a firing order of {1,3,4,2,5}.

The pulse train duration defined in Equation (62) has an overall duration of NT. If a single array (set of sub-arrays) is used for transmission and reception, there exists a minimum detectable range. For example, if the first sub-pulse transmitted at F_1 travels to the target and the reflected signal returns to the array before the last pulse in the train is transmitted, the returned signal may not be detected. Therefore, the propagation time from array to target must be greater than NT/2 which yields a minimum range resolution of

$$R_{min} = v\left[\frac{NT}{2}\right] \tag{71}$$

where v is the velocity of propagation. If separate arrays are used for transmission and reception, no minimum range exists.

The maximum range in terms of signal structure is given by the pulse train repetition period (i.e., the time between the starting points of adjacent pulse trains). After a pulse train has been transmitted, the

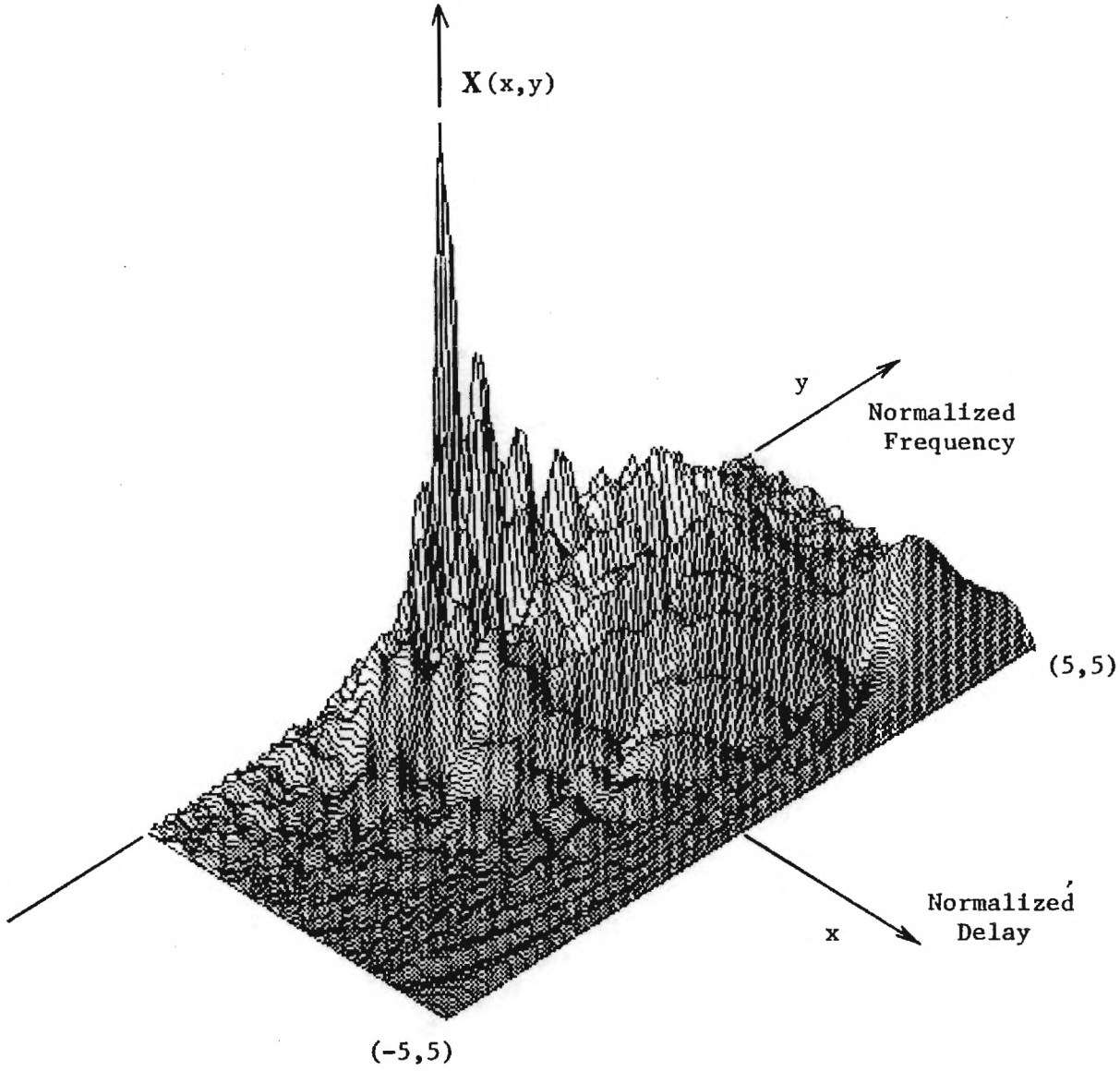

Figure 8. N=5 Costas Array Sequence (1,3,4,2,5) Ambiguity Function.

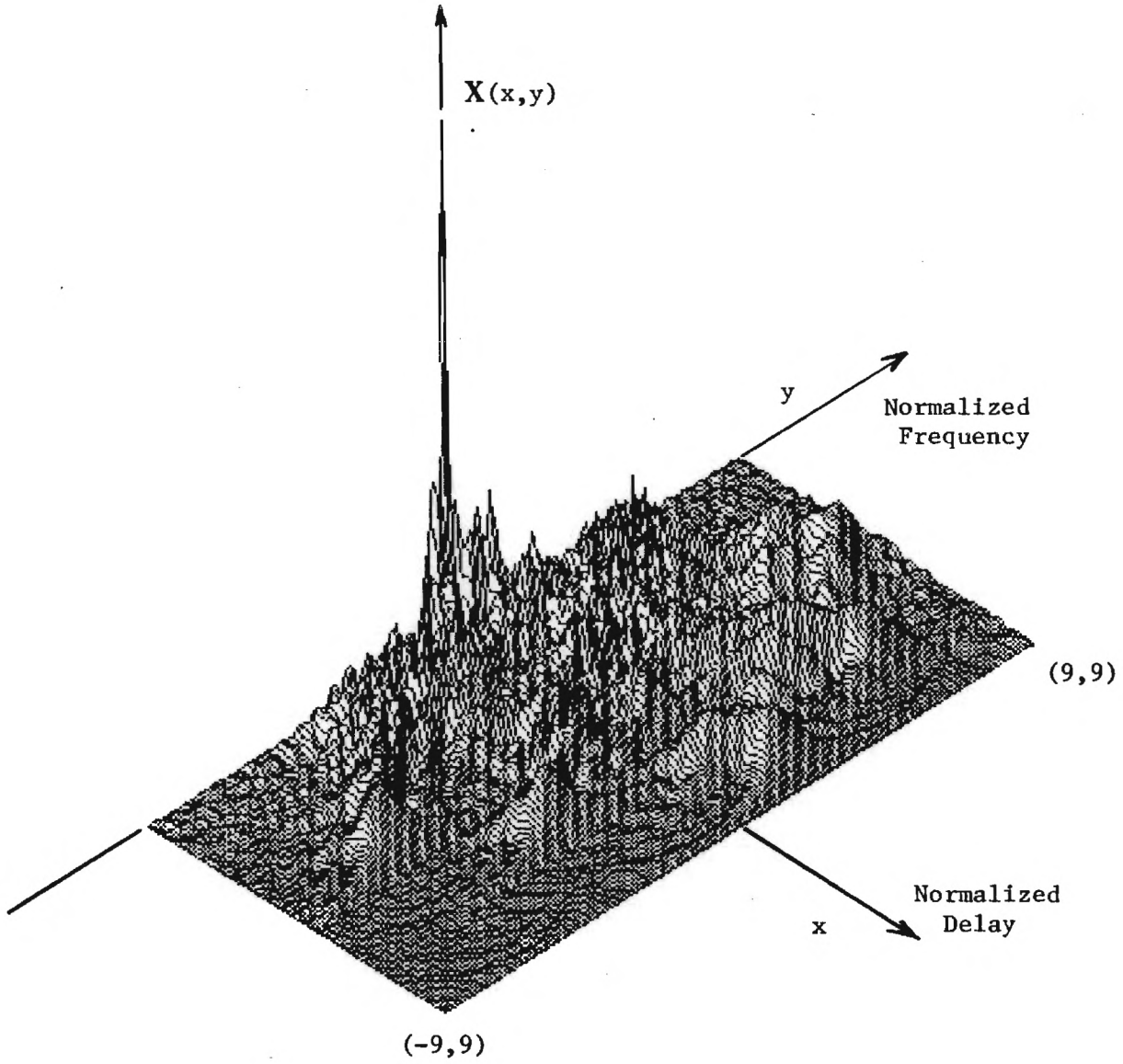

Figure 9. N=9 Costas Array Sequence (1,2,6,4,9,8,5,7,3) Ambiguity Function.

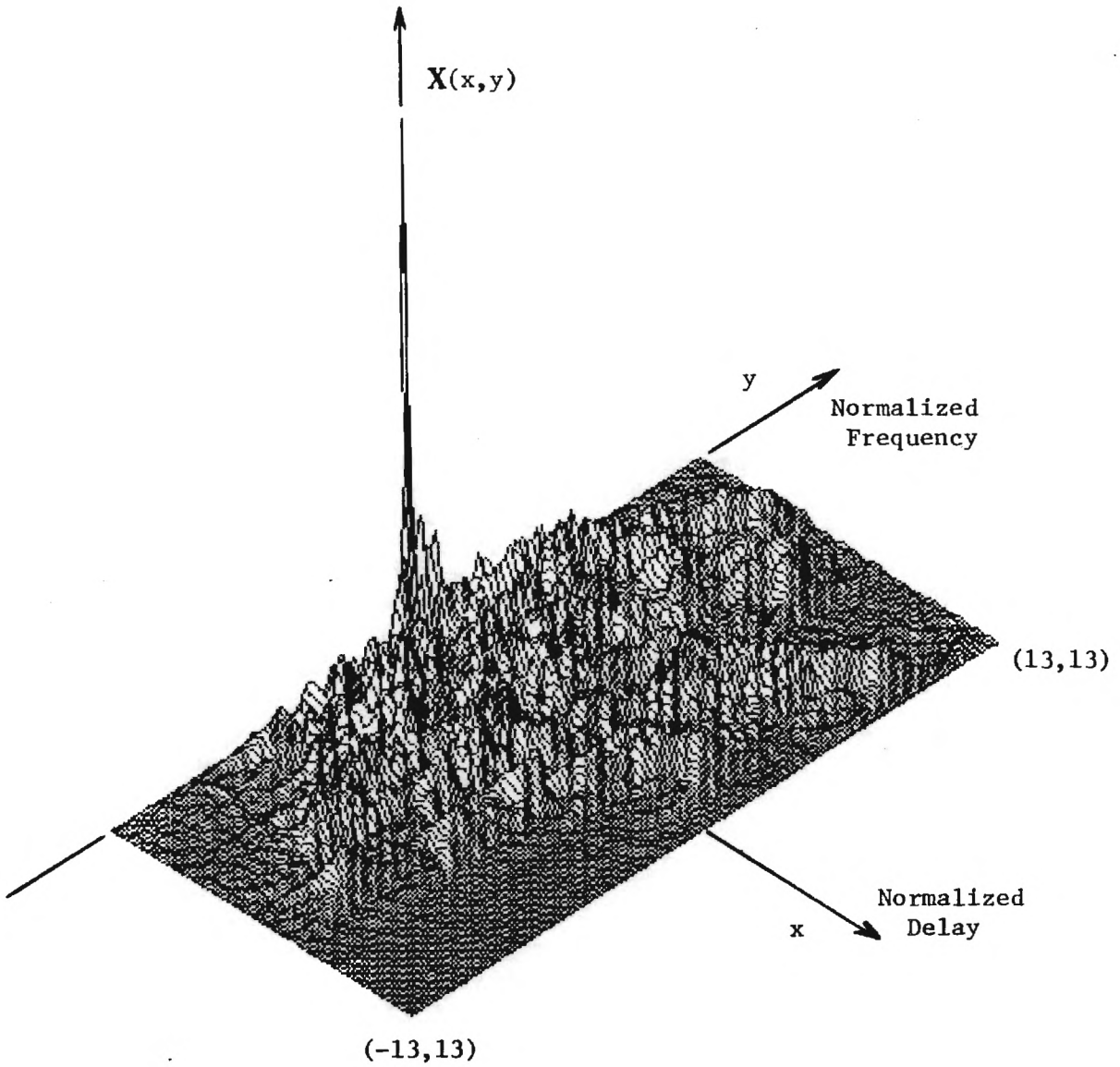

Figure 10. N=13 Costas Array Sequence (1,2,4,9,13,6,12,11,7,5,8,3,10) Ambiguity Function.

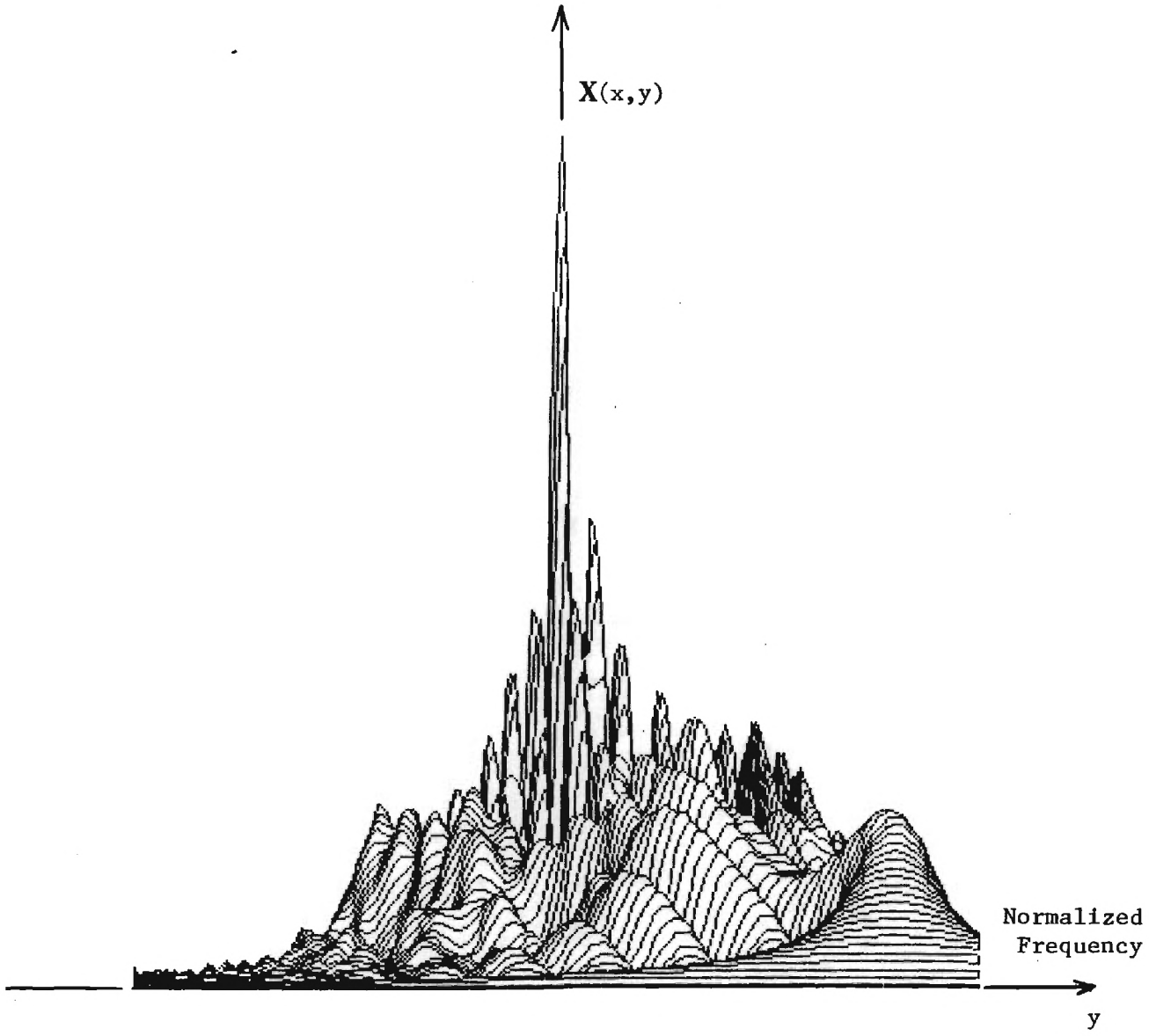

Figure 11. N=5 Costas Array Sequence (1,3,4,2,5) Ambiguity Function Sidelobe Presentation.

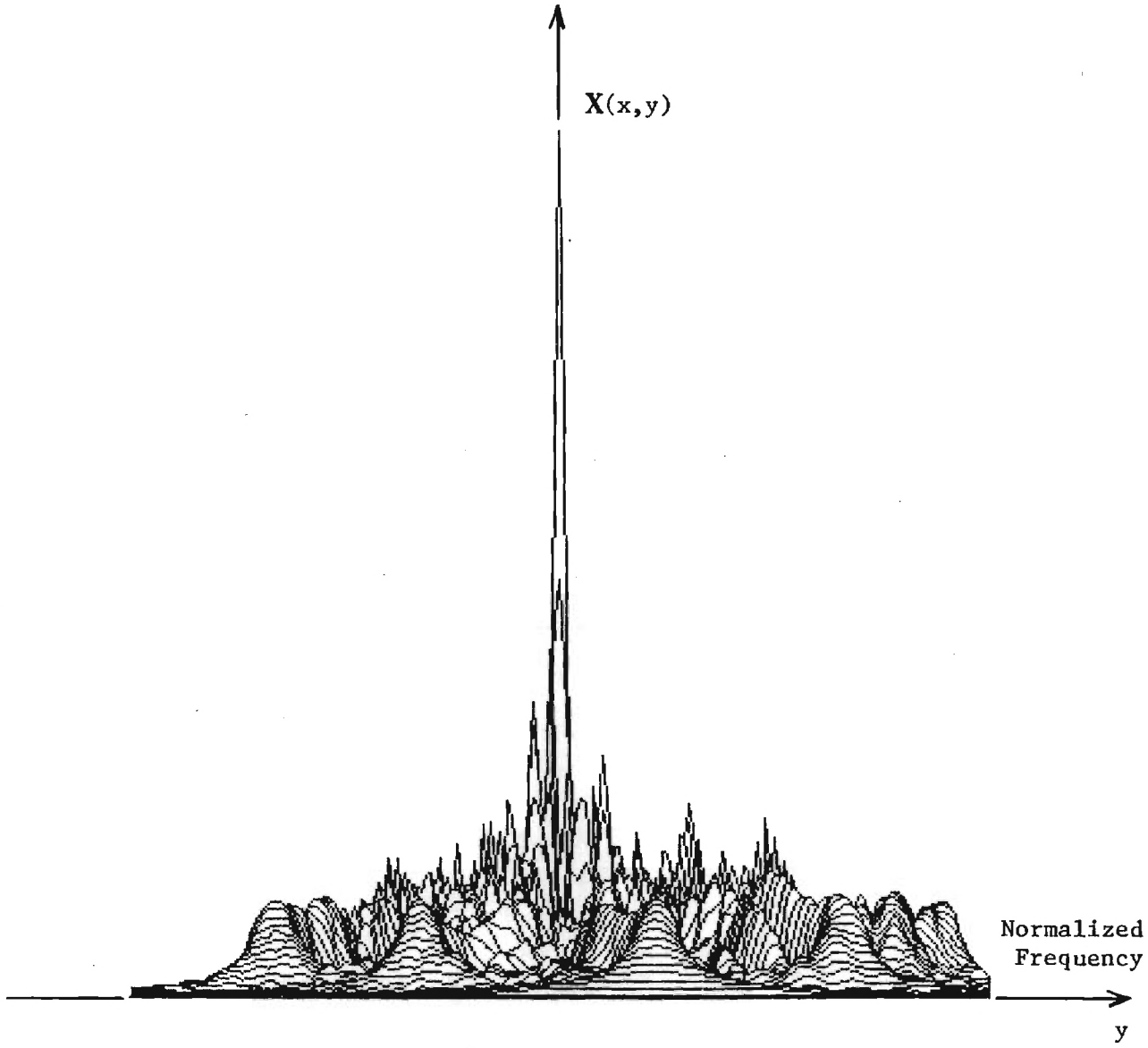

Figure 12. N=9 Costas Array Sequence (1,2,6,4,9,8,5,7,3) Ambiguity Function Sidelobe Presentation.

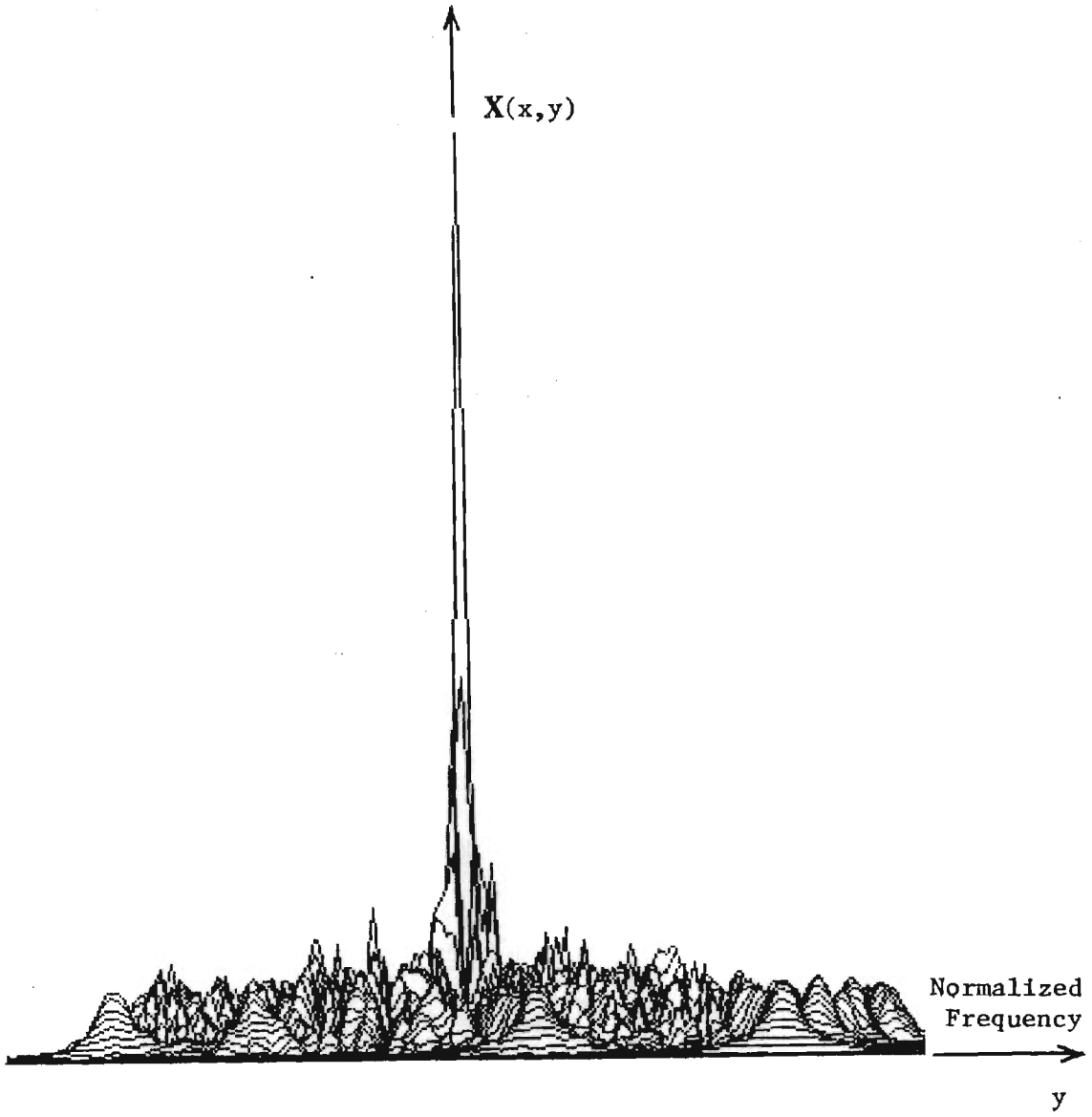

Figure 13. N=13 Costas Array Sequence (1,2,4,9,13,6,12,11,7,5,8,3,10) Ambiguity Function Sidelobe Presentation.

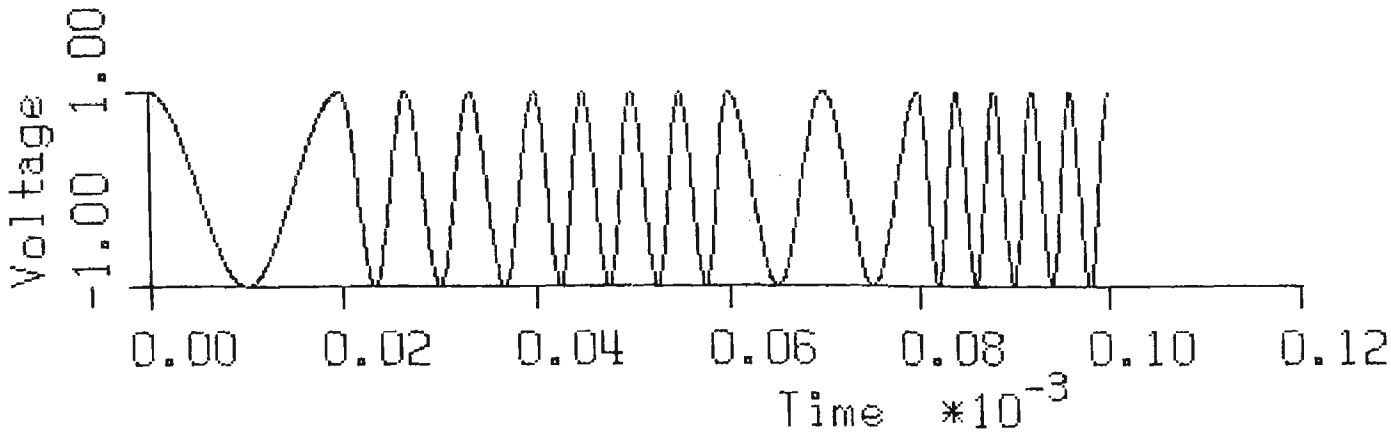

Figure 14. Frequency-Hopped Signal with N=5, F_L=50 kHz, F_H=250 kHz and firing order of (1,3,4,2,5).

entire returned signal must arrive at the array before the next transmission, assuming one transmit/receive array. If the repetition period of the pulse train is T_p, the maximum range is given by

$$R_{max} = v\left[\frac{T_p - NT}{2}\right] \quad . \tag{72}$$

Equation (72) may be used to select a pulse repetition rate given a specified maximum range. If separate arrays are used for transmission and reception, no maximum range exists in terms of signal structure assuming no firing order is repeated in the transmitted pulse trains.

3.0 PROPERTIES OF THE ARRAY, BEAMFORMER AND RECEIVER

The characteristics of a frequency-hopped signal consisting of N sub-pulses of distinct frequencies were considered in Section 2. The user has several advantages over the interceptor in terms of the ability to enhance the reception of this frequency-hopped signal. Since the number of possible firing orders grows rapidly with N, there exists a low probability that the interceptor could correctly guess the sequential order of the incoming sub-pulses. The user may utilize his knowledge of the transmitted signal firing order to improve the properties of the received signal. By detecting the envelopes of the separate returned sub-pulses and delaying each such they are coincident in time, the sub-pulse envelopes may be summed to yield an enhanced signal. The sub-pulse properties (frequency and duration) will also affect the ability of the interceptor receiver to detect the transmitted signal.

3.1 RECEIVER STRUCTURE

The receiver used to detect the multiple frequency per pulse signal discussed in Section 1 must be capable of processing narrowband signals over a wide range of frequencies. The basic structure of a receiver used to detect such a pulse is shown in Figure 2(b). The actual implementation of this receiver over such a wide frequency band (50-250 kHz) entails several frequency-dependent considerations concerning the acoustic transducers. The incorporation of the beamformer with the receiver at each of the frequencies of interest must also be considered. The overall beamformer/receiver structure is shown in Figure 15. The properties of the operation of the beamformer/receiver are discussed in what follows.

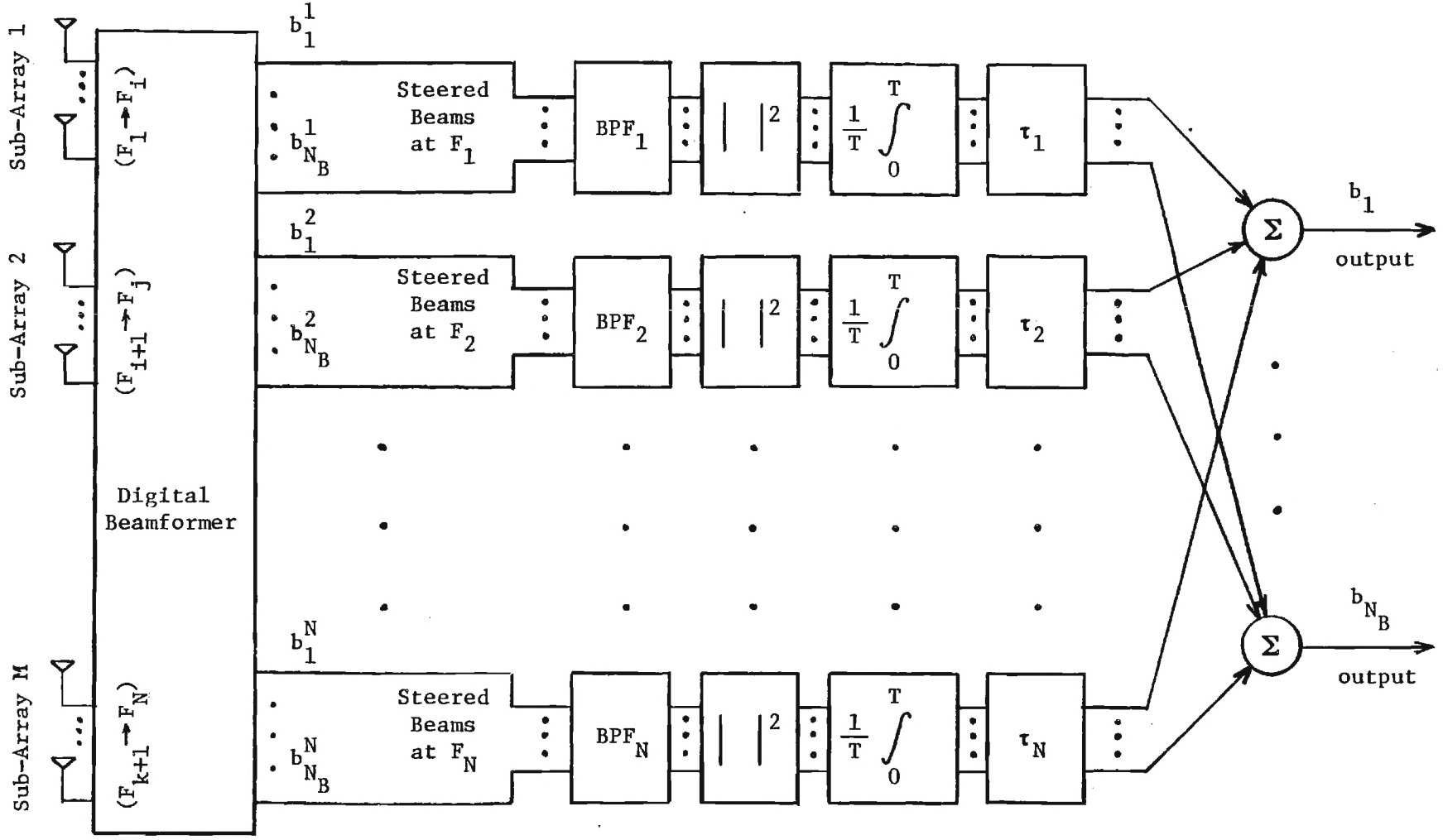

Figure 15. Beamformer/Receiver Structure.

The multiple frequency per pulse signal consists of narrowband signals which cover a wide band of frequencies. The receiving array must therefore consist of multiple sub-arrays due to the bandwidth limitations on the array elements. The design aspects of the sub-arrays are discussed in detail in Section 3.2.1. Assuming a total of M sub-arrays provide adequate coverage of the frequency band of interest, each sub-array will operate over a sub-band of the overall frequency band. Each sub-array is connected to a beamformer which produces a uniform coverage of the field of view at the frequencies in the respective sub-bands (i.e., the directions of the steered beams at each of the sub-band frequencies are the same). The directions of the steered beams must in fact be uniform for all frequencies because these outputs are subsequently summed. The steered beams are represented by b_n^m which denotes the n^{th} steered beam at the m^{th} frequency. There are N_B steered beams at each frequency.

The steered beams are passed through a band-pass filter at the respective frequencies to remove extraneous responses at adjacent frequencies. The filter response must be chosen such that a Doppler-shifted return at the frequency of interest is passed while that of an adjacent frequency is not.

The envelopes of the filtered steered beam responses are then detected by squaring each signal followed by an integration of the squared signal. The envelope of each filtered steered beam is then delayed by some time value τ_n which is dictated by the firing order of the transmitted signal. The delay time values are chosen so that all of the delayed envelopes of the filtered steered beams will occupy the same time slot. The delayed envelopes of the filtered steered beams at a given angle are then summed together. Thus, the receiver output consists of enhanced responses at each of the steered beam angles.

3.2 BEAMFORMER AND ARRAY STRUCTURES

The beamformer shown in Figure 15 is a conventional, time-domain, digital beamformer which produces N_B steered beams at N distinct narrowband frequencies. This beamformer may be implemented through commonly used techniques such as phase-shift beamforming [11] or quadrature beamforming [12]. The sets of delay and shading coefficients required to form N_B steered beams at N separate frequencies simultaneously may each be stored in a two-dimensional array indexed by frequency and element number. Among the sub-array characteristics which must be determined to employ such a beamformer are the number of elements per sub-array, element spacing, element bandwidth, the number of active elements at each frequency and the number of frequencies per sub-array.

3.2.1 SUB-ARRAY SENSOR CHARACTERISTICS

Among the most limiting factors in the design of sub-arrays to receive signals over a wide band is the element bandwidth. Current technology can produce hydrophone elements with minimum quality factors in the range of 2.0 to 1.5 which yields bandwidths in the range of 50% to 67% of the center frequency. To receive signals ranging from 50 to 250 kHz ($F_H = 5F_L$) would obviously require several sub-arrays. The most efficient array design (the minimum number of sub-arrays) depends on the bandwidth of the transmitted signals. The selection of the sensor center frequencies is illustrated in Figure 16. The sensors of sub-array 1 are designed to receive signals in the range of F_1 through F_i. The transmitted signals at all frequencies have a bandwidth (90% energy BW) of 2/T. Thus, the frequency range from $F_1 - \frac{1}{T}$ to $F_i + \frac{1}{T}$ must lie within the bandwidth of the sensors in sub-array 1.

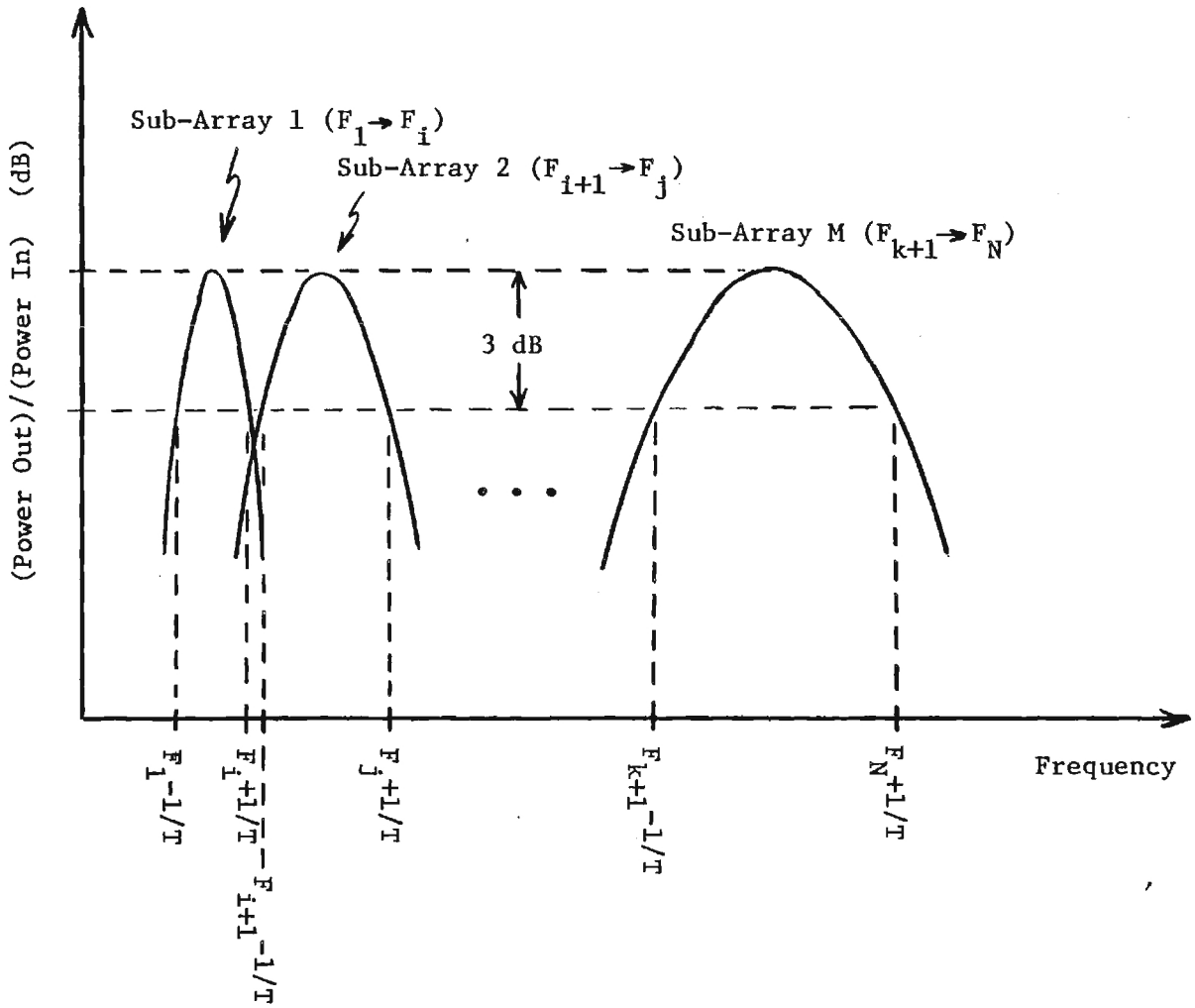

Figure 16. Frequency Response of the Sub-Array Sensors in Terms of the Hopped Frequencies.

Similar relationships hold for sub-arrays 2 through M. Assuming a constant Q for all sensors yields larger bandwidths at higher center frequencies. Therefore, the bandwidth of sub-array M will contain more frequencies than that of sub-array 1 assuming a uniform frequency distribution.

3.2.2 SUB-ARRAY DESIGN CONCERNING THE FIELD OF VIEW COVERAGE

As discussed in Section 3.2, the beamformer is required to produce N_B steered beams for N frequencies and the distribution of beam pointing angles must be identical at each frequency. The beamwidths of the steered beams must also be equivalent to ensure the capability of isolating the angle at which the target lies.

The maximum spacing of the elements is assumed to be one-half wavelength to prevent any spatial aliasing. Therefore, the maximum element spacing for a given sub-array is one-half wavelength at the highest frequency of interest. If the spacing d is chosen so that each sub-array has $d = \lambda/2$ at the highest frequency of interest ($\lambda_{min}/2$ is 1/2 wavelength at F_{max}), the number of elements in the n^{th} sub-array N_E^n required to obtain a certain broadside beamwidth at F_{max} is approximated by

$$\text{BROADSIDE BEAMWIDTH} \simeq \frac{101.8}{N_E^n} . \qquad (\lambda/2 \text{ spacing}) \tag{73}$$

Equation (73) is more accurate for larger values of N_E^n. Thus, 102 elements are required to produce a 1° beamwidth at F_{max} if $d = \lambda_{min}/2$. The total physical length of the n^{th} sub-array is given by

$$L_n = (N_E^n - 1)\, d_n \tag{74}$$

where d_n is the element spacing of the n^{th} sub-array.

Given the N_E^n value determined at F_{max} ($d = \lambda min/2$), the effective length of the sub-array becomes smaller as the frequency of operation is decreased. A smaller effective length at the lower frequencies produces a wider beamwidth. Assuming sub-array n must operate at F_1 and F_2 with $F_2 > F_1$ and $F_2 = F_{max}$ ($d = \lambda_2/2$), then to produce the same beamwidth at F_1 as obtained at F_2, the effective length of the sub-array at F_1 must be increased by adding elements. The beamwidths of the steered beams at F_1 may be reduced to those at F_2 by adding elements with $\lambda/2$ spacing at F_2. The actual number of active elements required at F_1 may be determined by equating the effective lengths of the sub-array at F_1 and F_2. If we let $F_2 = 2F_1$ ($\lambda_1 = 2\lambda_2$) and $d = \lambda_2/2$, a sub-array with N_E elements has an effective length at F_1 which is one-half of the effective length at F_2. To determine a general formula for the number of active elements required at each of the lower frequencies of a certain sub-array, the maximum frequency of operation will be denoted by F' while the lower frequency will be given by F. The number of active elements required at F' and F are N_E' and N_E, respectively. Equating the effective lengths of the sub-array at F' and F yields

$$(N_E' - 1)\frac{\lambda}{2} = (N_E - 1)k\lambda \tag{75}$$

where the elements spacing is $d = \lambda/2$ at F' and $d = k\lambda$ at F with k being a constant. The constant k is determined by writing the wavelengths in terms of frequency as given by

$$d = \frac{1}{2}\frac{c}{F'} = k\frac{c}{F} \tag{76a}$$

or

$$k = \frac{1}{2}\frac{F}{F'} \quad . \tag{76b}$$

The effective sub-array lengths become

$$(N_E' - 1)\frac{\lambda}{2} = (N_E - 1)\frac{\lambda}{2}\frac{F}{F'} \tag{77}$$

which yields

$$N_E = \frac{F'}{F}(N_E' - 1) + 1 \tag{78}$$

for the number of active elements required at F. The actual design of sub-arrays used to receive multiple frequencies is illustrated in the design example of Section 4.0.

4.0 DESIGN EXAMPLE

The most important parameter to be chosen in the design of the frequency-hopping system discussed in the previous sections is the number of frequencies (N). The choice of N affects the minimum range of the interceptor receiver, the allowable Doppler shifts and the ambiguity function sidelobe magnitudes. The allowable Doppler shifts are also affected by the sub-pulse duration (T) which depends on the minimum cycles per sub-pulse at F_L. For a given value of N, the allowable Doppler shifts increase in magnitude as T increases since the 90% BW of the separate sub-pulse signals is inversely proportional to T. Yet, as N is increased, the allowable Doppler shift is decreased because the frequency spacing Δf is decreased for a given bandwidth. Thus, the number of frequencies must be chosen in conjunction with the minimum cycles per sub-pulse. This point is illustrated by investigating the energy spectral density of a single transmission consisting of N sub-pulses.

The energy spectral density [E(f)] of the N consecutive sub-pulses described in (62) is given by

$$E(f) = |U(f)|^2 \tag{79}$$

where U(f) is the Fourier transform of the signal given in (62). The energy spectral density of the frequency-hopped signal becomes

$$\begin{aligned} E(f) = \frac{T^2}{4} \sum_{n=0}^{N-1} \sum_{m=0}^{N-1} (-1)^{\theta_m+\theta_n} \cos[2\pi f(n-m)T] \\ \cdot \left[\operatorname{sinc}(ft+\theta_m) + \operatorname{sinc}(fT-\theta_m) \right] \\ \cdot \left[\operatorname{sinc}(fT+\theta_n) + \operatorname{sinc}(fT-\theta_n) \right] \end{aligned} \tag{80}$$

The energy spectral density (ESD) given in Equation (80) represents the output of an interceptor spectrum analyzer assuming the interceptor integrates over the entire received signal period (NT). Figures 17, 18, 19 and 20 show the ESD of N=5 waveforms with 1, 2, 3 and 12 minimum cycles per pulse, respectively. The characteristics of these waveforms are described in Table 4 of Section 2.2.2. With a minimum of one cycle per sub-pulse, spectral interaction between adjacent frequencies produces ESD peaks away from the transmitted frequencies. These peaks make the signal easier to detect from the standpoint of the interceptor. Increasing the minimum number of cycles per sub-pulse reduces the spectral interaction by concentrating the energy of the sub-pulses at the actual frequency of transmission. The so-called ''dead zones'' between spectral peaks grow in width as the number of cycles per sub-pulse is increased. The widths of the dead zones must be large enough to account for the maximum Doppler shift as discussed in Section 2.1. Table 5 summarizes the required frequency spacings as defined in Equation (55) for the various sub-pulse durations of interest assuming F_N = 250 kHz with relative velocities of 10 and 20 knots. A comparison of Table 5 with Table 4 yields the various sequences which may be used to implement the frequency-hopping system under the given design constraints. For a maximum relative speed of 10 knots, the maximum value of N is 17 (ΔF = 12.5 kHz, T = 240 μs) while a maximum relative speed of 20 knots yields a maximum N of 13 (ΔF = 16.67 kHz, T = 240μs). The N = 17 (v = 10 knots) case will be considered in the following design example.

The firing order of an N = 17 sequence may be determined using the Welch construction technique as discussed in Section 2.2.1. The Welch-17 firing order determined from p = 19, α = 2 (N = p - 2) is

1,3,7,15,12,6,13,8,17,16,14,10,2,5,11,4,9.

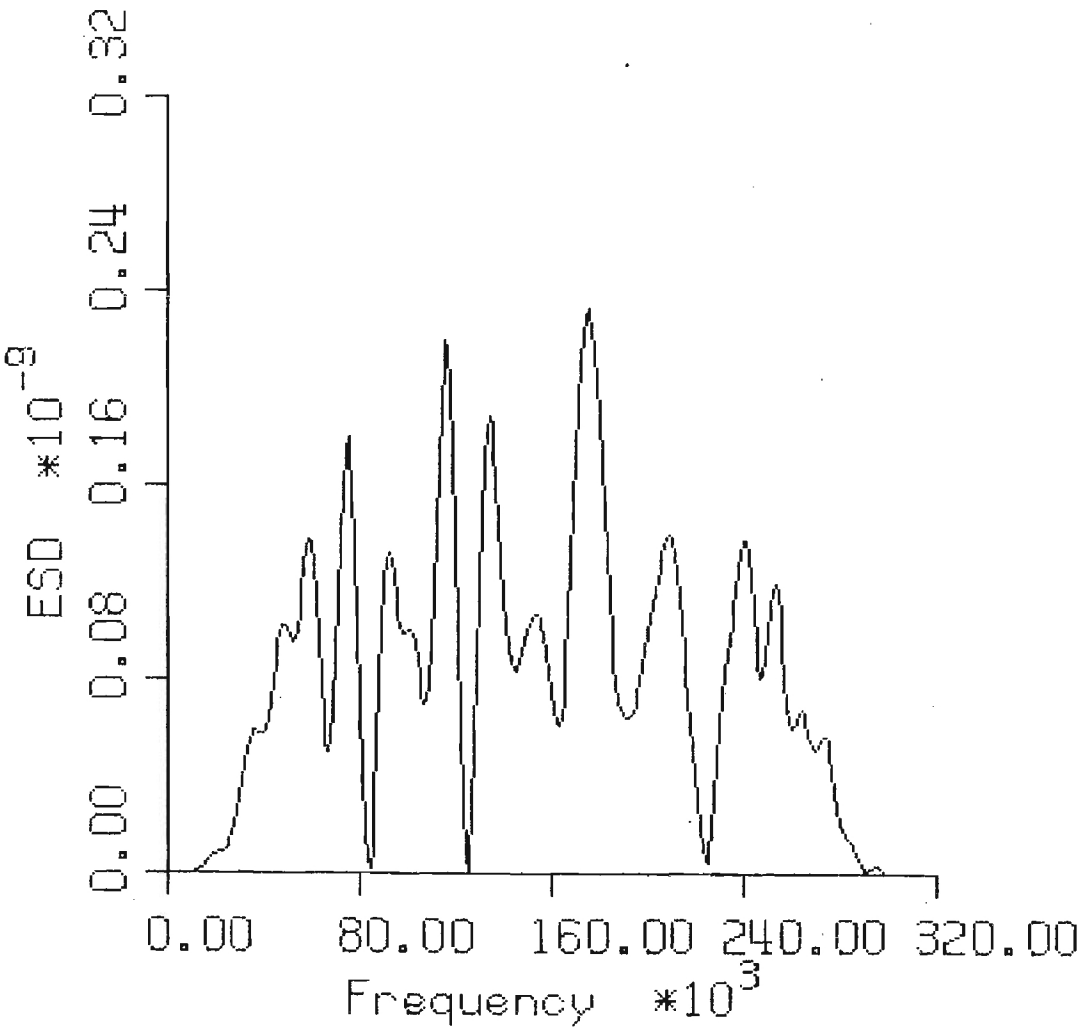

Figure 17. Energy Spectral Density of an N=5 Sequence with a Minimum of One Cycle Per Sub-Pulse (1,3,4,2,5), T=20 μs.

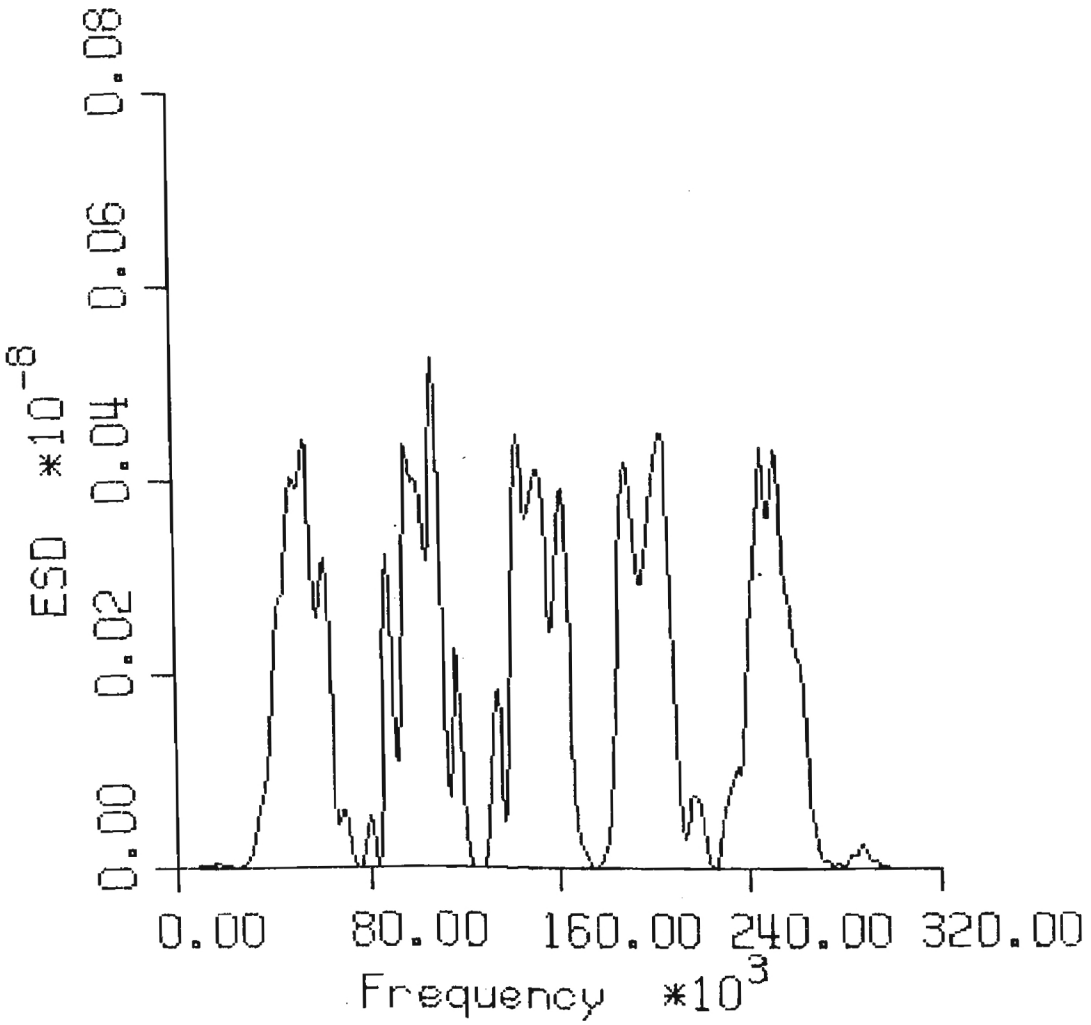

Figure 18. Energy Spectral Density of an N=5 Sequence with a Minimum of Two Cycles Per Sub-Pulse (2,6,8,4,10), T=40 μs.

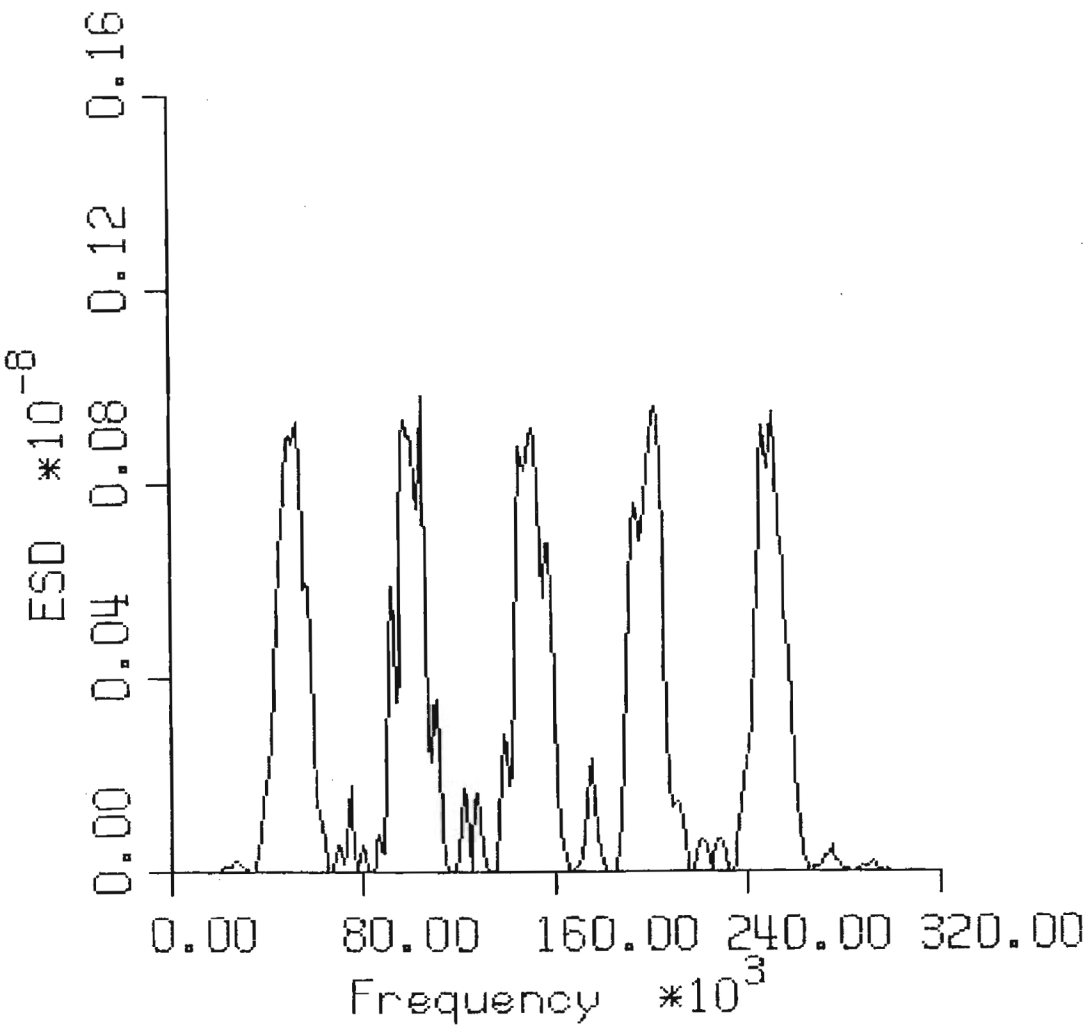

Figure 19. Energy Spectral Density of an N=5 Sequence with a Minimum of Three Cycles Per Sub-Pulse (3,9,12,6,15), T=60 μs.

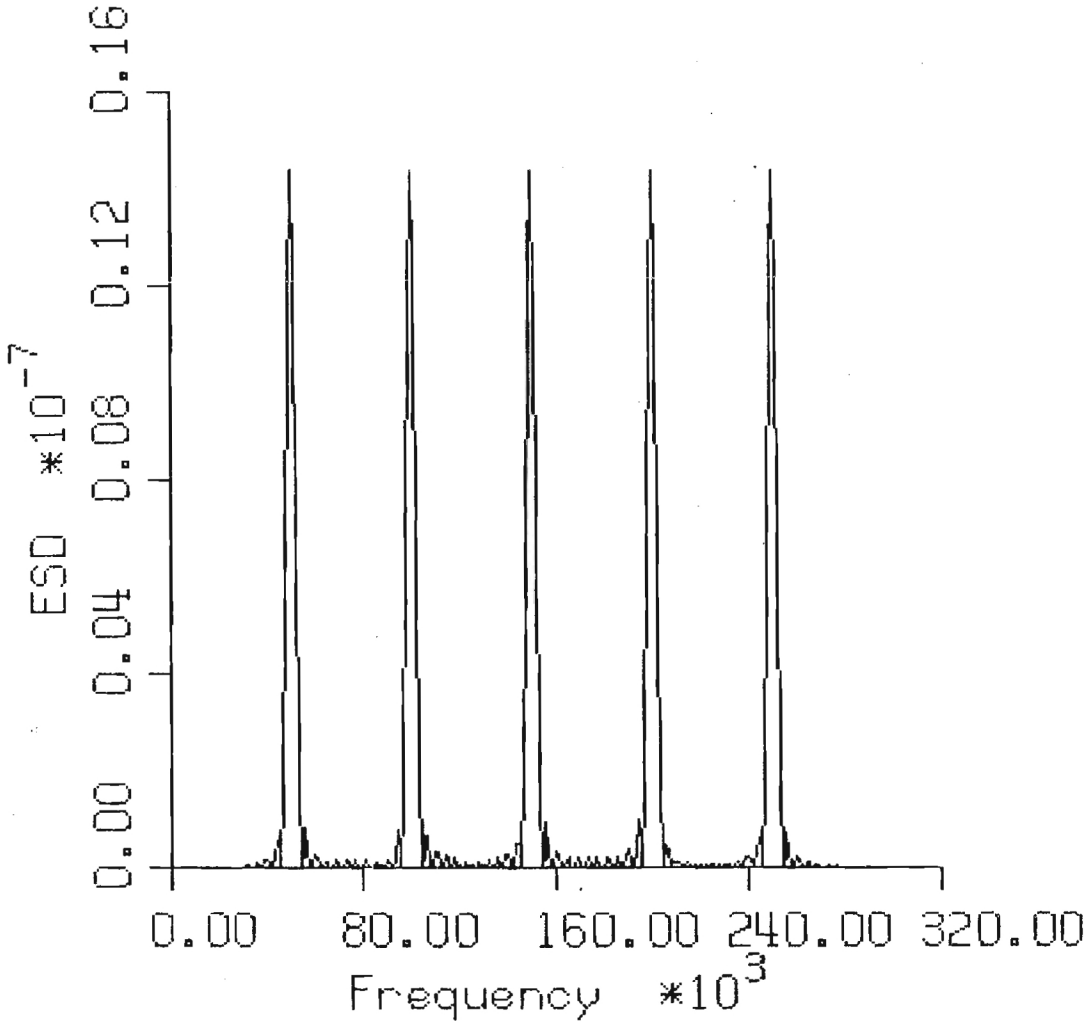

Figure 20. Energy Spectral Density of an N=5 Sequence with a Minimum of Twelve Cycles Per Sub-Pulse (12,36,48,24,60), T=240 μs.

SUB-PULSE PERIOD T (μs)	ΔF_{min} (kHz) v = 10 knots	ΔF_{min} (kHz) v = 20 knots
20	102.7	105.4
40	53.1	56.1
60	36.5	39.7
80	28.2	31.4
100	23.3	26.5
120	20.0	23.2
140	17.6	20.9
160	15.8	19.1
180	14.4	17.7
200	13.3	16.6
220	12.4	15.7
240	11.7	15.0
260	11.1	14.4

Table 5. Minimum Frequency Spacings for Various Sub-Pulse Durations Assuming F_H = 250 kHz with v = 10 knots and v = 20 knots.

To increase the minimum number of cycles per pulse from one to four, every sequence element is incremented by three. The resulting sequence is then multiplied by three to obtain the sequence values shown in Table 4. The firing order becomes

12,18,30,54,45,27,48,33,60,57,51,39,15,24,42,21,36 .

The ESD of the previous sequence is shown in Figure 21. The frequencies of transmission for the previous sequence are 50, 62.5, 75, 87.5, 100, 112.5, 125, 137.5, 150, 162.5, 175, 187.5, 200, 212.5, 225, 237.5 and 250 kHz.

The design of the sub-arrays used to implement the given frequency coverage is now considered. All sensors are assumed to have a bandwidth (BW) centered about the frequency F_o described by

$$BW = F_{3dB+} - F_{3dB-} \tag{81}$$

and

$$F_o = \frac{F_{3dB+} + F_{3dB-}}{2} \tag{82}$$

where F_{3dB+} and F_{3dB-} are the upper and lower 3dB frequencies, respectively, as shown in Figure 22. The Q and BW of the sensors are related by

$$BW = \frac{F_o}{Q} \tag{83}$$

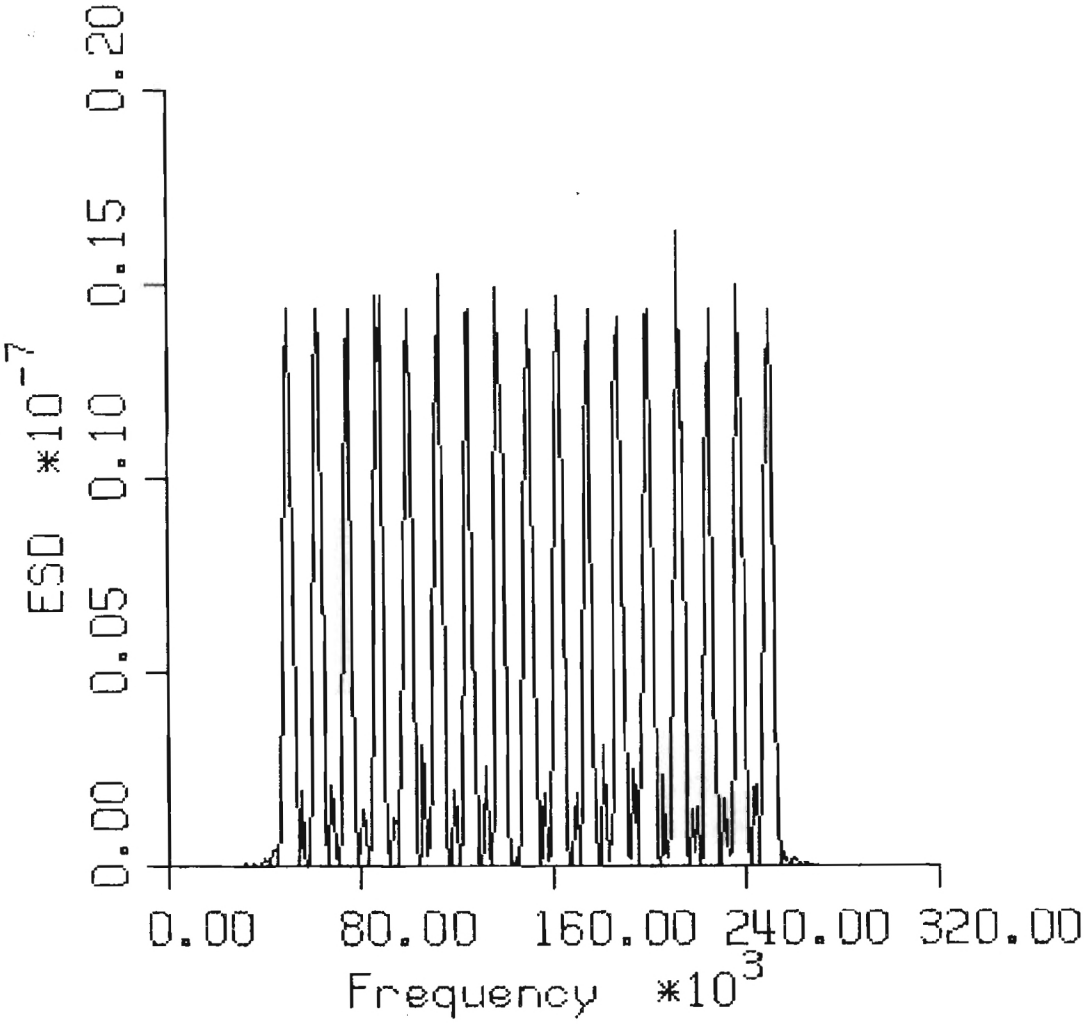

Figure 21. Energy Spectral Density of the Design Example Signal: N=17, (12,18,30,54,45,27,48,33,60,57,51,39,15,24,42,21,36), T=240 s.

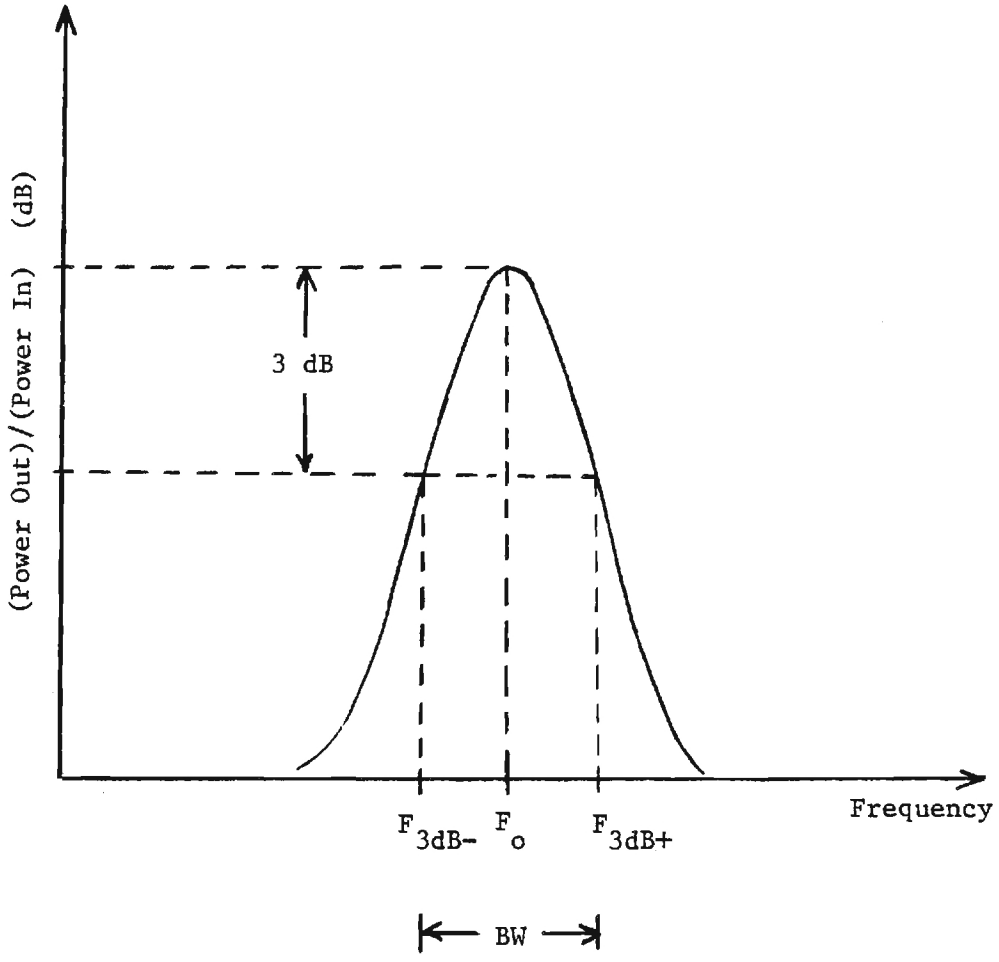

Figure 22. Sensor Frequency Response Parameters.

so that a relationship between Q and the 3dB frequencies may be obtained by using (81) and (82) in (83) to yield

$$Q = \frac{1}{2}\left[\frac{F_{3dB+} + F_{3dB-}}{F_{3dB+} - F_{3dB-}}\right] \tag{84}$$

or

$$F_{3dB-} = F_{3dB+}\left[\frac{Q - \frac{1}{2}}{Q + \frac{1}{2}}\right] \quad . \tag{85}$$

Equation (85) may be used to determine the range of frequencies covered by a sub-array with sensors of a given Q. For the design example of N = 17 and T = 240 μs, the upper 3dB frequency of sub-array M is chosen as

$$F^m_{3dB+} = F_N + \frac{1}{T} = (250 + 4.2)\ \text{kHz} = 254.2\ \text{kHz} \quad .$$

For sensors with Q = 2, the lower 3dB frequency of sub-array M is computed using Equation (85) and found to be 152.5 kHz. The 90% bandwidths of F_{10} = 162.5 kHz through F_{17} = 250 kHz lie within the bandwidth of the sensors of sub-array M. The center frequency of sub-array M (F^m_o) may be chosen midway between F_{10} and F_{17} to ensure maximum response at both end frequencies. The center frequency of the elements in sub-array M becomes

$$F^m_o = \frac{F_{10} + F_{17}}{2} = 206.25\ \text{kHz} \quad . \tag{86}$$

The technique used to determine the frequency coverage of sub-array M is then applied to the remaining frequency range to yield the following results:

$$F_{3dB+}^{m} = F_{17} + \frac{1}{T} = 254.2 \text{ kHz} \qquad F_{3dB-}^{m} = 152.5 > F_{10} - \frac{1}{T}$$

$$F_{3dB+}^{m-1} = F_{9} + \frac{1}{T} = 154.2 \text{ kHz} \qquad F_{3dB-}^{m-1} = 92.5 > F_{5} + \frac{1}{T}$$

$$F_{3dB+}^{m-2} = F_{4} + \frac{1}{T} = 91.7 \text{ kHz} \qquad F_{3dB-}^{m-2} = 55.0 > F_{2} + \frac{1}{T}$$

$$F_{3dB+}^{m-3} = F_{1} + \frac{1}{T} = 54.2 \text{ kHz} \qquad F_{3dB-}^{m-3} = 32.5 > F_{1} + \frac{1}{T}$$

Thus, four sub-arrays are required to provide adequate coverage of the 50 - 250 kHz band for the given example (Q = 2 for all sensors, N = 17, T = 240 μs). The center frequency of each sub-array is chosen as shown in Equation (86). The element spacing is $\lambda/2$ at the highest sub-array frequency to prevent spatial aliasing.

The number of active sub-array elements required at each sub-array frequency is determined as shown in Section 3.2.2. Assuming a broadside beamwidth of 1°, each sub-array consists of 102 active elements at the highest frequency of operation (Equation (73)). The number of active elements at each of the lower frequencies is calculated using Equation (78). The number of active elements which must be added at the lower frequencies is assumed to be an even number so that an equal number of elements may be added on both ends of the sub-array. The number of active elements at each of the N frequencies is shown in Table 6 along with other sub-array design characteristics.

	Element Center Frequency (kHz)	Element Spacing (cm)	Total Number of Sub-Array Elements	Total Sub-Array Length (m)	Frequency (kHz)	Number of Active Elements	Broadside Beamwidth (Degrees)	45° Beamwidth
SUB-ARRAY 1	50	1.50	102	1.52	$F_1 = 50$	102	0.995	1.417
SUB-ARRAY 2	75	0.857	144	1.23	$F_2 = 62.5$	144	0.987	1.405
					$F_3 = 75$	120	0.987	1.405
					$F_4 = 87.5$	102	0.995	1.417
SUB-ARRAY 3	125	0.500	154	0.765	$F_5 = 100$	154	0.988	1.408
					$F_6 = 112.5$	136	0.995	1.417
					$F_7 = 125$	124	0.982	1.398
					$F_8 = 139.5$	112	0.988	1.408
					$F_9 = 150$	102	0.995	1.417
SUB-ARRAY 4	206	0.300	158	0.471	$F_{10} = 162.5$	158	0.988	1.407
					$F_{11} = 175$	146	0.993	1.414
					$F_{12} = 187.5$	136	0.995	1.417
					$F_{13} = 200$	128	0.991	1.411
					$F_{14} = 212.5$	120	0.995	1.417
					$F_{15} = 225$	114	0.989	1.408
					$F_{16} = 237.5$	108	0.989	1.408
					$F_{17} = 250$	102	0.995	1.417

Table 6. Characteristics of the Sub-Arrays Used to Implement the Design Example (N = 17, T = 240μs, Element Q = 2)

The field of view is assumed to be 90° (± 45° measured from broadside). The beam coverage data is given in Tables 7a through 7q for each of the 17 frequencies. The data in these tables was obtained using no shading coefficients. The angles given in the previous tables are measured in degrees with respect to broadside. Results are shown for only 0° to 45° due to the summetry of the beam coverage. As the beams are steered from broadside to ± 45°, the beamwidths of the sub-arrays at ± 45° for all of the frequencies of interest are approximately 1.4° compared with 1° at broadside. The phase shifts computed in Tables 7a through 7q represent the required phase differences between adjacent elements. The characteristics of the sub-arrays used in this design are summarized in Table 6.

The transmitted signal for this design example consists of 17 consecutive sub-pulses. Each sub-pulse duration is 240 μs giving a total transmit time per pulse train of 4.08 μs. If the same array is used for transmit and receive, the minimum range given by Equation (71) is 3.06 m. The pulse train frequency of the N = 17 signal may be computed using Equation (72). For a maximum range of 100 m, the pulse train period must be at least 0.137 s for a pulse train transmission rate of 7.3 Hz.

Finally, the ambiguity function of the N = 17 Welch signal is shown in Figures 23 and 24. The ambiguity function exhibits the general shape of the ideal ''thumbtack'' function with a maximum sidelobe to main peak ratio of less than 0.1176 or -18.6 dB.

Table 7a. Steered Beam Coverage at F_1.

Sub-Array 1 F_1

102 active elements at 50.000 kHz d= .500 wavelengths

Beam #	Max. Response	Lower 3dB	Upper 3dB	Beamwidth	Phase Shift
1	.000	-.497	.497	.995	.000
2	.995	.497	1.492	.995	3.125
3	1.990	1.492	2.488	.995	6.251
4	2.986	2.488	3.484	.996	9.376
5	3.983	3.484	4.481	.997	12.502
6	4.981	4.481	5.480	.999	15.627
7	5.980	5.480	6.480	1.000	18.753
8	6.981	6.480	7.483	1.002	21.878
9	7.985	7.483	8.487	1.005	25.003
10	8.991	8.487	9.495	1.007	28.129
11	9.999	9.495	10.505	1.010	31.254
12	11.011	10.505	11.518	1.014	34.380
13	12.026	11.518	12.535	1.017	37.505
14	13.046	12.535	13.557	1.021	40.631
15	14.069	13.557	14.582	1.026	43.756
16	15.097	14.582	15.613	1.030	46.881
17	16.130	15.613	16.648	1.036	50.007
18	17.168	16.648	17.690	1.041	53.132
19	18.213	17.690	18.737	1.047	56.258
20	19.263	18.737	19.791	1.054	59.383
21	20.320	19.791	20.852	1.061	62.509
22	21.385	20.852	21.920	1.068	65.634
23	22.457	21.920	22.997	1.077	68.759
24	23.538	22.997	24.082	1.085	71.885
25	24.628	24.082	25.176	1.094	75.010
26	25.727	25.176	26.281	1.104	78.136
27	26.837	26.281	27.396	1.115	81.261
28	27.957	27.396	28.522	1.126	84.387
29	29.090	28.522	29.660	1.138	87.512
30	30.235	29.660	30.812	1.152	90.637
31	31.393	30.812	31.978	1.166	93.763
32	32.566	31.978	33.158	1.181	96.888
33	33.754	33.158	34.355	1.197	100.014
34	34.959	34.355	35.569	1.214	103.139
35	36.182	35.569	36.801	1.233	106.265
36	37.425	36.801	38.054	1.253	109.390
37	38.688	38.054	39.329	1.275	112.515
38	39.975	39.329	40.627	1.298	115.641
39	41.286	40.627	41.951	1.324	118.766
40	42.623	41.951	43.303	1.352	121.892
41	43.991	43.303	44.686	1.383	125.017
42	45.390	44.686	46.103	1.417	128.143

Table 7b. Steered Beam Coverage at F_2.

Sub-Array 2 F_2

144 active elements at 62.500 kHz d= .357 wavelengths

Beam #	Max. Response	Lower 3dB	Upper 3dB	Beamwidth	Phase Shift
1	.000	-.493	.493	.987	.000
2	.995	.502	1.488	.987	2.232
3	1.990	1.497	2.484	.987	4.465
4	2.986	2.492	3.480	.988	6.697
5	3.983	3.488	4.477	.989	8.930
6	4.981	4.486	5.476	.990	11.162
7	5.980	5.484	6.476	.992	13.395
8	6.981	6.485	7.478	.994	15.627
9	7.985	7.487	8.483	.996	17.860
10	8.991	8.491	9.490	.999	20.092
11	9.999	9.499	10.501	1.002	22.324
12	11.011	10.509	11.514	1.005	24.557
13	12.026	11.522	12.531	1.009	26.789
14	13.046	12.540	13.552	1.013	29.022
15	14.069	13.561	14.578	1.017	31.254
16	15.097	14.587	15.608	1.022	33.487
17	16.130	15.617	16.644	1.027	35.719
18	17.168	16.653	17.685	1.033	37.952
19	18.213	17.694	18.733	1.039	40.184
20	19.263	18.741	19.786	1.045	42.417
21	20.320	19.795	20.847	1.052	44.649
22	21.385	20.856	21.916	1.060	46.881
23	22.457	21.925	22.992	1.068	49.114
24	23.538	23.001	24.077	1.076	51.346
25	24.628	24.086	25.172	1.085	53.579
26	25.727	25.181	26.276	1.095	55.811
27	26.837	26.285	27.391	1.106	58.044
28	27.957	27.400	28.517	1.117	60.276
29	29.090	28.527	29.656	1.129	62.509
30	30.235	29.665	30.807	1.142	64.741
31	31.393	30.817	31.973	1.156	66.973
32	32.566	31.982	33.153	1.171	69.206
33	33.754	33.163	34.350	1.187	71.438
34	34.959	34.360	35.563	1.204	73.671
35	36.182	35.574	36.796	1.222	75.903
36	37.425	36.806	38.049	1.242	78.136
37	38.688	38.059	39.323	1.264	80.368
38	39.975	39.334	40.621	1.287	82.601
39	41.286	40.632	41.945	1.313	84.833
40	42.623	41.957	43.297	1.341	87.066
41	43.991	43.309	44.680	1.371	89.298
42	45.390	44.692	46.097	1.405	91.530

Table 7c. Steered Beam Coverage at F_3.

Sub-Array 2 F_3

120 active elements at 75.000 kHz d= .429 wavelengths

Beam #	Max. Response	Lower 3dB	Upper 3dB	Beamwidth	Phase Shift
1	.000	-.493	.493	.987	.000
2	.995	.502	1.488	.987	2.679
3	1.990	1.497	2.484	.987	5.358
4	2.986	2.492	3.480	.988	8.037
5	3.983	3.488	4.477	.989	10.716
6	4.981	4.486	5.476	.990	13.395
7	5.980	5.484	6.476	.992	16.074
8	6.981	6.485	7.478	.994	18.753
9	7.985	7.487	8.483	.996	21.431
10	8.991	8.491	9.490	.999	24.110
11	9.999	9.499	10.501	1.002	26.789
12	11.011	10.509	11.514	1.005	29.468
13	12.026	11.522	12.531	1.009	32.147
14	13.046	12.540	13.552	1.013	34.826
15	14.069	13.561	14.578	1.017	37.505
16	15.097	14.587	15.608	1.022	40.184
17	16.130	15.617	16.644	1.027	42.863
18	17.168	16.653	17.685	1.033	45.542
19	18.213	17.694	18.733	1.039	48.221
20	19.263	18.741	19.786	1.045	50.900
21	20.320	19.795	20.847	1.052	53.579
22	21.385	20.856	21.916	1.060	56.258
23	22.457	21.925	22.992	1.068	58.937
24	23.538	23.001	24.077	1.076	61.616
25	24.628	24.086	25.172	1.085	64.295
26	25.727	25.181	26.276	1.095	66.973
27	26.837	26.285	27.391	1.106	69.652
28	27.957	27.400	28.517	1.117	72.331
29	29.090	28.527	29.656	1.129	75.010
30	30.235	29.665	30.807	1.142	77.689
31	31.393	30.817	31.973	1.156	80.368
32	32.566	31.982	33.153	1.171	83.047
33	33.754	33.163	34.350	1.187	85.726
34	34.959	34.360	35.563	1.204	88.405
35	36.182	35.574	36.796	1.222	91.084
36	37.425	36.806	38.049	1.242	93.763
37	38.688	38.059	39.323	1.264	96.442
38	39.975	39.334	40.621	1.287	99.121
39	41.286	40.632	41.945	1.313	101.800
40	42.623	41.957	43.297	1.341	104.479
41	43.991	43.309	44.680	1.371	107.158
42	45.390	44.692	46.097	1.405	109.836

Table 7d. Steered Beam Coverage at F_4.

Sub-Array 2 F_4

102 active elements at 87.500 kHz d= .500 wavelengths

Beam #	Max. Response	Lower 3dB	Upper 3dB	Beamwidth	Phase Shift
1	.000	-.497	.497	.995	.000
2	.995	.497	1.492	.995	3.125
3	1.990	1.492	2.488	.995	6.251
4	2.986	2.488	3.484	.996	9.376
5	3.983	3.484	4.481	.997	12.502
6	4.981	4.481	5.480	.999	15.627
7	5.980	5.480	6.480	1.000	18.753
8	6.981	6.480	7.483	1.002	21.878
9	7.985	7.483	8.487	1.005	25.003
10	8.991	8.487	9.495	1.007	28.129
11	9.999	9.495	10.505	1.010	31.254
12	11.011	10.505	11.518	1.014	34.380
13	12.026	11.518	12.535	1.017	37.505
14	13.046	12.535	13.557	1.021	40.631
15	14.069	13.557	14.582	1.026	43.756
16	15.097	14.582	15.613	1.030	46.881
17	16.130	15.613	16.648	1.036	50.007
18	17.168	16.648	17.690	1.041	53.132
19	18.213	17.690	18.737	1.047	56.258
20	19.263	18.737	19.791	1.054	59.383
21	20.320	19.791	20.852	1.061	62.509
22	21.385	20.852	21.920	1.068	65.634
23	22.457	21.920	22.997	1.077	68.759
24	23.538	22.997	24.082	1.085	71.885
25	24.628	24.082	25.176	1.094	75.010
26	25.727	25.176	26.281	1.104	78.136
27	26.837	26.281	27.396	1.115	81.261
28	27.957	27.396	28.522	1.126	84.387
29	29.090	28.522	29.660	1.138	87.512
30	30.235	29.660	30.812	1.152	90.637
31	31.393	30.812	31.978	1.166	93.763
32	32.566	31.978	33.158	1.181	96.888
33	33.754	33.158	34.355	1.197	100.014
34	34.959	34.355	35.569	1.214	103.139
35	36.182	35.569	36.801	1.233	106.265
36	37.425	36.801	38.054	1.253	109.390
37	38.688	38.054	39.329	1.275	112.515
38	39.975	39.329	40.627	1.298	115.641
39	41.286	40.627	41.951	1.324	118.766
40	42.623	41.951	43.303	1.352	121.892
41	43.991	43.303	44.686	1.383	125.017
42	45.390	44.686	46.103	1.417	128.143

Table 7e. Steered Beam Coverage at F_5.

Sub-Array 3 F_5

154 active elements at 100.000 kHz d= .333 wavelengths

Beam #	Max. Response	Lower 3dB	Upper 3dB	Beamwidth	Phase Shift
1	.000	-.494	.494	.988	.000
2	.995	.501	1.489	.989	2.084
3	1.990	1.496	2.485	.989	4.167
4	2.986	2.491	3.481	.990	6.251
5	3.983	3.487	4.478	.991	8.334
6	4.981	4.485	5.477	.992	10.418
7	5.980	5.483	6.477	.994	12.502
8	6.981	6.484	7.479	.996	14.585
9	7.985	7.486	8.484	.998	16.669
10	8.991	8.491	9.491	1.001	18.753
11	9.999	9.498	10.501	1.004	20.836
12	11.011	10.508	11.515	1.007	22.920
13	12.026	11.522	12.532	1.011	25.003
14	13.046	12.539	13.553	1.015	27.087
15	14.069	13.560	14.579	1.019	29.171
16	15.097	14.586	15.609	1.024	31.254
17	16.130	15.616	16.645	1.029	33.338
18	17.168	16.652	17.686	1.035	35.422
19	18.213	17.693	18.734	1.041	37.505
20	19.263	18.740	19.787	1.047	39.589
21	20.320	19.794	20.848	1.054	41.672
22	21.385	20.855	21.917	1.061	43.756
23	22.457	21.924	22.993	1.070	45.840
24	23.538	23.000	24.078	1.078	47.923
25	24.628	24.085	25.173	1.087	50.007
26	25.727	25.180	26.277	1.097	52.090
27	26.837	26.284	27.392	1.108	54.174
28	27.957	27.399	28.518	1.119	56.258
29	29.090	28.526	29.657	1.131	58.341
30	30.235	29.664	30.808	1.144	60.425
31	31.393	30.816	31.974	1.158	62.509
32	32.566	31.981	33.154	1.173	64.592
33	33.754	33.162	34.351	1.189	66.676
34	34.959	34.359	35.565	1.206	68.759
35	36.182	35.573	36.797	1.225	70.843
36	37.425	36.805	38.050	1.245	72.927
37	38.688	38.058	39.324	1.266	75.010
38	39.975	39.333	40.623	1.290	77.094
39	41.286	40.631	41.947	1.315	79.178
40	42.623	41.955	43.299	1.343	81.261
41	43.991	43.308	44.681	1.374	83.345
42	45.390	44.691	46.098	1.408	85.428

Table 7f. Steered Beam Coverage at F_6.

Sub-Array 3 F_6

136 active elements at 112.500 kHz d= .375 wavelengths

Beam #	Max. Response	Lower 3dB	Upper 3dB	Beamwidth	Phase Shift
1	.000	-.497	.497	.995	.000
2	.995	.497	1.492	.995	2.344
3	1.990	1.492	2.488	.995	4.688
4	2.986	2.488	3.484	.996	7.032
5	3.983	3.484	4.481	.997	9.376
6	4.981	4.481	5.480	.999	11.720
7	5.980	5.480	6.480	1.000	14.064
8	6.981	6.480	7.483	1.002	16.408
9	7.985	7.483	8.487	1.005	18.753
10	8.991	8.487	9.495	1.007	21.097
11	9.999	9.495	10.505	1.010	23.441
12	11.011	10.505	11.518	1.014	25.785
13	12.026	11.518	12.535	1.017	28.129
14	13.046	12.535	13.557	1.021	30.473
15	14.069	13.557	14.582	1.026	32.817
16	15.097	14.582	15.613	1.030	35.161
17	16.130	15.613	16.648	1.036	37.505
18	17.168	16.648	17.690	1.041	39.849
19	18.213	17.690	18.737	1.047	42.193
20	19.263	18.737	19.791	1.054	44.537
21	20.320	19.791	20.852	1.061	46.881
22	21.385	20.852	21.920	1.068	49.225
23	22.457	21.920	22.997	1.077	51.570
24	23.538	22.997	24.082	1.085	53.914
25	24.628	24.082	25.176	1.094	56.258
26	25.727	25.176	26.281	1.104	58.602
27	26.837	26.281	27.396	1.115	60.946
28	27.957	27.396	28.522	1.126	63.290
29	29.090	28.522	29.660	1.138	65.634
30	30.235	29.660	30.812	1.152	67.978
31	31.393	30.812	31.978	1.165	70.322
32	32.566	31.978	33.158	1.181	72.666
33	33.754	33.158	34.355	1.197	75.010
34	34.959	34.355	35.569	1.214	77.354
35	36.182	35.569	36.801	1.233	79.698
36	37.425	36.801	38.054	1.253	82.043
37	38.688	38.054	39.329	1.275	84.387
38	39.975	39.329	40.627	1.298	86.731
39	41.286	40.627	41.951	1.324	89.075
40	42.623	41.951	43.303	1.352	91.419
41	43.991	43.303	44.686	1.383	93.763
42	45.390	44.686	46.103	1.417	96.107

Table 7g. Steered Beam Coverage at F_7.

Sub-Array 3 F_7

124 active elements at 125.000 kHz d= .417 wavelengths

Beam #	Max. Response	Lower 3dB	Upper 3dB	Beamwidth	Phase Shift
1	.000	-.491	.491	.982	.000
2	.995	.504	1.486	.982	2.605
3	1.990	1.499	2.481	.983	5.209
4	2.986	2.494	3.478	.983	7.814
5	3.983	3.491	4.475	.984	10.418
6	4.981	4.488	5.474	.986	13.023
7	5.980	5.486	6.474	.987	15.627
8	6.981	6.487	7.476	.989	18.232
9	7.985	7.489	8.481	.992	20.836
10	8.991	8.494	9.488	.994	23.441
11	9.999	9.501	10.498	.997	26.045
12	11.011	10.511	11.512	1.000	28.650
13	12.026	11.525	12.529	1.004	31.254
14	13.046	12.542	13.550	1.008	33.859
15	14.069	13.563	14.576	1.012	36.463
16	15.097	14.589	15.606	1.017	39.068
17	16.130	15.619	16.642	1.022	41.672
18	17.168	16.655	17.683	1.028	44.277
19	18.213	17.696	18.730	1.034	46.881
20	19.263	18.744	19.784	1.040	49.486
21	20.320	19.798	20.845	1.047	52.090
22	21.385	20.859	21.913	1.055	54.695
23	22.457	21.927	22.990	1.063	57.299
24	23.538	23.004	24.075	1.071	59.904
25	24.628	24.089	25.169	1.080	62.509
26	25.727	25.183	26.274	1.090	65.113
27	26.837	26.288	27.388	1.101	67.718
28	27.957	27.403	28.515	1.112	70.322
29	29.090	28.529	29.653	1.124	72.927
30	30.235	29.668	30.805	1.137	75.531
31	31.393	30.819	31.970	1.150	78.136
32	32.566	31.985	33.150	1.165	80.740
33	33.754	33.166	34.347	1.181	83.345
34	34.959	34.362	35.561	1.198	85.949
35	36.182	35.576	36.793	1.217	88.554
36	37.425	36.809	38.046	1.237	91.158
37	38.688	38.062	39.320	1.258	93.763
38	39.975	39.337	40.618	1.282	96.367
39	41.286	40.635	41.942	1.307	98.972
40	42.623	41.960	43.294	1.335	101.576
41	43.991	43.312	44.677	1.365	104.181
42	45.390	44.695	46.094	1.398	106.785

Table 7h. Steered Beam Coverage at F_8.

Sub-Array 3 F_8

112 active elements at 137.500 kHz d= .458 wavelengths

Beam #	Max. Response	Lower 3dB	Upper 3dB	Beamwidth	Phase Shift
1	.000	-.494	.494	.988	.000
2	.995	.501	1.489	.989	2.865
3	1.990	1.496	2.485	.989	5.730
4	2.986	2.491	3.481	.990	8.595
5	3.983	3.487	4.478	.991	11.460
6	4.981	4.485	5.477	.992	14.325
7	5.980	5.483	6.477	.994	17.190
8	6.981	6.484	7.479	.996	20.055
9	7.985	7.486	8.484	.998	22.920
10	8.991	8.491	9.491	1.001	25.785
11	9.999	9.498	10.501	1.004	28.650
12	11.011	10.508	11.515	1.007	31.515
13	12.026	11.522	12.532	1.011	34.380
14	13.046	12.539	13.553	1.015	37.245
15	14.069	13.560	14.579	1.019	40.110
16	15.097	14.586	15.609	1.024	42.975
17	16.130	15.616	16.645	1.029	45.840
18	17.168	16.652	17.686	1.035	48.705
19	18.213	17.693	18.734	1.041	51.570
20	19.263	18.740	19.787	1.047	54.435
21	20.320	19.794	20.848	1.054	57.300
22	21.385	20.855	21.917	1.061	60.164
23	22.457	21.924	22.993	1.070	63.029
24	23.538	23.000	24.078	1.078	65.894
25	24.628	24.085	25.173	1.087	68.759
26	25.727	25.180	26.277	1.097	71.624
27	26.837	26.284	27.392	1.108	74.489
28	27.957	27.399	28.518	1.119	77.354
29	29.090	28.526	29.657	1.131	80.219
30	30.235	29.664	30.808	1.144	83.084
31	31.393	30.816	31.974	1.158	85.949
32	32.566	31.981	33.154	1.173	88.814
33	33.754	33.162	34.351	1.189	91.679
34	34.959	34.359	35.565	1.206	94.544
35	36.182	35.573	36.797	1.225	97.409
36	37.425	36.805	38.050	1.245	100.274
37	38.688	38.058	39.324	1.266	103.139
38	39.975	39.333	40.623	1.290	106.004
39	41.286	40.631	41.947	1.315	108.869
40	42.623	41.955	43.299	1.343	111.734
41	43.991	43.308	44.681	1.374	114.599
42	45.390	44.691	46.098	1.408	117.464

Table 7i. Steered Beam Coverage at F_9.

Sub-Array 3 F_9

102 active elements at 150.000 kHz d= .500 wavelengths

Beam #	Max. Response	Lower 3dB	Upper 3dB	Beamwidth	Phase Shift
1	.000	-.497	.497	.995	.000
2	.995	.497	1.492	.995	3.125
3	1.990	1.492	2.488	.995	6.251
4	2.986	2.488	3.484	.996	9.376
5	3.983	3.484	4.481	.997	12.502
6	4.981	4.481	5.480	.999	15.627
7	5.980	5.480	6.480	1.000	18.753
8	6.981	6.480	7.483	1.002	21.878
9	7.985	7.483	8.487	1.005	25.003
10	8.991	8.487	9.495	1.007	28.129
11	9.999	9.495	10.505	1.010	31.254
12	11.011	10.505	11.518	1.014	34.380
13	12.026	11.518	12.535	1.017	37.505
14	13.046	12.535	13.557	1.021	40.631
15	14.069	13.557	14.582	1.026	43.756
16	15.097	14.582	15.613	1.030	46.881
17	16.130	15.613	16.648	1.036	50.007
18	17.168	16.648	17.690	1.041	53.132
19	18.213	17.690	18.737	1.047	56.258
20	19.263	18.737	19.791	1.054	59.383
21	20.320	19.791	20.852	1.061	62.509
22	21.385	20.852	21.920	1.068	65.634
23	22.457	21.920	22.997	1.077	68.759
24	23.538	22.997	24.082	1.085	71.885
25	24.628	24.082	25.176	1.094	75.010
26	25.727	25.176	26.281	1.104	78.136
27	26.837	26.281	27.396	1.115	81.261
28	27.957	27.396	28.522	1.126	84.387
29	29.090	28.522	29.660	1.138	87.512
30	30.235	29.660	30.812	1.152	90.637
31	31.393	30.812	31.978	1.166	93.763
32	32.566	31.978	33.158	1.181	96.888
33	33.754	33.158	34.355	1.197	100.014
34	34.959	34.355	35.569	1.214	103.139
35	36.182	35.569	36.801	1.233	106.265
36	37.425	36.801	38.054	1.253	109.390
37	38.688	38.054	39.329	1.275	112.515
38	39.975	39.329	40.627	1.298	115.641
39	41.286	40.627	41.951	1.324	118.766
40	42.623	41.951	43.303	1.352	121.892
41	43.991	43.303	44.686	1.383	125.017
42	45.390	44.686	46.103	1.417	128.143

Table 7j. Steered Beam Coverage at F_{10}.

Sub-Array 4 F_{10}

158 active elements at 162.500 kHz d= .325 wavelengths

Beam #	Max. Response	Lower 3dB	Upper 3dB	Beamwidth	Phase Shift
1	.000	-.494	.494	.988	.000
2	.995	.501	1.489	.988	2.032
3	1.990	1.496	2.485	.989	4.063
4	2.986	2.491	3.481	.989	6.095
5	3.983	3.488	4.478	.990	8.126
6	4.981	4.485	5.477	.992	10.158
7	5.980	5.483	6.477	.993	12.189
8	6.981	6.484	7.479	.995	14.221
9	7.985	7.486	8.484	.998	16.252
10	8.991	8.491	9.491	1.000	18.284
11	9.999	9.498	10.501	1.003	20.315
12	11.011	10.508	11.515	1.007	22.347
13	12.026	11.522	12.532	1.010	24.378
14	13.046	12.539	13.553	1.014	26.410
15	14.069	13.560	14.579	1.019	28.441
16	15.097	14.586	15.609	1.023	30.473
17	16.130	15.616	16.645	1.029	32.504
18	17.168	16.652	17.686	1.034	34.536
19	18.213	17.693	18.733	1.040	36.567
20	19.263	18.741	19.787	1.047	38.599
21	20.320	19.794	20.848	1.054	40.631
22	21.385	20.855	21.917	1.061	42.662
23	22.457	21.924	22.993	1.069	44.694
24	23.538	23.000	24.078	1.078	46.725
25	24.628	24.086	25.173	1.087	48.757
26	25.727	25.180	26.277	1.097	50.788
27	26.837	26.284	27.392	1.107	52.820
28	27.957	27.399	28.518	1.119	54.851
29	29.090	28.526	29.657	1.131	56.883
30	30.235	29.664	30.808	1.144	58.914
31	31.393	30.816	31.974	1.158	60.946
32	32.566	31.982	33.154	1.172	62.977
33	33.754	33.162	34.351	1.188	65.009
34	34.959	34.359	35.564	1.206	67.040
35	36.182	35.573	36.797	1.224	69.072
36	37.425	36.805	38.050	1.244	71.104
37	38.688	38.058	39.324	1.266	73.135
38	39.975	39.333	40.622	1.289	75.167
39	41.286	40.631	41.946	1.315	77.198
40	42.623	41.956	43.298	1.343	79.230
41	43.991	43.308	44.681	1.373	81.261
42	45.390	44.691	46.098	1.407	83.293

Table 7k. Steered Beam Coverage at F_{11}.

Sub-Array 4 F_{11}

146 active elements at 175.000 kHz d= .350 wavelengths

Beam #	Max. Response	Lower 3dB	Upper 3dB	Beamwidth	Phase Shift
1	.000	-.496	.496	.993	.000
2	.995	.498	1.491	.993	2.188
3	1.990	1.493	2.487	.994	4.376
4	2.986	2.489	3.483	.994	6.563
5	3.983	3.485	4.480	.995	8.751
6	4.981	4.482	5.479	.997	10.939
7	5.980	5.481	6.479	.998	13.127
8	6.981	6.481	7.482	1.000	15.315
9	7.985	7.484	8.486	1.003	17.502
10	8.991	8.488	9.494	1.005	19.690
11	9.999	9.495	10.504	1.008	21.878
12	11.011	10.506	11.517	1.012	24.066
13	12.026	11.519	12.534	1.015	26.254
14	13.046	12.536	13.556	1.019	28.441
15	14.069	13.558	14.581	1.024	30.629
16	15.097	14.583	15.612	1.028	32.817
17	16.130	15.614	16.647	1.034	35.005
18	17.168	16.649	17.689	1.039	37.193
19	18.213	17.691	18.736	1.045	39.380
20	19.263	18.738	19.790	1.052	41.568
21	20.320	19.792	20.851	1.059	43.756
22	21.385	20.853	21.919	1.066	45.944
23	22.457	21.921	22.996	1.074	48.132
24	23.538	22.998	24.081	1.083	50.319
25	24.628	24.083	25.175	1.092	52.507
26	25.727	25.177	26.280	1.102	54.695
27	26.837	26.282	27.395	1.113	56.883
28	27.957	27.397	28.521	1.124	59.071
29	29.090	28.523	29.659	1.136	61.258
30	30.235	29.662	30.811	1.149	63.446
31	31.393	30.813	31.976	1.163	65.634
32	32.566	31.979	33.157	1.178	67.822
33	33.754	33.159	34.353	1.194	70.010
34	34.959	34.356	35.567	1.212	72.197
35	36.182	35.570	36.800	1.230	74.385
36	37.425	36.802	38.053	1.250	76.573
37	38.688	38.055	39.327	1.272	78.761
38	39.975	39.330	40.626	1.296	80.949
39	41.286	40.628	41.950	1.321	83.136
40	42.623	41.952	43.302	1.350	85.324
41	43.991	43.304	44.685	1.380	87.512
42	45.390	44.687	46.101	1.414	89.700

Table 71. Steered Beam Coverage at F_{12}.

Sub-Array 4 F_{12}

136 active elements at 187.500 kHz d= .375 wavelengths

Beam #	Max. Response	Lower 3dB	Upper 3dB	Beamwidth	Phase Shift
1	.000	-.497	.497	.995	.000
2	.995	.497	1.492	.995	2.344
3	1.990	1.492	2.488	.995	4.688
4	2.986	2.488	3.484	.996	7.032
5	3.983	3.484	4.481	.997	9.376
6	4.981	4.481	5.480	.999	11.720
7	5.980	5.480	6.480	1.000	14.064
8	6.981	6.480	7.483	1.002	16.408
9	7.985	7.483	8.487	1.005	18.753
10	8.991	8.487	9.495	1.007	21.097
11	9.999	9.495	10.505	1.010	23.441
12	11.011	10.505	11.518	1.014	25.785
13	12.026	11.518	12.535	1.017	28.129
14	13.046	12.535	13.557	1.021	30.473
15	14.069	13.557	14.582	1.026	32.817
16	15.097	14.582	15.613	1.030	35.161
17	16.130	15.613	16.648	1.036	37.505
18	17.168	16.648	17.690	1.041	39.849
19	18.213	17.690	18.737	1.047	42.193
20	19.263	18.737	19.791	1.054	44.537
21	20.320	19.791	20.852	1.061	46.881
22	21.385	20.852	21.920	1.068	49.225
23	22.457	21.920	22.997	1.077	51.570
24	23.538	22.997	24.082	1.085	53.914
25	24.628	24.082	25.176	1.094	56.258
26	25.727	25.176	26.281	1.104	58.602
27	26.837	26.281	27.396	1.115	60.946
28	27.957	27.396	28.522	1.126	63.290
29	29.090	28.522	29.660	1.138	65.634
30	30.235	29.660	30.812	1.152	67.978
31	31.393	30.812	31.978	1.165	70.322
32	32.566	31.978	33.158	1.181	72.666
33	33.754	33.158	34.355	1.197	75.010
34	34.959	34.355	35.569	1.214	77.354
35	36.182	35.569	36.801	1.233	79.698
36	37.425	36.801	38.054	1.253	82.043
37	38.688	38.054	39.329	1.275	84.387
38	39.975	39.329	40.627	1.298	86.731
39	41.286	40.627	41.951	1.324	89.075
40	42.623	41.951	43.303	1.352	91.419
41	43.991	43.303	44.686	1.383	93.763
42	45.390	44.686	46.103	1.417	96.107

Table 7m. Steered Beam Coverage at F_{13}.

Sub-Array 4 F_{13}

128 active elements at 200.000 kHz d= .400 wavelengths

Beam #	Max. Response	Lower 3dB	Upper 3dB	Beamwidth	Phase Shift
1	.000	-.495	.495	.991	.000
2	.995	.499	1.491	.991	2.500
3	1.990	1.494	2.486	.992	5.001
4	2.986	2.490	3.482	.992	7.501
5	3.983	3.486	4.479	.993	10.001
6	4.981	4.483	5.478	.995	12.502
7	5.980	5.482	6.478	.996	15.002
8	6.981	6.482	7.481	.998	17.502
9	7.985	7.485	8.485	1.001	20.003
10	8.991	8.489	9.493	1.003	22.503
11	9.999	9.496	10.503	1.006	25.003
12	11.011	10.507	11.516	1.010	27.504
13	12.026	11.520	12.533	1.013	30.004
14	13.046	12.537	13.555	1.017	32.504
15	14.069	13.559	14.580	1.022	35.005
16	15.097	14.584	15.611	1.026	37.505
17	16.130	15.615	16.646	1.032	40.005
18	17.168	16.650	17.688	1.037	42.506
19	18.213	17.692	18.735	1.043	45.006
20	19.263	18.739	19.789	1.050	47.506
21	20.320	19.793	20.850	1.057	50.007
22	21.385	20.854	21.918	1.064	52.507
23	22.457	21.922	22.995	1.072	55.008
24	23.538	22.999	24.080	1.081	57.508
25	24.628	24.084	25.174	1.090	60.008
26	25.727	25.178	26.279	1.100	62.509
27	26.837	26.283	27.393	1.111	65.009
28	27.957	27.398	28.520	1.122	67.509
29	29.090	28.524	29.658	1.134	70.010
30	30.235	29.663	30.810	1.147	72.510
31	31.393	30.814	31.975	1.161	75.010
32	32.566	31.980	33.156	1.176	77.511
33	33.754	33.160	34.352	1.192	80.011
34	34.959	34.357	35.566	1.209	82.511
35	36.182	35.571	36.799	1.228	85.012
36	37.425	36.804	38.052	1.248	87.512
37	38.688	38.056	39.326	1.270	90.012
38	39.975	39.331	40.624	1.293	92.513
39	41.286	40.629	41.948	1.319	95.013
40	42.623	41.954	43.300	1.347	97.513
41	43.991	43.306	44.683	1.378	100.014
42	45.390	44.689	46.100	1.411	102.514

Table 7n. Steered Beam Coverage at F_{14}.

Sub-Array 4 F_{14}

120 active elements at 212.500 kHz d= .425 wavelengths

Beam #	Max. Response	Lower 3dB	Upper 3dB	Beamwidth	Phase Shift
1	.000	-.497	.497	.995	.000
2	.995	.497	1.492	.995	2.657
3	1.990	1.492	2.488	.995	5.313
4	2.986	2.488	3.484	.996	7.970
5	3.983	3.484	4.481	.997	10.626
6	4.981	4.481	5.480	.999	13.283
7	5.980	5.480	6.480	1.000	15.940
8	6.981	6.480	7.483	1.002	18.596
9	7.985	7.483	8.487	1.005	21.253
10	8.991	8.487	9.495	1.007	23.910
11	9.999	9.495	10.505	1.010	26.566
12	11.011	10.505	11.518	1.014	29.223
13	12.026	11.518	12.535	1.017	31.879
14	13.046	12.535	13.557	1.021	34.536
15	14.069	13.557	14.582	1.026	37.193
16	15.097	14.582	15.613	1.030	39.849
17	16.130	15.613	16.648	1.036	42.506
18	17.168	16.648	17.690	1.041	45.162
19	18.213	17.690	18.737	1.047	47.819
20	19.263	18.737	19.791	1.054	50.476
21	20.320	19.791	20.852	1.061	53.132
22	21.385	20.852	21.920	1.068	55.789
23	22.457	21.920	22.997	1.077	58.445
24	23.538	22.997	24.082	1.085	61.102
25	24.628	24.082	25.176	1.094	63.759
26	25.727	25.176	26.281	1.104	66.415
27	26.837	26.281	27.396	1.115	69.072
28	27.957	27.396	28.522	1.126	71.729
29	29.090	28.522	29.660	1.138	74.385
30	30.235	29.660	30.812	1.152	77.042
31	31.393	30.812	31.978	1.165	79.698
32	32.566	31.978	33.158	1.181	82.355
33	33.754	33.158	34.355	1.197	85.012
34	34.959	34.355	35.569	1.214	87.668
35	36.182	35.569	36.801	1.233	90.325
36	37.425	36.801	38.054	1.253	92.982
37	38.688	38.054	39.329	1.275	95.638
38	39.975	39.329	40.627	1.298	98.295
39	41.286	40.627	41.951	1.324	100.951
40	42.623	41.951	43.303	1.352	103.608
41	43.991	43.303	44.686	1.383	106.265
42	45.390	44.686	46.103	1.417	108.921

Table 7o. Steered Beam Coverage at F_{15}.

Sub-Array 4 F_{15}

114 active elements at 225.000 kHz d= .450 wavelengths

Beam #	Max. Response	Lower 3dB	Upper 3dB	Beamwidth	Phase Shift
1	.000	-.495	.495	.989	.000
2	.995	.500	1.490	.989	2.813
3	1.990	1.495	2.485	.990	5.626
4	2.986	2.491	3.481	.990	8.439
5	3.983	3.487	4.478	.991	11.252
6	4.981	4.484	5.477	.993	14.064
7	5.980	5.483	6.477	.994	16.877
8	6.981	6.483	7.480	.996	19.690
9	7.985	7.486	8.484	.999	22.503
10	8.991	8.490	9.492	1.001	25.316
11	9.999	9.497	10.502	1.004	28.129
12	11.011	10.508	11.515	1.008	30.942
13	12.026	11.521	12.532	1.011	33.755
14	13.046	12.538	13.554	1.015	36.567
15	14.069	13.560	14.579	1.020	39.380
16	15.097	14.585	15.610	1.024	42.193
17	16.130	15.616	16.645	1.030	45.006
18	17.168	16.651	17.687	1.035	47.819
19	18.213	17.693	18.734	1.041	50.632
20	19.263	18.740	19.788	1.048	53.445
21	20.320	19.794	20.849	1.055	56.258
22	21.385	20.855	21.917	1.062	59.071
23	22.457	21.923	22.994	1.070	61.883
24	23.538	23.000	24.079	1.079	64.696
25	24.628	24.085	25.173	1.088	67.509
26	25.727	25.180	26.277	1.098	70.322
27	26.837	26.284	27.392	1.108	73.135
28	27.957	27.399	28.519	1.120	75.948
29	29.090	28.525	29.657	1.132	78.761
30	30.235	29.664	30.809	1.145	81.574
31	31.393	30.815	31.974	1.159	84.387
32	32.566	31.981	33.155	1.174	87.199
33	33.754	33.162	34.351	1.190	90.012
34	34.959	34.358	35.565	1.207	92.825
35	36.182	35.572	36.798	1.225	95.638
36	37.425	36.805	38.050	1.245	98.451
37	38.688	38.058	39.325	1.267	101.264
38	39.975	39.332	40.623	1.291	104.077
39	41.286	40.631	41.947	1.316	106.890
40	42.623	41.955	43.299	1.344	109.703
41	43.991	43.307	44.682	1.375	112.515
42	45.390	44.690	46.099	1.408	115.328

Table 7p. Steered Beam Coverage at F_{16}.

Sub-Array 4 F_{16}

108 active elements at 237.500 kHz d= .475 wavelengths

Beam #	Max. Response	Lower 3dB	Upper 3dB	Beamwidth	Phase Shift
1	.000	-.495	.495	.989	.000
2	.995	.500	1.490	.989	2.969
3	1.990	1.495	2.485	.990	5.938
4	2.986	2.491	3.481	.990	8.907
5	3.983	3.487	4.478	.991	11.877
6	4.981	4.484	5.477	.993	14.846
7	5.980	5.483	6.477	.994	17.815
8	6.981	6.483	7.480	.996	20.784
9	7.985	7.486	8.484	.999	23.753
10	8.991	8.490	9.492	1.001	26.722
11	9.999	9.497	10.502	1.004	29.692
12	11.011	10.508	11.515	1.008	32.661
13	12.026	11.521	12.532	1.011	35.630
14	13.046	12.538	13.554	1.015	38.599
15	14.069	13.560	14.579	1.020	41.568
16	15.097	14.585	15.610	1.024	44.537
17	16.130	15.616	16.645	1.030	47.506
18	17.168	16.651	17.687	1.035	50.476
19	18.213	17.693	18.734	1.041	53.445
20	19.263	18.740	19.788	1.048	56.414
21	20.320	19.794	20.849	1.055	59.383
22	21.385	20.855	21.917	1.062	62.352
23	22.457	21.923	22.994	1.070	65.321
24	23.538	23.000	24.079	1.079	68.291
25	24.628	24.085	25.173	1.088	71.260
26	25.727	25.180	26.277	1.098	74.229
27	26.837	26.284	27.392	1.108	77.198
28	27.957	27.399	28.519	1.120	80.167
29	29.090	28.525	29.657	1.132	83.136
30	30.235	29.664	30.809	1.145	86.106
31	31.393	30.815	31.974	1.159	89.075
32	32.566	31.981	33.155	1.174	92.044
33	33.754	33.162	34.351	1.190	95.013
34	34.959	34.358	35.565	1.207	97.982
35	36.182	35.572	36.798	1.225	100.951
36	37.425	36.805	38.050	1.245	103.921
37	38.688	38.058	39.325	1.267	106.890
38	39.975	39.332	40.623	1.291	109.859
39	41.286	40.631	41.947	1.316	112.828
40	42.623	41.955	43.299	1.344	115.797
41	43.991	43.307	44.682	1.375	118.766
42	45.390	44.690	46.099	1.408	121.735

Table 7q. Steered Beam Coverage at F_{17}.

Sub-Array 4 F_{17}

102 active elements at 250.000 kHz d= .500 wavelengths

Beam #	Max. Response	Lower 3dB	Upper 3dB	Beamwidth	Phase Shift
1	.000	-.497	.497	.995	.000
2	.995	.497	1.492	.995	3.125
3	1.990	1.492	2.488	.995	6.251
4	2.986	2.488	3.484	.996	9.376
5	3.983	3.484	4.481	.997	12.502
6	4.981	4.481	5.480	.999	15.627
7	5.980	5.480	6.480	1.000	18.753
8	6.981	6.480	7.483	1.002	21.878
9	7.985	7.483	8.487	1.005	25.003
10	8.991	8.487	9.495	1.007	28.129
11	9.999	9.495	10.505	1.010	31.254
12	11.011	10.505	11.518	1.014	34.380
13	12.026	11.518	12.535	1.017	37.505
14	13.046	12.535	13.557	1.021	40.631
15	14.069	13.557	14.582	1.026	43.756
16	15.097	14.582	15.613	1.030	46.881
17	16.130	15.613	16.648	1.036	50.007
18	17.168	16.648	17.690	1.041	53.132
19	18.213	17.690	18.737	1.047	56.258
20	19.263	18.737	19.791	1.054	59.383
21	20.320	19.791	20.852	1.061	62.509
22	21.385	20.852	21.920	1.068	65.634
23	22.457	21.920	22.997	1.077	68.759
24	23.538	22.997	24.082	1.085	71.885
25	24.628	24.082	25.176	1.094	75.010
26	25.727	25.176	26.281	1.104	78.136
27	26.837	26.281	27.396	1.115	81.261
28	27.957	27.396	28.522	1.126	84.387
29	29.090	28.522	29.660	1.138	87.512
30	30.235	29.660	30.812	1.152	90.637
31	31.393	30.812	31.978	1.166	93.763
32	32.566	31.978	33.158	1.181	96.888
33	33.754	33.158	34.355	1.197	100.014
34	34.959	34.355	35.569	1.214	103.139
35	36.182	35.569	36.801	1.233	106.265
36	37.425	36.801	38.054	1.253	109.390
37	38.688	38.054	39.329	1.275	112.515
38	39.975	39.329	40.627	1.298	115.641
39	41.286	40.627	41.951	1.324	118.766
40	42.623	41.951	43.303	1.352	121.892
41	43.991	43.303	44.686	1.383	125.017
42	45.390	44.686	46.103	1.417	128.143

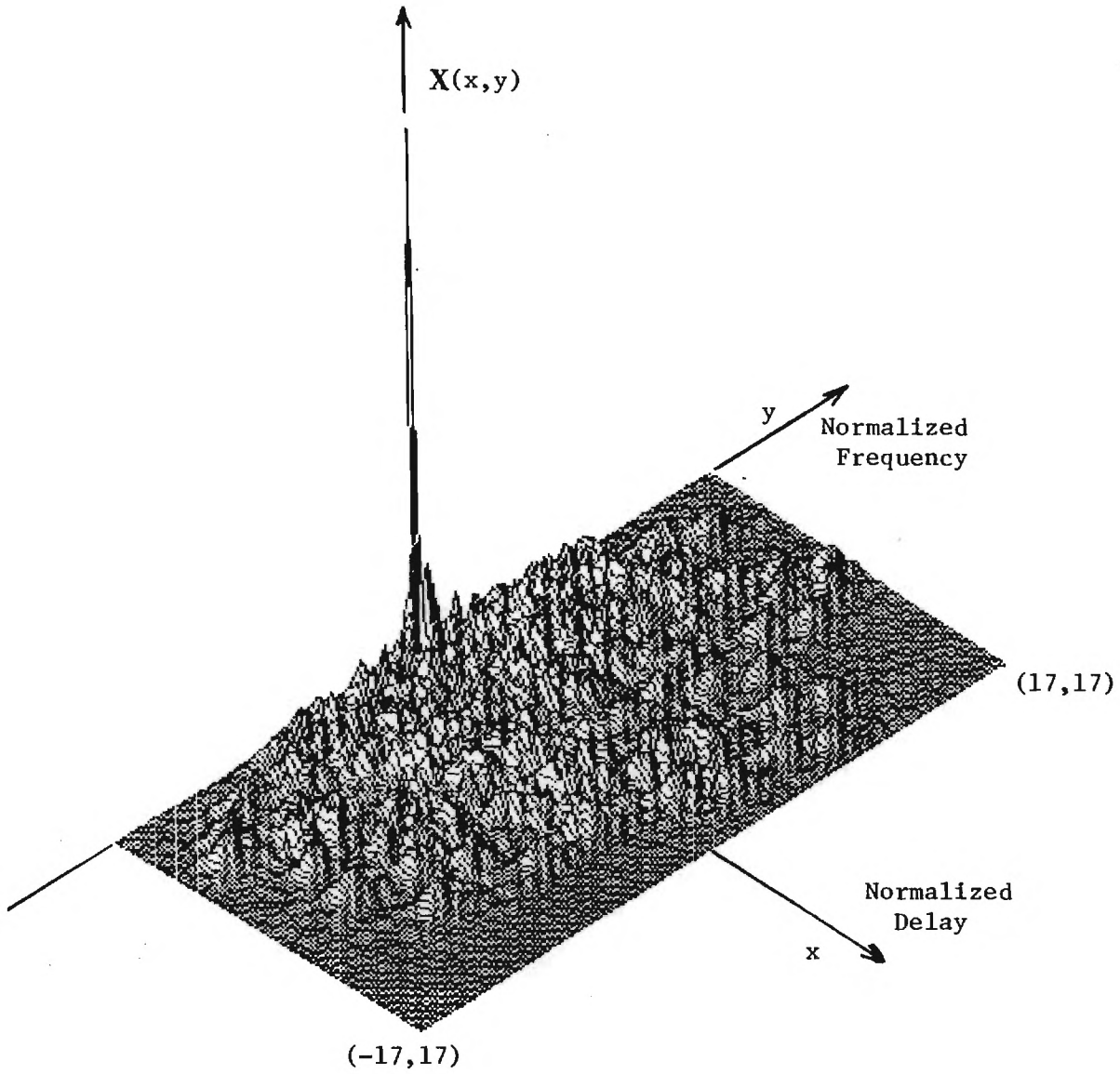

Figure 23. Ambiguity Function of the Design Example Sequence (N=17).

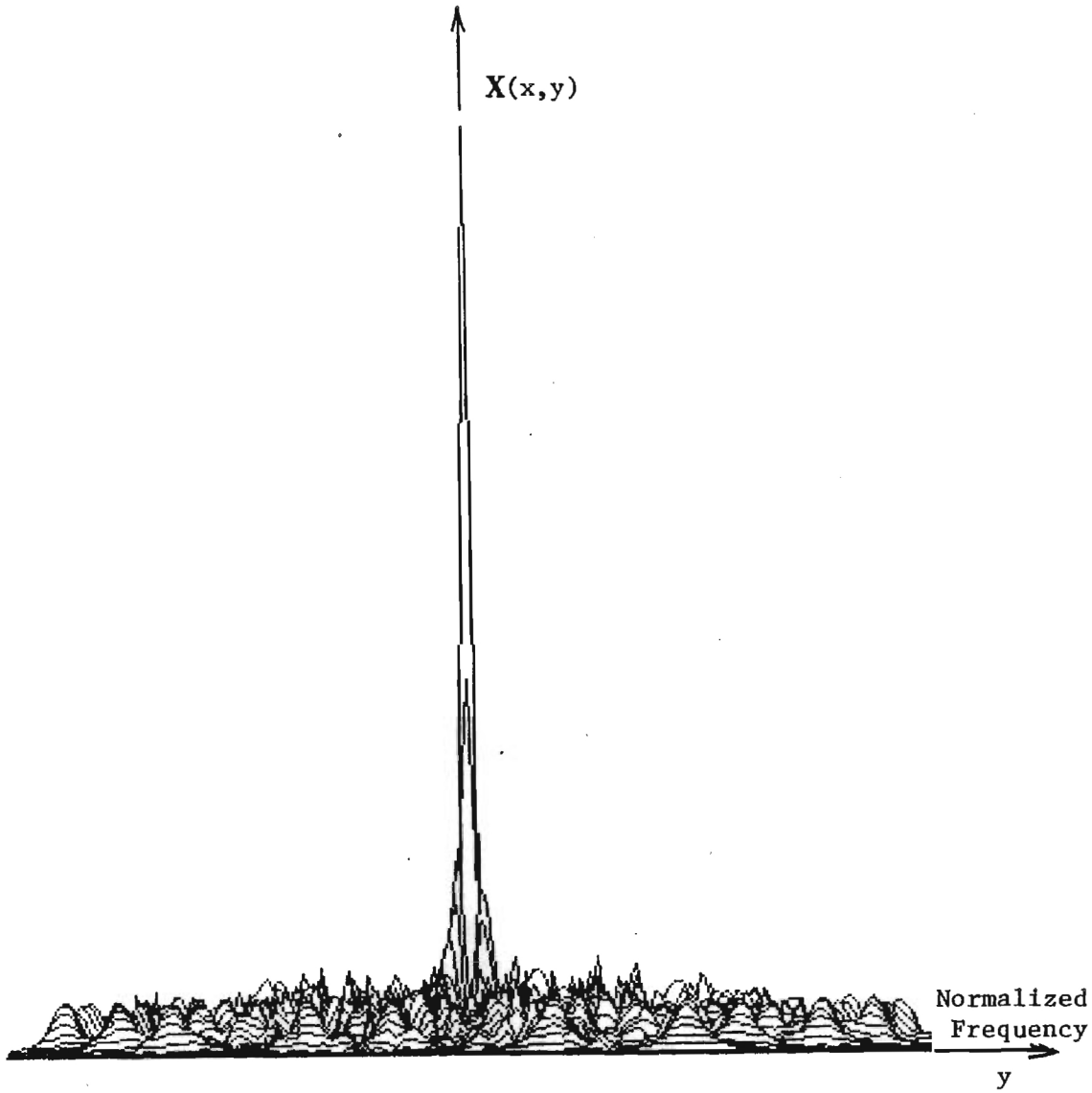

Figure 24. Ambiguity Function Sidelobe Presentation of the Design Example Sequence (N=17).

5.0 CONCLUSIONS

5.1 COMMENTS

A sonar system designed to achieve a low probability of intercept over a wide frequency band has been demonstrated in this research. The low probability of intercept sonar signal is designed to avoid detection by energy spreading through frequency-hopping or instantaneous spectral spreading or both. Thus, the signal is designed to force an interceptor receiver to come within the detection range of the user before the interceptor can detect the presence of an emitter.

The signal structure and interceptor range and a simplified signal design scheme are discussed in Section 1. The use of Welch sequence Costas arrays is discussed in Section 2, and properties of the wide frequency band beamforming arrays are discussed in Section 3. A design example for array construction, choice of frequencies, number of sub-pulses and number of array elements is presented in Section 4.

The signal scheme is a viable technique and can provide a Doppler tolerant, low probability of intercept, wide frequency band, obstacle avoidance sonar system. In the following section, some suggestions are made in terms of the operation of the sonar system to ensure a low probability of interception over a wide range.

5.2 OPERATIONAL SUGGESTIONS

The viability of forcing a potential signal interceptor to move within the detection range of the user's sonar has been demonstrated. This technique has the virtue of robust variation in application. Some of the possibilities are:

1. Start an obstacle search with low power (minimum user range) pings using a high N(SF) product. This would allow detection of objects or intruders before they could detect the user emissions. To achieve the maximum N(SF) product, the desired range resolution could be relaxed for one or two master ping pulses. As the surroundings are mapped the resolution could be optimized with the reduction of the N(SF) product. Longer ranges then could be investigated and mapped by relaxing the N(SF) product master pulse by master pulse.

2. The use of different Welch sequences of the same length or of different lengths from master pulse to master pulse will prevent an interceptor from a fortunate guess on one master pulse and extrapolating to the next pulse. In essence, even if the interceptor is listening to the correct frequencies, the interceptor will not be able to integrate the N pulses. Rather the interceptor will be forced to work with the single sub-pulse energy over an N pulse period, resulting in low SNR. This technique is not a current technique in the literature but reference [13] comments both on adjusting the period length and of a pseudo periodic version, in which the frequency code is changed from period to period, as possible variants under consideration for radar applications that are currently under study. This reference serves to confirm the appeal of the concept.

3. The spectral spreading factor varies from sub-pulse to sub-pulse since the number of cycles per sub-pulse goes up as the frequency of the sub-pulse increases. This can be utilized as increased spreading or

the width of higher frequency pulses can be reduced and the same spreading factor maintained. The variable pulse width would serve to maintain a mismatched integrator time in the interceptor receiver.

4. Time hopping is also possible with these same sequences, making the interceptor receiver more unlikely to be initiating signal processing at the correct time, thereby reducing the performance of the interceptor receiver.

5. Spreading the energy of the pulses requires phase coherent reception of the return bi-phase modulated sub-pulse. Although the phase coherency frequency to frequency may not be required, it is desirable to allow rapid acquisition for despreading of the pulses. If this phase coherency is not possible or unlikely, then higher values of N may be used in lieu of a smaller value of N combined with a spreading factor.

6. For the purposes of acquisition of the spread pulses, it is desirable to have the most cycles per sub-pulse possible. This could be optimized by raising the lower frequency of the operating frequency band, F_L, on a temporary basis while using spreading.

Appendix I

Signal-To-Noise Ratio From Energy Detector and Finite Time Integrator

Consider the energy detector and finite time integrator circuit of Figure A.1.

If the input at point A is White Gaussian noise with

$$R_n(\tau) = \frac{N_o}{2}\,\delta(\tau) \quad \text{and} \quad S_n(f) = \frac{N_o}{2} \qquad \text{A.1}$$

and a signal X(t) as

$$X(t) = \prod (t/T_s)\,\cos W_c t \qquad \text{A.2}$$

Then at point B the noise is also Gaussian bandlimited with [A1]

$$R_{nB}(t) = N_o\beta\,\delta(\tau) = \sigma^2_{nB} \qquad \text{A.3}$$

and the signal at point B, S(t), is a bandlimited version of x(t) as

$$S(t) = x(t) * h_{BPF}(t) = F^{-1}\,[X(f)\,H_{BPF}(f)] \qquad \text{A.4}$$

or

$$s(t) = F^{-1}\left[\frac{AT_S}{2}\,(\text{sinc}\,(f-f_c)\,T_s + \text{sinc}\,(f+f_c)\,T_s)\left(\prod(\frac{f-f_c}{\beta}) + \prod(\frac{f+f_c}{\beta})\right)\right] \qquad \text{A.5}$$

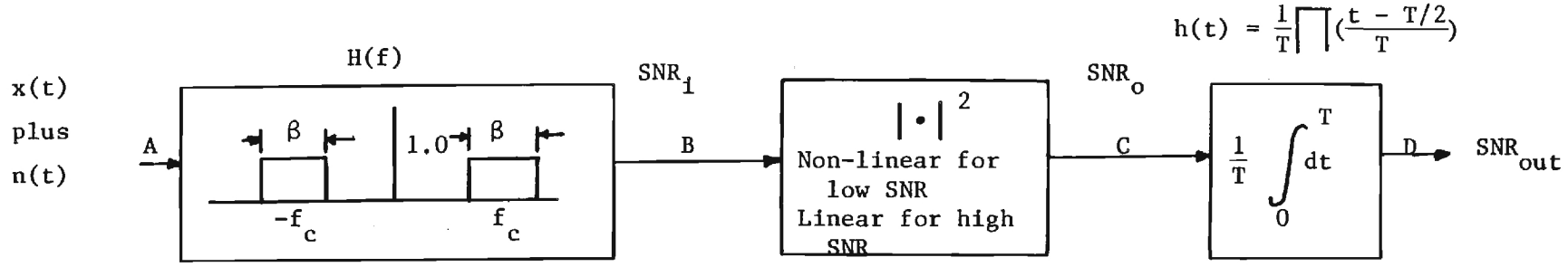

At point C: $S_c(f) = S_{ss}(f) + 4S_s(f)*S_n(f) + 2\sigma_s^2\sigma_n^2 S(f) + \sigma_n^4 S(f) + 2S_n(f)*S_n(f)$ Ref. 2

where all terms refer to the input at point B.

Figure A.1 Bandlimited, Square Law, Finite Time Integrator Detector

If the bandwidth β is wide compared with $2/T_s$, then the output s(t) is approximately equal to x(t). For example, if $\beta = 2/T_s$ the approximately ninety percent of the energy of X(t) is passed by the bandpass filter. If $\beta = 4/T_s$, then approximately 95% of the energy of x(t) is passed, etc. Thus a fair approximation of s(t) is

$$s(t) \sim \overline{\Pi}(t\beta) \cos w_c t, \quad \text{for } \beta \geq 2/T_s \quad . \qquad \text{A.6}$$

The signal power at point B is thus approximately

$$P_B \sim \frac{A^2}{2} \qquad \text{A.7}$$

and the signal-to-noise ratio at point B is

$$SNR_i = \frac{P_B}{N_o\beta} \sim \frac{A^2/2}{N_o\beta} \qquad \beta \geq 2/T_s \quad . \qquad \text{A.8}$$

The output of a square law envelope detector, point C, is analyzed in the literature and of these two are referenced [2] and [A2]. In general for the signal and noise as stated above the output signal-to-noise ratio is

$$SNR_0 \sim \frac{(A^2/2)^2}{\frac{1}{2}(2\beta N_o\beta) + N_o\beta A^2} = \frac{SNR_i^2}{1 + 2SNR_i} \quad . \qquad \text{A.9}$$

This relationship between input and output has two distinct regions of interest, low SNR_i and high SNR_i.

For the case of low SNR_i (the term $2SNR_i$ is less than one), the output SNR reduces to

$$SNR_0 \sim SNR_i^2 = \frac{(A^2/2)^2}{(N_o\beta)^2} \qquad \underline{\text{LOW } SNR_i} \quad , \qquad \text{A.10}$$

whereas in the case of high SNR_i (the term $2SNR_i$ is greater than one), the output SNR reduces to

$$SNR_0 \sim \frac{SNR_i}{2} = \frac{A^2/2}{2N_o\beta} \qquad \underline{\text{HIGH } SNR_i} \quad . \qquad \text{A.11}$$

For the case of Equation A.10, the noise statistics at point C have been shown to be CHI Squared with noise power $(N_o\beta)^2$ [A2]. The signal power is approximately $A^2/2$ with very small variance.

The output of a finite time integrator, point D, with small variance signal and CHI Squared noise statistics has been shown to be

$$SNR_D = T\beta \; SNR_C = T\beta \; SNR_i^2 \qquad \text{A.12}$$

or

$$SNR_D = T\beta \frac{(A^2/2)^2 (T_s/T)}{(N_o\beta)^2} \qquad \underline{\text{LOW } SNR_i} \qquad \text{A.13}$$

where T_s is the signal duration and T the integrator duration.

For the high SNR_i case, Equation A.11, the output is

$$SNR_0 \sim \frac{SNR_i}{2} = \frac{A^2/2}{2N_o\beta} \qquad \text{A.14}$$

and for this situation the square-law detector is almost linear for small deviations in SNR_i, hence the output noise is still approximately Gaussian in nature with variance

$$\sigma^2 = 2N_o\beta \quad . \qquad \text{A.15}$$

The output of a finite time integrator, point D, with small variance signal and Gaussian noise input is [A3]

$$SNR_D = \frac{(A^2/2)(T_s/T)}{2N_o\beta} \qquad \underline{\text{HIGH } SNR_i} \qquad \text{A.16}$$

where T_s is the signal duration and T the integrator duration.

6.0 REFERENCES

1. Modern Communications and Spread Spectrums, G. Cooper and C. McGillem, McGraw Hill, 1986, page 310.

2. Ibid, page 80.

3. Ibid, page 90.

4. Underwater Acoustic System Analysis, W. Burdic, Prentice Hall, 1984, page 386.

5. Ibid, page 41.

6. Principles of Underwater Sound, R. Urick, McGraw Hill, 1983, page 303.

7. Ibid, page 324.

8. Principles of Underwater Sound, Urick, 1983, page 284.

9. A Study of a Class of Detection Waveforms Having Nearly Ideal Range-Dopper Ambiguity Properties, IEEE Proc., Vol. 72, No. 8, August, 1984, page 996.

10. Construction and Properties of Costas Arrays, S. W. Golomb and H. Taylor, IEEE Proc., Vol. 72, No. 9, September, 1984, page 1143.

11. Design and Implementation of a Digital Phase Shift Beamformer, S. P. Pitt, W. T. Adams and J. K. Vaughn, J. Acoust. Soc. AM, Vol. 64, No. 3, September, 1978, page 808.

12. Shifted Sideband Beamformer, Pridham, R. G. and Mucci, R. A., IEEE Trans. Acoustics, Speech and Signal Processing, Vol. ASSP-27, No. 6, December, 1979.

13. High Resolution Radar, Donald Wehner, Artech House, 1987, page 115.

A1. Digital and Analog Communication Systems, Couch, MacMillan, 1987, page 500.

A2. Underwater Acoustic Systems Analysis, W. Burdic, Prentice Hall, 1984, page 395.

A3. Probability Methods of Signal and System Analysis, Cooper and McGillem, HRW, 1986, page 316.